THE EFFECTS OF 2-D BEDROCK PROFILE ON SITE SPECIFIC SEISMIC AMPLIFICATIONS IN LEDA CLAY

by

Prasanthan Ramakrishnan

M.Sc. (PM), National University of Singapore, Singapore (2017)
B.Sc. (Eng.), University of Peradeniya, Sri Lanka (2012)

A thesis submitted to the Faculty of Graduate and Postdoctoral Affairs
in conformity with the requirements for the degree of

Master of Applied Science

in

Civil Engineering

Department of Civil and Environmental Engineering
Carleton University
Ottawa, Ontario

The Master of Applied Science in Civil Engineering is a joint program with the University of Ottawa, and is administered through the Ottawa-Carleton Institute for Civil Engineering.

Abstract

The primary objective of the research is to understand the significance of the effects of the bedrock profile on seismic amplifications in soft soil deposits. Inclined soil-bedrock interfaces lead to simultaneous primary and secondary wave loading on soils, and a numerical study has been undertaken to assess whether ignoring them may lead to design deficiencies. The response of a site in Orleans with a deep Leda clay deposit at the center, but with a concaved bedrock profile, leading to a soft soil-deposit "valley", is evaluated using 2-D numerical analysis.

The seismic response of Leda clay on a hypothetical horizontal bedrock (representing conventional practice), and two different natural bedrock basins has been studied. The National building code of Canada (NBCC 2015) design spectra compatible earthquake shaking was considered. The comparisons between the conventional practice and the response of the 2-D basin demonstrate that assessment of the cyclic loading intensity is significantly affected by the basin shape. Higher cyclic stress ratio (CSR) values are realized in the 2-D analysis due to basin geometry, and the magnitude of the CSR is dependent on the configuration of the basin. This indicates that ignoring basin geometry effects might lead to unsafe liquefaction susceptibility assessments.

Acknowledgments

Foremost, I would like to devote my sincere gratitude to my supervisor Professor Siva Sivathayalan for his exceptional guidance and support in all stages of my student life at Carleton University, which gave me comfort to complete my Master's research program. It would have been impossible without his guidance and support.

I take this opportunity to thank my seniors and friends, especially Premnath, Senthooran and Theenathayarl, who gave their guidance and support full of care during this study period. Also, I would like to acknowledge all my teachers and mentors who inspired and guided me from childhood until the university level.

I would like to convey my special gratitude to my father Ramakrishnan, mother Nagaratnapoopathy and my siblings for their mental support.

Finally, I would like to thank my wife Lakshiya and daughter Saathvika for their unconditional love, encouragement and understanding throughout my studies and life.

Statement of Originality

I hereby certify that all of the work described within this thesis is the original work of the author. Any published (or unpublished) ideas and/or techniques from the work of others are fully acknowledged in accordance with the standard referencing practices.

Prasanthan Ramakrishnan

(December, 2021)

Table of Contents

List of Figures

List of Tables

CHAPTER 1

INTRODUCTION

1.1 BACKGROUND

Earthquake shaking can cause various failures such as landslides, lateral spreading, and liquefaction in soils. Geotechnical failures due to ground shaking, and associated soil liquefaction, are often responsible for most of the damage during seismic events. Seismic shaking events may consist of different types of wave forms, and various frequencies at different amplitudes. A combination of the various components of the waves represents the actual seismic loading, and it may trigger large deformations, or even structural failures. Both the dynamic properties of soils at the site and the characteristics of the incoming motion, which is mainly a function of the magnitude and distance of the earthquake, dictate the intensity of the seismic loading at a site.

Earthquakes occur in many parts of the world, and the need to perform seismic analysis as a part of the design process has been progressively recognized over the years. Depending on the geology, earthquakes may occur at the interface of tectonic plates or within the plate. Inter-plate earthquakes occurring as a result of the accumulation of energy between tectonic plates tend to be larger but occur less frequently. The largest earthquakes in Canada are expected on the West coast where the North American plate and the Pacific plate interface to create a subduction zone (Mazzotti et al., 2008), and earthquakes as large as magnitude 9 may be possible in this region (NRC, 2022). Earthquakes in Eastern Canada are generally due to fault rupture. Ottawa is an earthquake-prone city located in the Western

Quebec seismic zone, and the 2010 Val-des-Bois earthquake with the magnitude of 5.0 centered at 56 km north of Ottawa (Atkinson & Assatourians, 2010) caused the strongest shaking in this region in many years. The 1989 Saguenay earthquake, magnitude 5.9, was the largest earthquake located in Eastern Canada during the 20th century (Drysdale & Cajka, 1989).

Seismic waves are classified into two major types; body waves that travel through the body of the earth, and surface waves, that are caused by the interaction of body waves with surficial soil layers, travel along the surface of the earth. Body waves are further categorized as primary waves (p-waves) and secondary waves (s-waves) depending on the nature of particle movement given the wave propagation direction. P-waves propagate by compression-dilation pulses, and s-waves by shear deformation. Among the surface waves, Rayleigh waves that include particle movement in both horizontal and vertical directions are commonly encountered due to large, distant earthquakes. Simultaneous loading due to p-waves and s-waves, or loading due to Rayleigh waves cause both normal and shear stress increments. The effects of such combined cyclic loading with incremental shear and normal stress components are not considered in current practice. The principal stress directions continuously rotate during cyclic loading, and this differs from the conventional characterization using the cyclic stress ratio, originally defined as $CSR = 0.65 \times (a_{max}/g) \times (\sigma/\sigma') \times r_d$ by Seed & Idriss (1971).

Soil behavior during earthquakes is generally evaluated by considering the response of soils due to vertically propagating shear waves. This is because seismic waves approaching a soil deposit (at the bedrock interface) tend to travel vertically due to the natural variations in density and wave velocity with depth. P-wave intensity is typically less than s-wave

intensity (except in the case of shallow earthquakes with shorter epicentral distances), and since structures are already designed to withstand their weight ("1g" loading) in the vertical direction, the focus in practice is generally limited to shear wave loading, Thus, the occurrences of soil liquefaction are often linked to shear wave loading, and hence the a_{max} used in practice corresponds to the shear wave. Further, typical dynamic analysis considers 1D wave propagation through the soil layers in order to determine the cyclic stress ratio (CSR) to evaluate the factor of safety against soil liquefaction.

The presumption of vertically propagating shear waves within the soil medium is valid only if the underlying bedrock is horizontal. Sites with inclined bedrock are very common in nature, and in such cases, the incoming p- or s-wave would refract into both p- and s-waves. Such simultaneous loading by p- and s-waves, or loading by Rayleigh waves, would lead to a complex loading path within the soil deposits with particle movement in both horizontal and vertical directions. In such cases, the principal stress direction with respect to the direction of deposition continuously rotates during cyclic loading. Proper consideration of this change in the loading paths may be critical given that soil behavior is stress path dependent. The current Cyclic Resistance Ratio (CRR) based design approach may have to be re-evaluated to account for stress path effects under such loading. Also, the maximum cyclic shear stress (used in determining the CSR, and hence liquefaction potential) under these loading conditions could be higher than that obtained by considering a vertically propagating shear wave alone.

Local site conditions largely influence the amplification of seismic waves. In addition to the intensity and the frequency characteristics of the input motion, the mechanical properties of soil and rock, including the relative seismic impedance influence seismic

wave propagation, and the reflection and refraction at the interfaces. The basin shape may focus or spread the seismic energy towards upper layers (Frankel et al., 2002, 2009; Pratt et al., 2003).

Normally dynamic analysis or the factor of safety assessment against liquefaction relies on 1-D wave propagation to assess seismic amplification and CSR calculations. This presumes soil-bedrock interface is horizontal, but it is normal to have irregularities in bedrock profiles and the soil-bedrock interface can be inclined or concave or convex shaped. So, the vertically propagating shear wave will reflect/ refract differently depending on the incidence angle. This could produce complex loading on soil deposits. A simple 1D "SHAKE analysis", which is common in practice, may not properly capture the effects of the interactions of different wave types within the soil deposit when the bedrock-soil interface is not horizontal.

This research focus herein is on the effects of the basin geometry on the assessment of earthquake loading in soil deposits, and contrast the general loading cases with conventional cyclic resistant calculations considering 1-Dimensional wave propagation. For this purpose, a real site profile is selected from Orleans, Ottawa. The selected Orleans site contains a deep Leda clay deposit at the center with a concave shaped bedrock soil interface. It is modelled using the 2-D FLAC software to understand the significance of site geometry on the seismic response of soft clays. In addition, a horizontal rock profile is also modelled in FLAC in order to compare the effect of the bedrock shape and contrast it with conventional practice. Further, this horizontal rock profile is also modelled using "SHAKE analysis" to enable comparisons with the FLAC results.

Multiple earthquake motions, both from artificial time histories as well as from real earthquake histories, are used as input to assess the characteristics of wave propagation at the site. Accelerations and stresses obtained at different locations within the soil deposit have been used to compute cyclic stress ratio and were compared against the 1-dimensional analysis to address the significance of seismic response on local site geology.

Real earthquakes data are obtained from the 2010 Val-des-Bois earthquake and were scaled by using a new procedure to match the expected loading intensity at the site at NBCC 2015 design loads. Artificial earthquakes are generated to match the target design spectrum according to NBCC 2015 seismic provisions. Since the response of the site was assessed using 2D characterization, two cross sections of the valley (5.5km x 100m, and 4.0km x 100m) are considered in the analysis to represent different basin shapes. The results were compared to current practice, which is either empirical or simple 1D wave propagation.

1.2 SCOPE & OBJECTIVE

This research study aims to understand the significance of the combined compression (P-wave) and shear (S-wave) wave loading on soil deposits. A soft soil site in the Orleans suburb, located in the Eastern part of Ottawa, is selected for the analysis. The local geology has a concave bedrock-soil interface and has been well characterized by the Earth Scientists at the Geological Survey of Canada (Hunter et al., 2010). The response of the soils in this valley was considered in the seismic analysis to evaluate the actual cyclic stress ratio and compare it to the conventional analysis.

Site response is assessed using both artificial earthquake records that are generated to match the design spectrum, and instrument recorded motions scaled to match the design

spectrum in order assess the suitability of using artificial motions for seismic analysis. A total of eight time-history records are used as input earthquake motions with three site profiles. The soil model used was limited to non-linear elastic, with no consideration of plasticity, since the intent was to compare the response with current practice, which is based on equivalent linear analysis.

The wave propagation analysis is used to compute the stress increments, and calculate the cyclic stress ratio at different locations within the Leda clay deposit. These values are contrasted with the CSR computed using the "Simplified Approach" of Seed & Idriss (1971) that is widely used by practicing engineers. Finally, the implications of simultaneous primary and secondary wave loading on soils due to the local geology and liquefaction potential are discussed based on the typical response of Leda clay under cyclic loading at different CSR values. This permits a conclusion of the significance of local geology on seismic design.

1.3 ORGANIZATION OF THESIS

The general behavior of soils under cyclic loading is presented in Chapter 2 which follows this introductory chapter. Concepts relating to seismic wave propagation, soil liquefaction, and geological influence on wave propagations are discussed in detail. The current approach to seismic analysis is discussed and its deficiencies, in light of the research is being carried out, are noted at the end of the chapter.

Chapter 3 discusses the basics of numerical modelling using FLAC. The modelling concepts and steps involved in the analysis of cyclic nonlinear analysis of two-dimensional model are discussed in detail. Details about the methods used in artificial earthquake

generation and scaling of real earthquakes to use as input to the seismic analysis are discussed.

Chapter 4 presents the analysis and interpretation of results from the output of numerical study. Stating from the validation of FLAC numerical model, a comparison of seismic effects on different geological profiles on different earthquake motions is discussed. Also, a comparison of the seismic response among artificial earthquakes and real earthquakes are presented. At the end, the spectral ratio method is used to visualize the amplification or attenuation of input earthquake at different elevations of both 2D profiles of Orleans valley.

Chapter 5 presents the conclusions derived from the numerical analysis presented in the previous chapters, and summarizes the implications of this study to geotechnical engineering practice.

CHAPTER 2

GENERAL SOIL BEHAVIOR UNDER CYCLIC LOADING

2.1 INTRODUCTION

Cyclic loading during an earthquake may lead to a reduction in the shear strength of soil. Soil liquefaction is the phenomenon associated with catastrophic failures during or following dynamic loading. The term liquefaction has been used to refer to both zero effective stress, and to excessive deformation in the literature. The strength reduction or excessive deformation becomes the reason for the failure of many structures on the ground surface as well as underground. As earthquakes are a short period events, the soil response in-situ is undrained. So, a knowledge of the undrained behavior of soil under cyclic loading is important in construction if the design has to have a seismic resistant structure.

Various parameters influence the deformation characteristics of soil during cyclic loading; predominant factors are void ratio, effective confining stress, fabric structure, stress path, and stress-strain history (Castro, 1969; Vaid & Sivathayalan, 2000). In addition, the local site geology influences the cyclic stress ratio and amplification or attenuation of earthquake motion. Typical seismic analysis in current practice is based on one dimensional wave propagation where the bedrock is assumed to be horizontal and the incoming seismic shear wave approaches the interface at a normal incidence angle. This is commonly referred to as the vertically propagating shear wave in the literature and used for numerical analysis of soil deposit under seismic loadings. The current understanding of soil behaviour under earthquake loading conditions have been very much based on the response of soil under vertically propagating shear waves.

The nature of loading changes if the bedrock-soil interface is not horizontal. So, the level of amplification might differ within the same region due to the variation in bedrock/soil profile. Such observations are recorded in the past where the amplification of up to 10 was observed with reference to the bedrock motion (Gutenberg, 1957) among 25 different seismic stations. So, the geological properties particularly the geometry and the nonlinearity of soil/bedrock profile should also be taken into consideration together with the physical properties of soil deposit during the seismic analysis of a local site.

2.1.1 Anisotropy of soils

The anisotropic nature of soil has been discussed by many researchers in the literature (Philips & May, 1967; Arthur & Menzies, 1972; Arthur et al., 1977; Wong & Arthur, 1985; Mahmood & Mitchell, 1974; Lade & Kirkgard, 2000; Vaid et al., 2001) which is basically due to natural pedogenesis. The formation of particles in geo-materials plays an important role in its strength. Generally, the soil layers are formed by particles of sediments under gravity either in the marine environment or in the air. Due to this directionality in the formation, the physical property of soil layers is not the same in all directions. Cohesive materials like Leda clay are formed in the marine environment and exposed out to become land after several years.

Casagrande & Carillo (1944) explains that the nature of anisotropy is formed in two stages. In the first stage, the anisotropy is due to the shape and directional deposition of particles. This has been called the inherent anisotropy. Subsequently, the soil layers experience additional loading due to geological changes such as overburden pressure accumulated by additional layers on top, infiltration and erosion, and other environmental changes that

influence the nature of anisotropy. This is referred to as induced anisotropy. Both inherent and induced anisotropy influence the soil structure and the properties of soil layers such as soil strength, permeability, swelling/shrinkage, and these effects become directionally dependent.

2.1.2 Sensitive clay

Most of the landmass in Ottawa and the surrounding areas were covered underneath the Champlain Sea several thousand years ago. As the area began to rebound due to retreating glaciers, the Seawater retreated leading to the landmass. Sedimentation of particles in such marine environment slowly formed these sensitive clays. Positively charged ions in minerals bind to the deposited particles and formed sediments. Such sensitive clays hold its strength due to its fabric arrangement. This fabric structure of clay material also due to the depositional environment, geological and stress history (Locat et al., 1984). If the fabric is disturbed then the shear strength reduces rapidly (Skempton & Northey, 1952; Craig, 2004). Fabric structure can be disturbed by applying excessive stress or physical remolding of such clays and result in considerable loss of strength, which may lead to excessive deformation. This reduction in strength due to its loss of fabric/structure is referred to as sensitivity. Mathematically, sensitivity is the measure that represents the loss of shear strength of a sensitive clay due to the loss of its fabric. Sensitivity of clay defined from the ratio of shear strength between in-situ condition and remolded condition.

$$Sensitivity, S_t = \frac{Undisturbed\ shear\ strength}{Remoulded\ shear\ strength} = \frac{S_u}{S_{u(r)}}$$

Based on the sensitivity index S_t soils are classified as insensitive, low sensitive, medium sensitive, sensitive, extra sensitive and quick clays (Skempton & Northey, 1952). Current Canadian Engineering Manual CFEM (2006) 4th edition proposes five classifications of sensitivity, ranging from low sensitivity to quick clays. The reduction in strength happens regardless of water content (Skempton & Northey, 1952) and there is a significant reduction in shear strength between undisturbed/in-situ clay and remolded clay under identical water content conditions. This observation implies the loss of fabric structure causes the strength reduction. Such loss of fabric may also be a major factor during cyclic loading.

2.2 UNDRAINED CYCLIC BEHAVIOR OF SOIL

Response of a saturated soil without volume change is classified as undrained. It occurs due to insufficient time to dissipate excess pore water pressure either on account of the fast-loading rate or low permeability. Shear strength reduction and deformation of such material under dynamic loading depends on various parameters such as frequency content of incoming seismic waves, duration of earthquake and distance from the epicenter (Ansal & Erken, 1989). But the response of soil or the amplification or attenuation of incoming seismic waves is not the same even if the site is located at the same epicentral distance. There are many site-specific factors such as physical properties of soil, geological variation of soil/bedrock interface, stress path etc. that influence the amplification of incoming seismic motion. Various research works have been carried out to understand the undrained cyclic behavior of soil (Sangrey et al., 1969; Andersen et al.,1988; Malek el al., 1989; Zergoun & Vaid, 1994; Ishihara, 1996; Boulanger & Idriss, 2004). All the studies explicitly

state that cyclic loading increases the pore pressure and reduces the effective stress. As a result, the soil liquefies and deforms excessively. Also, shear modulus or the stiffness of the soil reduces as the effective stress decreases, and the stress vs strain hysteresis loop gets larger with every cycle of loading. The shear modulus of the liquefied soil is essentially zero (Sivathayalan and Mehrabi Yazdi, 2014).

2.2.1 Liquefaction

The term liquefaction has been used in different contexts in the literature over the years. Theoretically, liquefaction happens in granular soils when the soil reaches zero effective stress due to generation of excess pore water pressure that caused by external loading under undrained condition. Generally, the liquefaction phenomenon has been related to granular materials (Castro, 1969; Ishihara, 1996; Vaid & Chern, 1985). Clayey materials are considered as non-liquefiable soil (Thiers & Seed, 1969; Seed et al., 1983) because zero effective stress state in clayey material does not necessarily lead to zero shear strength due to its interparticle cohesion. But, the zero-effective stress-based definition of liquefaction is not relied upon in current practice, and liquefaction is deemed to be a state where soil shows excessive deformation under cyclic loading in undrained condition. It is recognized that zero effective stress is not the only critical condition, but excessive deformation can also lead to major disasters. The term liquefaction is used in this research to refer to the phenomenon in both sandy and clayey materials with the concept of excessive deformation. Further, the soil response following liquefaction has been studied by many researchers, and it has been found that soil gains its strength at post liquefaction state (Vaid Thomas, 1995; Vaid & Sivathayalan, 1996). The studies on soil deformation under post liquefaction load

condition in Seed et al. (2003) and Sivathayalan & Ha (2011) indicates that deformation in that case it associated with dilation.

In precise terms, it is hypothetical to define a soil layer as purely drained or undrained. In real cases, the drainage conditions cannot be easily classified to its extreme cases of truly drained vs undrained states. The actual state will be in between the two extreme states where it can be deemed partially drained or partially undrained in an element, and typically undrained response is considered to be weaker than the drained response. This may not necessarily be the case in dilative materials. Further, in-situ pore pressure variations during earthquake loading in boundary values problems can lead to more complex drainage conditions in soil elements, and scenarios weaker than undrained may be realized (Sivathayalan & Logeswaran, 2008). In granular material (e.g., sands), if liquefaction occurred in shallow layers, it can be observed through sand boiling where the pore water migrates to the ground surface due to the generation of excess pore water pressure. But it will not be so evident at the ground level if the deep soil layer got liquefied.

2.2.1.1 Liquefaction assessment in Fine grained soils

The liquefaction potential in fine grained soils was originally assessed by Wang (1979) who reported that fine soils have to meet all the following criteria to be susceptible to liquefaction.

1. Finer grains (less than 0.005mm) percentage is less than or equal 15%
2. Liquid limit less than or equal 35%
3. Natural water content greater than or equal 90% of liquid limit.
4. Liquidity Index, $LI = (WC - PI)/PI$ is greater than 0.75.

The above criteria were commonly known as the “Chinese criteria” in the literature and were modified by Finn (1994) who proposed the following as the requirement for liquefaction in fine grained soil

1. Finer grains (less than 0.005mm) percentage is less than or equal 20%
2. Liquid limit less than or equal 36%
3. Natural water content greater than or equal 90% of liquid limit.

In recent years, it has been recognized these criteria are not necessarily accurate since deformation characteristics of fine-grained soils are also dependent on plasticity index. Seed et al. (2003) and Boulanger and Idriss (2005) among others have proposed alternated means to assess liquefaction potential of fine-grained soils. Figure 2-1 shows such a proposal as summarized by Prakash and Puri (2010).

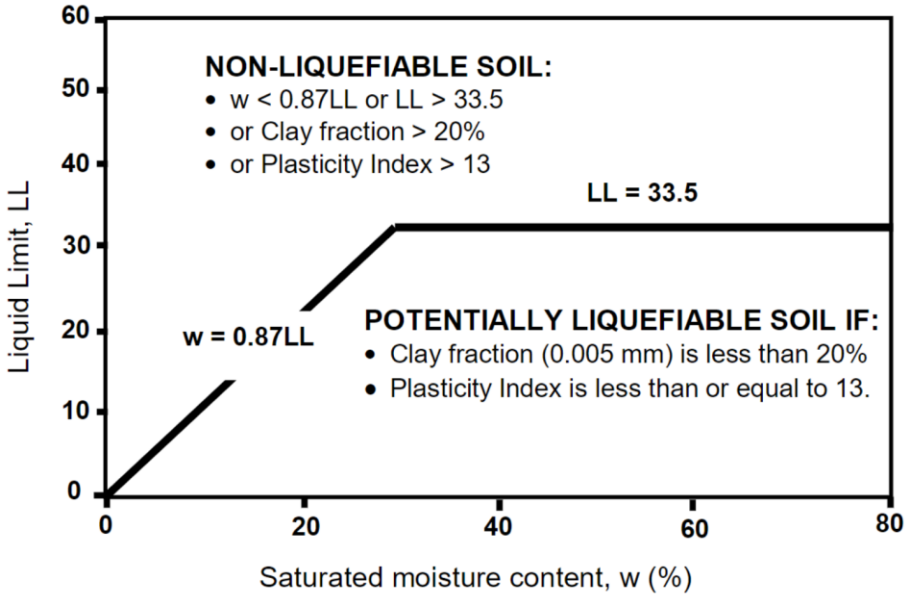

Figure 2-1: Chinese Criteria Adapted to ASTM Definitions of Soil Properties (Perlea et al., 1999)

It should be noted that when using the term liquefaction to represent large strains without regard to the strain development mechanisms or the development of large excess pore water pressure, soft soils that do not meet these criteria could also be deemed liquefied.

2.2.1.2 Liquefaction assessment in granular soils

Liquefaction assessment in sands is often based on empirical in-situ correlations in practice. Seed & Idriss (1971) originally proposed a chart to identify liquefiable sands based on SPT-N values. Commonly called the "Seed's chart" (Figure 2-2), it was essentially a boundary curve that separates liquefied soils from non-liquefied soils during earthquakes. It is based on in-situ observations of soil liquefaction in California, and was limited to liquefaction at relatively shallow depths (5-15m) on level ground, and earthquake magnitudes of about 7.5. Liquefaction potential is assessed by comparing the cyclic stress ratio to the cyclic resistance ratio.

Various improvements were made to this chart over the years to account for confining stress, initial static shear, fines content of the soil, and the earthquake magnitude. Dependency on confining stress level is accounted by the K_σ factor (Seed & Harder 1990; Vaid & Sivathayalan, 1996; Vaid et al., 2001) and a similar approach using K_α factor has been proposed to account for initial static shear. K_σ has been shown to be dependent on stress level (Seed & Harder 1990), and relative density (Vaid & Sivathayalan 1996). It varies systematically with increasing density and stress levels, and the chart provided by Youd et al. (2001) is widely used in current practice.

K_α has been shown to be dependent on many factors, including static shear stress ratio $\alpha = \tau_{st}/\sigma'$, relative density and loading mode (Vaid et al., 2001; Sivathayalan & Ha, 2011),

but its variation is complex and thus it is often not properly considered in practice (Youd et al., 2001). Since the chart was based on magnitude 7.5 earthquakes it has to be corrected for use with other earthquake magnitudes. Seed and Idriss (1982) first introduced the magnitude scaling factor, K_{MSF} to adjust the liquefaction assessment for different earthquake magnitudes.

In addition to the SPT N-value based liquefaction chart discussed above, correlations-based CPT data and shear wave velocity are also available in the literature (Youd et al., 2001). Typical in-situ correlation based empirical liquefaction assessment process begins with the Seed's chart, and the reference CRR obtained from the chart would be corrected for overburden stress, static shear and earthquake magnitude. This site-specific cyclic resistance would then be compared to the anticipated cyclic load at the site to determine the factor of safety against liquefaction as shown in the following equation. (which is discussed in detail in the following pages)

$$FS = \frac{CRR_{Chart} \times K_{MSF} \times K_{\sigma} \times K_{\alpha}}{CSR}$$

The soil liquefaction can happen at any depth, and if every other parameter remains constant deeper soils are more susceptible to liquefaction. However, the severity of the damage is higher if liquefaction occurs at shallow depths or near the ground level. In general, the damage potential is related to the thickness of un-liquified soil layers above the liquified soil layer (Ishihara, 1996).

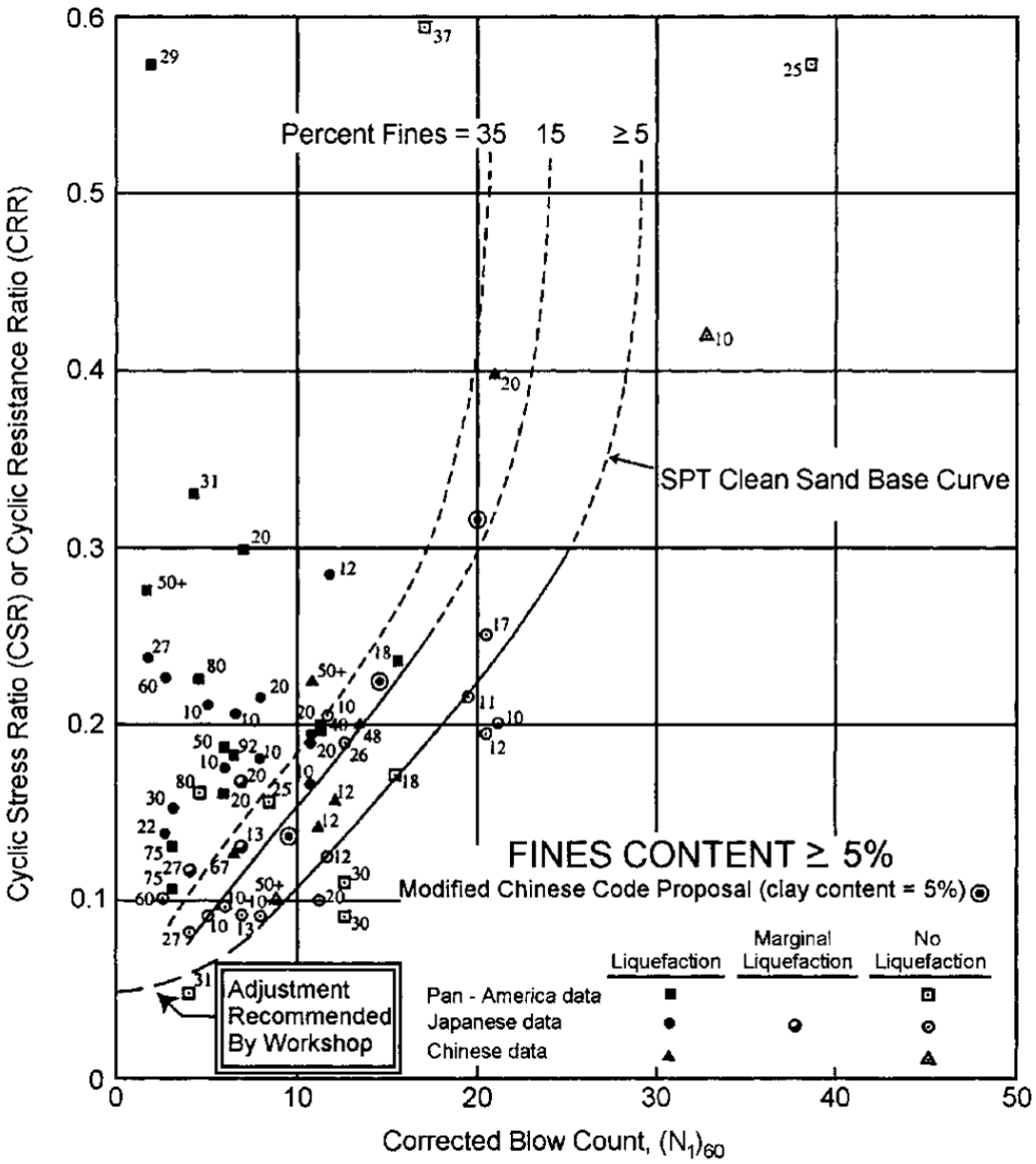

Figure 2-2: SPT Clean-Sand Base Curve for Magnitude 7.5 Earthquakes with Data from Liquefaction Case Histories (Modified from Seed et al., 1985)

2.2.2 Cyclic Stress Ratio (CSR)

The intensity of cyclic loading is generally represented by cyclic stress ratio (CSR) which is the ratio between the shear stress increment and the initial effective stress. It has been defined differently depending on the loading mode; in laboratory cyclic simple shear experiments it is customary to define $CSR = \tau_{cy}/\sigma'_{vc}$ and under cyclic triaxial it is typically defined as $CSR = \sigma_{d,cy}/2\sigma'_{3c}$ where $\sigma_{d,cy}$ is the cyclic deviatoric stress and is equal to $2\tau_{cy}$. In field problems, it has been defined as the ratio of shear stress induced by earthquake loading normalized by the vertical effective stress (Seed el al., 1983) and thus is identical to simple shear. The use of minor principal stress as the normalizing parameter has its origins in the early days when soil behaviour was characterized at isotropic consolidation states. Vaid et al. (2001) proposed a modified definition for CSR to account for non-hydrostatic initial stress states that is consistent with the simple shear definition. Their rationale was that the CSR be considered as a ratio between the maximum shear stress increment and the effective normal stress on the plane of maximum shear stress for the specimen under loading.

For in-situ applications, CSR is often determined from the horizontal acceleration record, according to the Seed and Idriss (1971) simplified formulation. They proposed $CSR = 0.65\left(\frac{a_{max}}{g}\right)\frac{\sigma_{vo}}{\sigma'_{vo}}r_d$. where a_{max}- Peak horizontal acceleration at ground surface generated by the earthquake, g – acceleration of gravity, σ_{vo} – total vertical overburden stress, σ'_{vo} - effective overburden stress, r_d stress reduction coefficient to account for the effects of increasing confining stress with depth.

While simple to use, the accuracy of this formulation is highly dependent on the chosen $r_{d_}$value since the formulation is based on surficial acceleration. If proper numerical analysis is conducted, the variation of acceleration, and shear stress increment with depth can be directly obtained. So, CSR is defined as ratio of the shear stress increment in $x-z$ plane and the initial vertical effective stress and the formula re-arranged and formed as $CSR = K\frac{\Delta\tau_{xz}}{\sigma'_{vo}}$. Here $\Delta\tau_{xz}$ is the shear stress increment in the horizontal plane, σ'_{vo} is the initial effective vertical stress, and K is a reduction factor to account for the fact that the seismic shaking is transient, and the peak value of $\Delta\tau_{xz}$ only happens momentarily and it will not cause any direct effect on the soil deposit. A factor of K = 0.65 has been originally proposed by Seed, but it has been suggested that it would be more appropriate to change the value of K depending on earthquake magnitude as $K = (M-1)/10$.

Under three-dimensional loading, the definition of CSR can be considered differently from the simpler definitions used in practice based on the shear stress increment on the horizontal plane. It would be logical to consider the maximum shear stress increment (which would eb consistent with the cyclic triaxial definition of CSR) since it would be the parameter that governs failure.

2.2.3 Number of cycles from earthquake magnitude

Earthquake motion can be represented as a combination of various frequencies of simple sinusoidal waves with different magnitude. The intensity of shaking at different frequencies are represented by a Fourier spectrum. Each of the waves involves in triggering the soil deposit or the structures depending its energy level. However, the overall earthquake motion can be simplified and represented with a single uniform sinusoidal wave

with a cyclic amplitude of (τ_{cy}) and a certain number of cycles (N) (Seed & Idriss, 1970; Seed & Idriss, 1982; Idriss I. , 1999). Even though many researchers proposed different way of representation of earthquake motion, the relationship shown in Figure 2-3 (Boulanger & Idriss, 2004) is widely adopted.

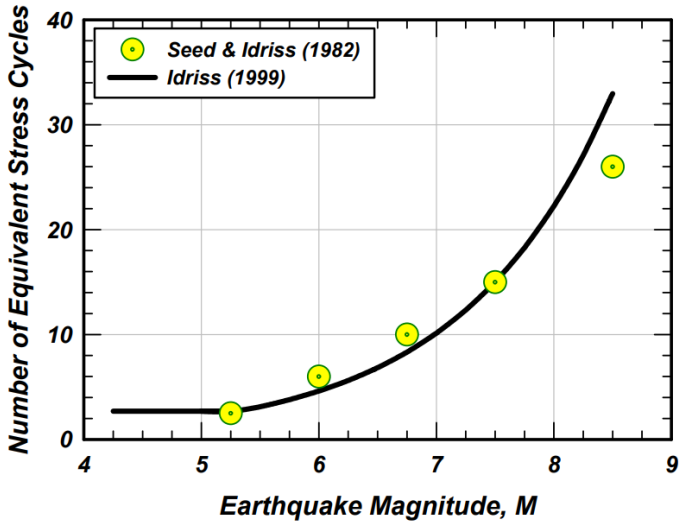

Figure 2-3: Relationship between earthquake magnitude and number of loading cycle (after Boulanger & Idriss, 2004)

2.2.4 Cyclic Resistance Ratio (CRR)

Cyclic resistance ratio (CRR) represents the capacity of the soil to resist liquefaction under dynamic loading condition for a given earthquake magnitude. It is derived from Cyclic Stress Ratio (CSR) after multiple laboratory experiments, or from Seed's chart. As noted previously, CSR is the intensity of the imparted cyclic loading during the earthquake, and the duration of the event is characterized by the equivalent number of constant stress amplitude loading cycles. A series of experiments at different CSR are conducted in the laboratory to develop a "cyclic resistance curve" and CRR is derived based on the curve

given the equivalent uniform stress cycles expected for a specific earthquake magnitude. CRR is generally qualified by the earthquake magnitude as $CRR_{M=7.5}$ or the corresponding equivalent number of uniform loading cycles as CRR_{15} based on the data shown in Figure 2-3. Higher earthquake magnitude corresponds to larger number of equivalent cycles, and results in lower cyclic resistance. The value of CRR reduces with the increase in number of cycles or the magnitude of earthquake hyperbolically (Ansal & Erken, 1989; Kodaka el al., 2010; Wichtmann et al., 2013).

2.2.5 Overburden stress

As noted earlier, in addition to earthquake magnitude, the cyclic resistance ratio depends on many other factors including confining (overburden) stress and static shear. Increasing overburden stress makes the sands more contractive and thus plays an important role in soil liquefaction susceptibility under dynamic loading. While increasing overburden stress with depth leads to increasing density (void ratio reduces) which enhances the cyclic resistance of the soil deposit, the gradual change from dilative to contractive with increasing confining stress reduces cyclic resistance. Proper comparisons of the effect of confining stress levels have to be made at fixed density levels. At fixed density the CRR reduces with increased confining stress. To address the effect of confining stress σ_v', that increases with respect to the depth of soil represented by a factor K_σ which is a ratio of the CRR at a certain confining stress and the CRR at a confining stress of 100kPa. If the factor K_σ approaches 1 it implies the capacity of soil is almost same at different confining stresses.

To standardize the cyclic resistance ratio calculation with respect to the overburden pressure, K_σ factor is introduced. K_σ factor standardizes the measured cyclic resistant ratio (CRR) at a certain overburden pressure against the 100kPa effective overburden pressure.

$$K_\sigma = \frac{CRR\ at\ confining\ stress\ \sigma'_v = \sigma'_v}{CRR\ at\ \ \sigma'_v = 100kPa}$$

K_σ factor is less than 1 if the effective overburden pressure is greater than 100 kPa. If the effective overburden pressure is smaller than 100kPa, then K_σ will be greater than one, and typically it is capped at about 1.7. So, by incorporating the K_σ factor, the cyclic resistance ratio will be,

$$CRR_\sigma = K_\sigma \times CRR_{\sigma=100kPa}$$

Followed by the case study on the Duncan dam (British Colombia) hydroelectricity project in early 90s, it was recognized that appropriate consideration should be taken not only of the effect of K_σ due to increased confining stress with depth, but also of the associated stress densification. Even though increment in confining stress with depth causes soil more susceptible to liquefaction, the density of the soil also increases with depth. In the case of Duncan Dam, it was found that both factors compensated each other and the CRR remained essentially the same throughout the depth (Pillai and Byrne, 1992). So, considering the overburden stress together with the physical properties of the soil deposit is crucial in seismic analysis.

2.2.6 Static shear stress

Similar to the overburden pressure, the static shear stress also influences the cyclic resistance ratio of the soil. Initial static shear present due to the sloping ground affects the

capacity of soil since the cyclic shear stress is now superimposed on shear stress already present on the material. The value of initial static shear is quantified by the static shear stress ratio, α which is a ratio of the static shear stress, τ_{st} to the vertical effective confining stress, σ'_{vc}. For loose sands, increasing α reduces CRR and increases liquefaction potential. In contrast, for dense sand, increasing α increases CRR and decreases liquefaction potential (Seed el al., 1983; Seed & Harder, 1990).

The static shear correction is considered through K_α factor which is a ratio of CRR with a static shear of a certain α to CRR with no static shear.

$$K_\alpha = \frac{CRR\ with\ static\ shear\ \ \frac{\tau_{st}}{\sigma'_{vc}} = \alpha}{CRR\ with\ no\ static\ shear}$$

The combination of overburden stress correction factor and static shear correction factor (Seed & Harder, 1990), the equation for cyclic resistant ratio (CRR) become to,

$$CRR_{\sigma,\alpha} = K_\sigma \times K_\alpha \times CRR$$

2.2.7 Magnitude Scaling Factor

As noted previously, the Seed's chart was based on earthquakes with magnitude 7.5. Soil capacity will be higher for smaller magnitude of earthquakes since they produce smaller number of equivalent uniform cycles. Thus, if the design earthquake has a different magnitude, an appropriate correction has to be considered. Seed & Idriss (1982) first introduced magnitude scaling factor, K_{MSF} to adjust the liquefaction assessment for different earthquake magnitudes. Improvements to the Seed and Idris K_{MSF} factors have

been proposed in the literature (Youd et al., 2001). Figure 2-4 shows the variation of K_{MSF} with earthquake magnitude.

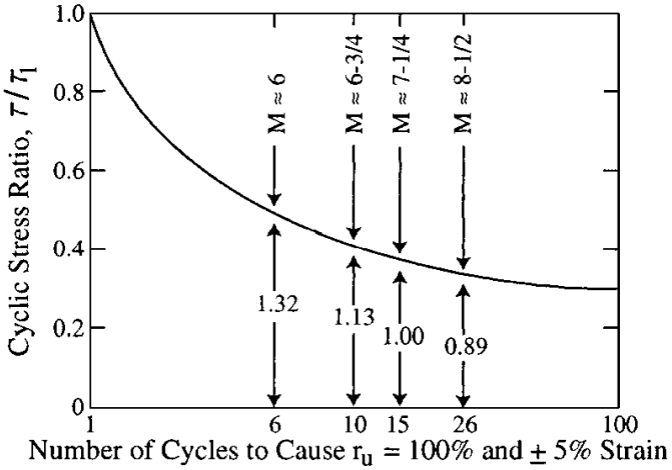

Figure 2-4: Representative Relationship between CSR and Number of Cycles to Cause Liquefaction (Reproduced from Seed & Idriss 1982)

Finally, the equation for site specific CRR becomes,

$$CRR_{M,\sigma,\alpha} = K_{MSF} \times K_{\sigma} \times K_{\alpha} \times CRR_{Reference}$$

The site-specific cyclic resistance ratio (CRR) includes the effect of overburden stress, static shear stress and the earthquake magnitude, and will determine whether there will be liquefaction at a site due to a given cyclic stress ratio imposed due to seismic shaking.

2.3 SEISMIC WAVE PROPAGATION

Earthquake waves are classified into two major types such as primary waves and shear waves. Transmission mechanism of primary waves is through compression and dilation where the direction of wave propagation is same direction as the particle motion. And the

secondary waves are transverse waves where the wave propagation is perpendicular to the particle motion. The Figure 2-5 illustrates the propagation of primary and secondary waves. Shear waves are further divided into two types, SH and SV waves depending on whether particles movement is in the horizontal plane or vertical plane. In a real scenario, the actual particle movement will be oriented in an oblique plane where it will have both vertical and horizontal components.

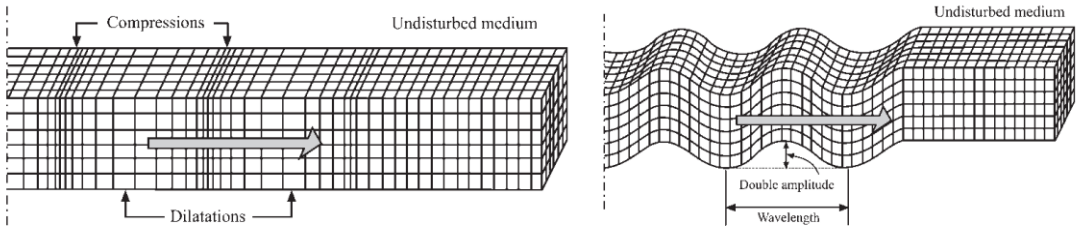

Figure 2-5: Propagation of body waves: Compression wave (left) and Shear wave (right) (adopted from Bolt, 1999)

The surface waves are formed due to trapping of body waves within surficial soil layers when the incident wave exceeds critical angle. Surface waves are again classified into two major types such as Love wave and Rayleigh wave as shown in Figure 2-6. Horizontal shear waves trapped within soft surficial soil layers result in Love wave and in these waves, there will not be any particle movement in the vertical direction. Interaction between p waves or SV waves and surficial layers result in a ground rolling wave called the Raleigh wave. In this case, there will be particles movement in both horizontal and vertical directions.

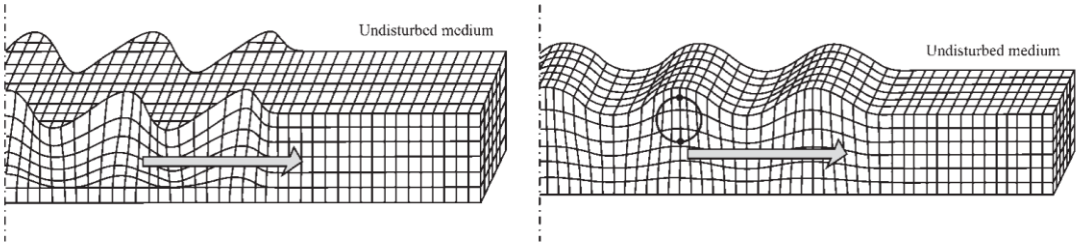

Figure 2-6: Propagation of shear waves: Love wave (left) and Rayleigh waves (right) (adapted from Bolt, 1999)

The combined effect of compressional and shear wave imposes complex loading on soil deposits that is analogous to that of Rayleigh waves. The principal stress direction rotates continuously with respect to the direction of soil deposition during the duration of earthquake. However, current practice of seismic analysis mostly assumes the incoming waves as vertically propagating shear waves that excite the soil deposit in the horizontal plane only.

The natural formation of soil is under gravity load leads to a transversely symmetric soil fabric that is axisymmetric about the vertical axis. This is typically called cross-anisotropy in geotechnical engineering. It is because the gravity force pulled each particle downwards during the formation. So, the soil strata will be more stable vertically compared to horizontal direction. So, the cyclic loading due to vertically propagating shear waves also acts horizontally that implies the cyclic loading shears the soil layers in the horizontal direction.

2.3.1 Reflection and refraction of seismic waves

Seismic wave propagation analysis is generally based on a presumed horizontal soil-bedrock interface. But, the assumption of horizontal stratification is not always true. Such

inclined interfaces, whether planer or non-planar changes the nature of wave refraction and reflection. The incoming wave reflects and refracts in to both P and S waves (Kramer, 1996) if it excites the particles at the interface both along and perpendicular to the interface. Figure 2-7 illustrates and compares the reflection and refraction of incoming wave at horizontal and non-linear interface. In addition to reflection and refraction, concave and convex interface focus or spread the earthquake energy towards the upper layer as illustrated in the Figure 2-7.

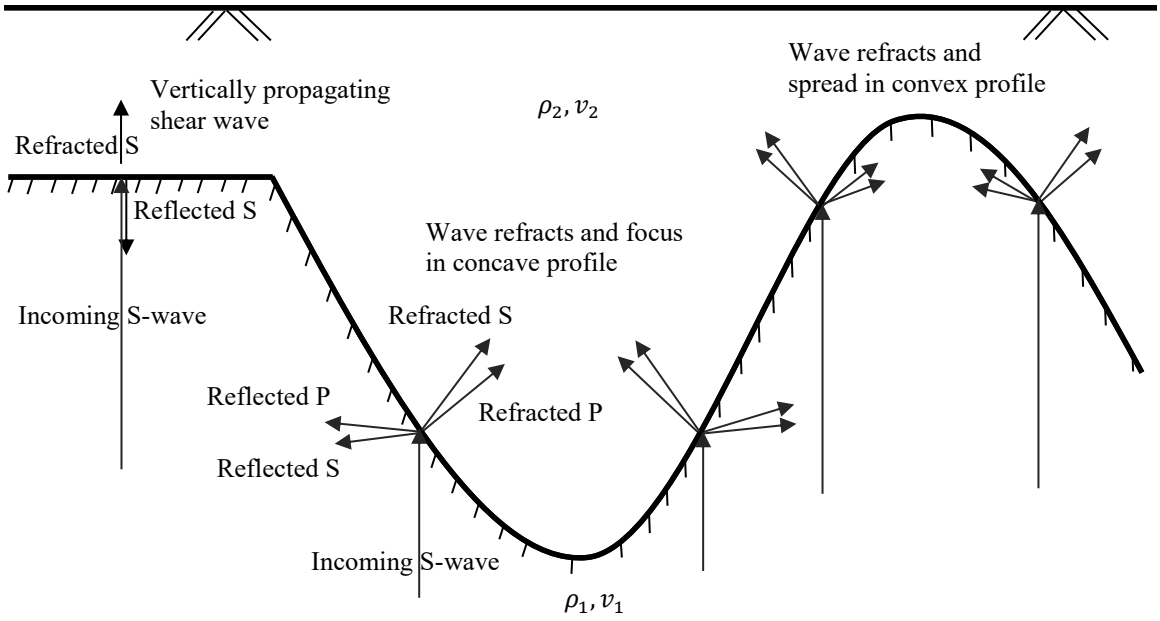

Figure 2-7: Reflection and Refraction of incoming vertically propagating seismic wave on different types of interfaces

2.3.2 Incident angle of seismic waves

Incident angle of seismic waves at the soil-bedrock interface influences the fundamental characteristics of wave propagation. In both planer and inclined interface, the wave reflection and refraction will take place. But the horizontal interface will have a normal incident wave where the reflected and refracted waves will have the same characteristic as the incoming wave. Here the assumption is that the incoming seismic waves approach to the local site bedrock soil interface vertically which is a widely accepted concept in seismic analysis. In contrast, the local geology may result in non-normal incident waves and leads to reflection and refraction of the incoming shear wave into both compressional and shear waves. Particle motion perpendicular to the interface causes the compressional wave, and that along the direction of the interfaces leads to the generation of shear wave.

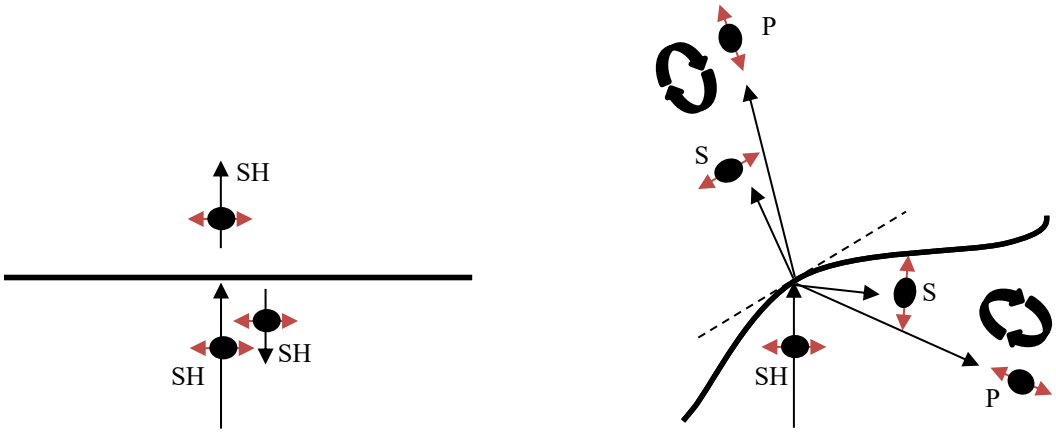

Figure 2-8: Wave reflection and refraction at horizontal and inclined soil-bedrock interfaces

As a result, the seismic waves within the soil deposit would have both compressional and shear waves (even if the incoming wave is only a compression wave or only a shear wave) and this leads to the particle rolling effect as shown in Figure 2-8. The resulting stress

increments in the soil deposit will be complex and the loading path would involve principal stress rotation.

The impacts of basin effect on the expected seismic amplifications in Seattle and the surrounding regions (Washington state, USA) have been studied by many researchers (Frankel et al., 2002, 2009; Pratt et al., 2003; Pratt & Brocher, 2006). Seismic Hazard Investigations of Puget Sound (SHIPS) experiments reported that basin effects in Seattle leads up to an amplification of ten or even more in the long period range from 1~5 seconds (Pratt et al., 2003). Recent studies on sedimentary basins in the Puget Lowland also show that the basin effect amplifies incoming shear waves and both the basin geometry and the impedance contrast between soil-bedrock interface results an increased shaking intensity and duration within the sedimentary basin (Thompson et al., 2020).

2.3.3 Effect of impedance contrast

Difference in seismic impedance ratio between two layers at the interface change the characteristic of the seismic waves and influence the amount of energy being refracted and reflected in-between those two layers. Seismic impedance is the product of density and shear wave velocity, $z = \rho v$. The impedance ratio between two layers is defined by $\alpha_z = \frac{\rho_2 v_2}{\rho_1 v_1}$ where ρ_1, ρ_2 and v_1, v_2 are the density and wave velocity of the layer 1 where the seismic wave approaches the interface and the layer 2 where the wave propagates through the interface.

For a simple harmonic incident wave, the stress due to the incident, reflected and transmitted waves is written as follows (Kramer, 1996).

$$\sigma_I(x,t) = \sigma_i e^{i(\omega t - k_1 t)} \quad (1)$$

$$\sigma_R(x,t) = \sigma_r e^{i(\omega t - k_1 t)} \quad (2)$$

$$\sigma_T(x,t) = \sigma_t e^{i(\omega t - k_1 t)} \quad (3)$$

Similarly, for the displacements of incident, reflected and transmitted waves are written as,

$$u_I(x,t) = u_i e^{i(\omega t - k_1 t)} \quad (3)$$

$$u_R(x,t) = u_r e^{i(\omega t - k_1 t)} \quad (4)$$

$$u_T(x,t) = u_t e^{i(\omega t - k_1 t)} \quad (5)$$

For the compatibility of displacement at the interface due to the seismic wave reflection and refraction, the summation of displacement of incoming, $u_I(x,t)$ and reflected, $u_R(x,t)$ wave in the layer 1 must be equal to the displacement of transmitted wave in the layer 2, $u_T(x,t)$.

$$u_I(x,t) + u_R(x,t) = u_T(x,t) \quad (6)$$

Similarly, the for the compatibility of stresses at the interface, the stress due to incident and reflected wave will be equal to the stress due to the refracted wave.

$$\sigma_I(x,t) + \sigma_R(x,t) = \sigma_T(x,t) \quad (7)$$

From that the relationship between the amplitudes of the incident, reflected and refracted seismic waves can be written as follows.

$x = 0$ at the interface where the wave reflection and refraction happen.

$$A_I(0,t) + A_R(0,t) = A_T(0,t) \quad (8)$$

$$\sigma_I(0,t) + \sigma_R(0,t) = \sigma_T \quad (9)$$

Here the incident (A_I), reflected (A_R) and transmitted (A_T) wave amplitudes can be written in the form of the impedance of those two materials.

$$A_r = \frac{z_1 - z_2}{z_1 + z_2} A_i \; and \; A_t = \frac{2z_1}{z_1 + z_2} A_i \quad (10)$$

It is also written in terms of impedance ratio $\alpha_z = \frac{z_2}{z_1}$,

$$A_r = \frac{1-\alpha_z}{1+\alpha_z} A_i \; and \; A_t = \frac{2}{1+\alpha_z} A_i \tag{11}$$

Similarly, the stress amplitude as follows,

$$\sigma_r = \frac{\alpha_z - 1}{1+\alpha_z} \sigma_i \; and \; \sigma_t = \frac{2\alpha_z}{1+\alpha_z} \sigma_i \tag{12}$$

Depending on the properties of soil layers, the impedance ratio also varies from layer to layer, and in homogeneous soil deposits the impedance ratio between the soil-rock is critical in how wave propagation progresses. If the wave approaches to the softer layer, then the impedance ratio will be lesser than 1. Otherwise, if the wave entering the stiffer layer then the impedance ratio will be greater than 1. Large variation in material properties leads to high impedance contrast that changes the fundamental characteristic of wave. Large contrast in seismic impedance between adjacent layers leads large amplifications or attenuation depend on the direction of wave approach (Tucket & Kind 1984; King & Tucker 1984).

Doubling effect of amplitude at the free surface also due to the impedance contrast. The impedance ratio of free surface is zero because the impedance of air is negligible compared to that of the soil layer. As a result, the transmitted displacement becomes two times the incident wave $A_t = 2A_i$ and the transmitted stress will be zero at the free surface. The reflected stress wave will be equal to the incident wave but with negative polarity, $\sigma_r = -\sigma_i$. If the impedance ratio is infinite, then it is considered as fixed boundary. Fixed boundary will not have any displacement. So, by satisfying the compatibility of displacements, the incident wave is completely reflected with the same amplitude as incident wave and negative polarity, $A_r = -A_i$. Here the stress amplitude of the

transmitted wave is twice the stress of incident wave, $\sigma_t = 2\sigma_i$ If the impedance ratio equals to 1, then there will not be any reflection and completely the incident wave energy will get transmitted without a change in polarity and amplitude.

As it is evident from the above discussion, impedance contrast plays a key role in seismic energy transmission across interfaces. Upon reaching the ground surface, the seismic wave will be fully reflected back downwards. At sites with high soil-bedrock impedance ratio, a significant portion of this downward travelling wave would be reflected back at the bedrock. This causes the "wave trapping" phenomenon where the soil deposited will subjected to elongated seismic motion due to repeated reflections of the earthquake waves between the ground surface and bedrock. If the soil-bedrock impedance is relatively small a large part of the energy of the downward propagating wave would be dissipated into the bedrock, which can be considered as an effective form of damping.

2.4 CURRENT DESIGN APPROACH

National Building Code of Canada (NBCC) proposed significant changes to its seismic design guidelines in its 2005 edition. These changes follow the National Earthquake Hazard Reduction Program (NEHRP) of United States but with some modifications (Finn and Whitman, 2003). The seismic provision in NBCC 2005 were then revised in 2010, and 2015 which is the latest version currently being practiced. The release of the updated 2020 edition of the building code has been delayed due to the covid pandemic. Recommendations given by the National Building Code of Canada (2015) for earthquake analysis considers the shear wave velocity in the first 30m ($V_{s,30}$) to the determine ground shaking level and ground response analysis. Peak ground acceleration (PGA), peak ground

velocity (PGV) and 5% damped spectral response acceleration values $S_s(T)$ are provided in NBCC for the reference site class C at different locations across the country. The seismic site class is determined according to the average shear wave velocity based $V_{s,30}$ and site-specific design spectral acceleration is obtained by interpolating the intermediate values of T and peak ground acceleration (PGA) of the reference site class C. These seismic classification system and amplification factors are defined by considering the impedance contrast of underlaying geotechnical material of upper 30m. In addition to time weighted average shear wave velocity ($V_{s,30}$), the site classification also correlates with the thickness weighted average standard penetration resistance or blow count (N_{60}) or thickness weighted average un-drained shear strength (S_u) as shown in Figure 2-9.

Site Class	Ground Profile Name	Average Properties in top 30m, as per Note A-4.1.8.4.(3) and Table 4.1.8.4.-A		
		Average Shear Wave Velocity, $\bar{V}_{s30}$, m/s	Average Standard Penetration Resistance, $\bar{N}_{60}$	Soil Undrained Shear Strength, S_u
A	Hard *rock* (1)(2)	$\bar{V}_{s30}$>1500	n/a	n/a
B	*Rock* (1)	760<$\bar{V}_{s30}$<1500	n/a	n/a
C	Very dense soil and soft rock	360<$\bar{V}_{s30}$<760	$\bar{N}_{60}$>50	S_u>100 kPa
D	Stiff soil	180<$\bar{V}_{s30}$<360	15 <$\bar{N}_{60}$< 50	50 kPa <S_u<100 kPa
E	Soft *soil*	$\bar{V}_{s30}$<180	$\bar{N}_{60}$ < 15	
		Any Profile more than 3m of soil with the following characteristics: • plasticity Index: PI >20 • moisture content: w≥40%, and • undrained shear strength: s_u<25 kPa		
F	Other *soils* (3)	Site-specific evaluation required		

(1) Site Classes A and B, hard rock and *rock*, are not to be used if there is more than 3m of softer materials between the *rock* and the underside of footing or mat *foundations*. The appropriate site class for such classes is determined on the basis of the average properties of the total thickness of the softer materials (see note A-4.1.8.4. (3) and Table 4.1.8.4.-A).

(2) Where $\bar{V}_{s30}$ has been measured in-situ, the F(T) values for Site Class A derived from Tables 4.1.8.4.-B to 4.1.8.4.-G are permitted to be multiplied by the factor 0.04 + $(1500/\bar{V}_{s30})^{1/2}$.

(3) Other *soils* includes:

(a) Liquefiable *soils*, quick and highly sensitive clays, collapsible weakly cemented soils, and other soils susceptible to failure or collapse under seismic loading,

(b) Peat and/or highly organic clays greater than 3 m in thickness,

(c) Highly plastic clays (PI>75) more than 8m thick, and

(d) Soft to medium stiff clays more than 30m thick.

Figure 2-9: Site Classification for seismic site response defined in NBCC-2015

According to NBCC 2015, the primary consideration of seismic site classification is based on average shear wave velocity of upper 30m layer of soil. The nonlinear soil/bedrock profile or the type of the soil below 30m from the ground level are not taken into consideration in the classification and the calculation of design spectra. But, sites like Orleans valley area have deep soil deposits with varying properties, and particularly the bedrock basin is concave with a narrow valley type of soil deposit at the middle. Such sites require site specific assessment because the general guidelines of assuming flat bedrock profile is not sufficient enough to address the seismic effect.

2.4.1 Numerical Site Response Analysis – Design Practice

Current seismic analysis practice generally relies on empirical formulations. Site specific analysis may be undertaken in important projects or in class F soils. Such analysis is typically based on the equivalent linear "SHAKE" analysis. Shake analysis assumes that earthquake shaking is caused by vertically propagating shear waves that comes through the bedrock formation beneath the soil deposit. Non-linear behavior of soil is captured through equivalent linear analysis based on the dynamic properties of shear modulus and damping ratio of soil. Maximum acceleration, predominant period and effective duration are considered as most important influencing parameters for earthquake response in the Shake analysis.

Shake is based on one dimensional equivalent linear analysis in frequency domain, and the soil stratifications are assumed to be horizontal regardless of the actual geology of the local site. Horizontal layers are assumed to extend infinitely in both horizontal directions and

the base is modeled as a semi-infinite half-space. This implies 1-D wave propagation in the vertical direction.

2.5 SUMMARY

Aspects related to seismic wave propagation and soil liquefaction are discussed in this chapter, and current design practice is summarized. The approximations made in the current design practice, whether design code based or numerical analysis based, may not be suitable in many sites. The research conducted in this study address some of the drawbacks in the current practice to assess whether those could lead to unsafe designs. In this research, a two-dimensional concave bedrock model of a soft clay basin will be created for the analysis of input earthquake motions to understand the dependence of seismic response on bedrock basin configurations, and whether the cyclic shear stresses induced under such conditions could be larger than those calculated using the conventional approach of horizontal stratification of soil and bedrock. The seismic shaking levels considered are compatible with the design spectral acceleration values proposed in the national building code of Canada (NBCC 2015). A 2-D finite difference code, FLAC, is used to run the analysis. This enables appropriate consideration of the basin geometry which is necessary to assess the effects of seismic wave refraction appropriately. Details of the modelling process with FLAC are discussed in the next chapter, followed by the results and discussion.

CHAPTER 3

MODELLING AND SEISMIC ANALYSIS IN FLAC

3.1 INTRODUCTION

Current practice evaluates seismic load effects on soil by assuming horizontal stratification of different layers including the bedrock-soil interface subjected to vertically incoming seismic waves. This leads to horizontal excitation since the interest is generally limited to vertically propagating shear waves. Given this approximation, wave propagation analysis is generally conducted using a "SHAKE" analysis (Seed et al., 1971), which considers one-dimensional wave propagation in soils using an equivalent linear model. While, two-dimensional equivalent linear analysis tools, such as FLUSH (Lysmer et al., 1971), have been proposed and available. But they are not commonly used by practicing engineers. The simplicity, and widespread experience have made 1D equivalent linear analysis method for seismic analysis in practice. The equivalent linear soil model and total stress analysis adopted in SHAKE are recognized as simplifying assumptions in SHAKE analysis. However, the effects of the implicit assumption of horizontal layering (inherent in the 1D model) have not received sufficient attention in the literature. Few researchers have considered the effects of basin-effects at a broader scale (Field E.H, 2000; Semblat et al., 2002) and the potential impacts on soil liquefaction are not well understood.

The main purpose of this research is to investigate the influence of the effects of local site geology in site specific analysis, and infer the implications of it on the potential for liquefaction in Leda clay sites. Excessive settlement or liquefaction potential is high for soft and loose soils, and the geology greatly influences the response of local sites during

earthquakes (Ohsaki, 1969; Seed, 1969). Liquefaction failure in the context of soft clayey soils is generally due to gradual softening and associated excessive deformation rather than the sudden deformation that is characteristic of loose sands on account of excess pore water pressure generation, and the associated effective stress reduction. A Leda clay site in the Orleans suburb of the city of Ottawa is studied to assess the implications of two-dimensional bedrock-soil interface on seismic amplification. The geology of the "Orleans valley" has been well characterized, and it is known to have a well-defined bedrock basin that consists of about 100m thick Leda clay at its center. The longest horizontal dimension of the valley is about 5km ("East-West"), and it is about 3km long "North-South" (Kaheshi Banab 2010). The bedrock is essentially outcropping at the edge of the valley. The soil deposit at the site has been classified into different layers, and approximated with soil parameters based on the data in the literature (Kaheshi Banab, 2010; Motazedian et al., 2011). The finite difference code FLAC (2D) was used to conduct the two-dimensional numerical analysis, and understand the effects of bedrock topography.

3.1.1 Site Model

FLAC 2D v8.0 (Itasca) finite difference analysis package is used for the 2-dimensional model creation and analysis of the site subjected to vertically propagating shear waves. The curvature of the bedrock profile implies that the incoming shear waves make non-normal incidence at the bedrock-soil interface. As discussed previously, this leads to reflections and refractions of p- and s- waves. Hence the soil particles will undergo loading due to incremental shear and normal stresses, and will undergo complex loading paths depending on the relative magnitudes of the shear and normal stresses. For comparison purposes, the

analysis was also conducted for a similar hypothetical site with horizontally layered soil bedrock profile.

Two perpendicular cross sections, one along the short axis (section A-B herein) and another along the long axis (labelled section C-D) were modelled. The maximum depth of the soil deposit was 94m, and a 6m thick bedrock was included in the model (for a total depth of 100m) to simplify the application of the incoming (vertically propagating) shear waves at the base. Thus, the actual 2D model was rectangular, and it captured the curvature of the bedrock-soil interface in each section. Section A-B stretches to about 4000m with the aspect ratio of 1:40, and section C-D stretches to 5550m with an aspect ratio of 1:50 approximately. The soil deposit was divided in to 12 layers including the top fill layer and the bottom alluvial deposit. A description of the methodology used by FLAC and details of the modelling approach are described in in the remainder of this chapter.

3.2 THE FLAC (FAST LAGRANGIAN ANALYSIS OF CONTINUA) PROGRAM

FLAC 2-dimensional finite difference program package is used for the modelling and analysis of geotechnical engineering problems. A 3-dimensional model would be more realistic and can be expected to capture all effects of the basin. However, it would significantly extend the run time[1] and thus was not considered practical nor essential. Current design practice uses simple 1-D formulation, and a 2-dimensional analysis is

[1] The time required for a FLAC run depends on the model size and complexity of the analysis, including the duration of the seismic shaking and frequency content of the input motion. The run-time for the FLAC 2D analysis conducted in this research varied from about six days to two weeks (depending on the cross section and input motion) using a 32-core 2.7GHz CPU with 512GB RAM running under Windows 2019. Due to time constraints, no attempts were made to conduct a sensitivity analysis or to assess the effects of different soil profiles.

expected to sufficiently good insights on the geological. The explicit formulation used by FLAC allows for the modelling of materials that have plastic flow following elastic behavior. The soil-bedrock model is created by specifying predefined grid sizes and nodes in order to form the different parts of the elements and their shapes. Since the objective herein was to assess the effect of non-normal incidence of incoming seismic waves and compare the response to typical SHAKE analysis the approach adopted was to simulate SHAKE analysis techniques as much as possible, except for the presumed horizontal bedrock-soil interface. Any compatible set of units can be used in FLAC, and the metric system of units has been used in this study.

3.2.1 2D Model Formulation

Dynamic soil properties of the model, estimated based on field data in the literature were provided as input to the program. For static analysis, the density, bulk modulus, shear modulus and shear wave velocity of each element have to be specified. Modulus reduction and damping ratio relationships with shear strain are specified for the specific soil type in order to capture the change in modulus and damping during the static and dynamic analysis. Soil-bedrock interface is created as two different types of layers, but without any interface elements. Modelling the soil-bedrock boundary with interface elements might improve the material behavior at the interface, but introduces many uncertainties due to the interface model, and the properties needed to implement the model. It is difficult to ascertain/predict whether using interface elements will lead to more accurate results in spite of it being a more complex model (which would lead to further extended run-times). It is noted that the use of interface elements may be preferred if the soil-bedrock interface is very steep, or

approaches vertical. The basin model in this research has 94m thick soil deposit but in a 4.0km (section A-B) or 5.5km (section C-D) wide site, and thus the soil-bedrock interface slopes are relatively mild (about 1V:5H or smaller. As a result, no interface elements are used in the model.

As a first step of the analysis, the gravitational acceleration is specified and a static analysis is performed in order to get an equilibrium state under gravity load. During the static analysis, the base boundary is specified as rigid by fixing it in both vertical and horizontal directions. Both sides of the boundary were restrained in horizontal direction to allow for vertical settlement freely under gravity load.

Following the initial static equilibrium, the water table is specified at the ground level to simulate the worst-case scenario in terms of effective stress, and the static equilibrium state was realized again to compute steady state ground water condition, and pore pressure distribution. The effective stresses within the soil mass are required to compute the cyclic stress ratio.

The objective of this study is to better understand the effects of basin geometry, and thus simplifying assumptions were made to avoid spending excessive time in coming up with exact soil properties as a function of depth. General trends due to the natural deposition process, and data from the literature were relied upon in estimating these parameters. The density and shear wave velocity of the soil and rock layers were obtained from the literature that specifically dealt with the same basin (Kaheshi Banab, 2010; Motazedian et al., 2011).

3.2.2 2-dimensional, plane strain, fully dynamic equivalent linear analysis.

FLAC analysis can be run two ways; equivalent linear analysis, and nonlinear analysis. Equivalent linear analysis (Idriss & Seed, 1968; Seed & Idriss, 1970; Kramer, 1996) is commonly used in earthquake engineering because of the difficulty of dealing with non-linear analysis as the material approaches failure. In the equivalent linear method, FLAC calculates the maximum shear stress in each zone using initial modulus, damping and applied stress history for each step. Dynamic parameters of shear modulus and damping ratios will be assumed at the beginning. At start, the strain values are low and the stress-strain relationship is linear. By performing the linear analysis for the applied stress history, it records the maximum shear strain and the shear strain history. From the shear strain history, equivalent harmonic effective shear strain will be calculated. Shear modulus and damping values will then be adjusted according to the computed effective shear strain, and the calculation repeated to estimate the shear strain history again. This loop will be repeated until the solution converges where the shear modulus and damping values from the effective shear strain become same as the values used for the estimation of shear strain within the tolerance level. However, the equivalent harmonic effective shear strain conversion may lead to unrealistic resonance on the system that may not happen in reality. FLAC solution process is based on the explicit finite difference scheme to solve full equations of motions. The masses are lumped to grid points from surrounding zones rather than using fictitious masses. More importantly the dynamic loading, boundary condition, wave transmission and mechanical damping are the four factors to be focused on the dynamic analysis. However, the outcome of the result required to be validated to show the accuracy of the FLAC 2-D dynamic model.

3.2.2.1 Dynamic multi-stepping

FLAC estimates the maximum time step required for convergence of the solution of a model in a given condition. The maximum time step will vary depending on the zone size and material stiffness. Even though major portions of the zones in a model can be run at significantly large time steps, a small portion will determine the critical time step which will extend the computation time. To resolve it, the FLAC uses the dynamic multistep option which estimates the local time step for each class of zones depending on its material stiffness and zone size and then transfers the information at an appropriate time (FLAC Manual, 2016).

3.2.2.2 Doubling effect of free surface

Boundary condition at the top of the model is defined as free surface. The free surface will double the amplitude of incoming waves and reflects them downwards. The doubling effect will influence up to a certain depth from the free surface. In order to have base grids vibrate freely to the applied stress field, the model has to have sufficient depth to avoid this effect has reaching the base of the model. The effect of increased amplitude of applied wave is observed within one-third to one-fourth (k factor) of the wave length associated with the dominant frequency. Although the real earthquake is made-up of many frequencies, the predominate range varies about 0.5~1Hz to about 15~20 Hz. The motion at frequencies less than 0.5 Hz and greater than 20Hz have little influence on earthquake shaking. The minimum frequency, f_{min} dominates on model depth, $d_{min} = k\frac{C_{s,min}}{f_{min}}$ where $C_{s,min}$ is the minimum shear wave velocity of the soil layer (FLAC Manual, 2016). For example, if the

shear wave velocity of top layer is 100 m/s and the frequency less than 0.5Hz considered as having no impact on response spectra, the minimum model depth should require at least $\frac{1}{4}\sim\frac{1}{3}$ of $\frac{C_{s,min}}{f_{min}} \rightarrow \frac{1}{4}\times\frac{100m/s}{0.5Hz}\, to\, \frac{1}{3}\times\frac{100m/s}{0.5Hz} \rightarrow 50m\sim67m$. The analysis conducted in this research uses a total model depth of 100m. Thus, the above conditions are being satisfied in order to apply desired stress field at the base.

3.2.2.3 Grid size determination

The largest grid size is recommended to be smaller than about 10% of the smallest wave length (FLAC Manual, 2016). The process discussed below to remove higher frequency from the margin of cut-off frequency is called filtering. Typically, 10~15Hz (or a maximum of 20Hz~25Hz) is the margin normally recommended for filtering. Frequencies above those values will not solicit much response from the soil or structure, since their strength is generally small and the soil will not be able to react to such a high rate of vibration. In addition, in order to analyze the model for high frequency (i.e., small wavelength), the grid size should be even smaller (less than 10% of the smallest wavelength) which would make the analysis even slower. So, for a relatively accurate wave propagation or the response in model the maximum zone size Δl is chosen to be 1 m. This satisfies the requirement that the grid size should be 10% of wave length associated with a higher frequency component of input wave (FLAC Manual, 2016). It should be noted that the 10% of wave length is a rough estimate. The intent of this is to allow the applied load to be properly felt by the zone. If the zone is bigger than the applied wave length, the zone will not get the complete effect due to applied stress wave.

3.2.2.4 Aspect ratio of zone

The grid points that are defined initially will deform during the analysis leading to grid distortion. Bad geometry error pops up if any of the grids overlap each other during the analysis. FLAC analysis will terminate if such overlap happens. FLAC manual recommends that the aspect ratio of each zone be 1:10 or less to improve the accuracy of the solution. In FLAC, zones are modelled as quadrilateral elements and divided into two triangular subzones. The area of each quadrilateral zone must have a positive value throughout the analysis and both triangular pairs of subzone areas that make up the zone should not be less than 20% of the total quadrilateral area. However, during an earthquake loading, it is normal to have large deformations, and chances of overlapping zones or distortion of zones from its original aspect ratio are high. Figure 3-1 shows examples of acceptable and problematic deformations. FLAC has an inbuilt automatic rezoning option in order to re-make the meshing by considering the deformed plastic boundary.

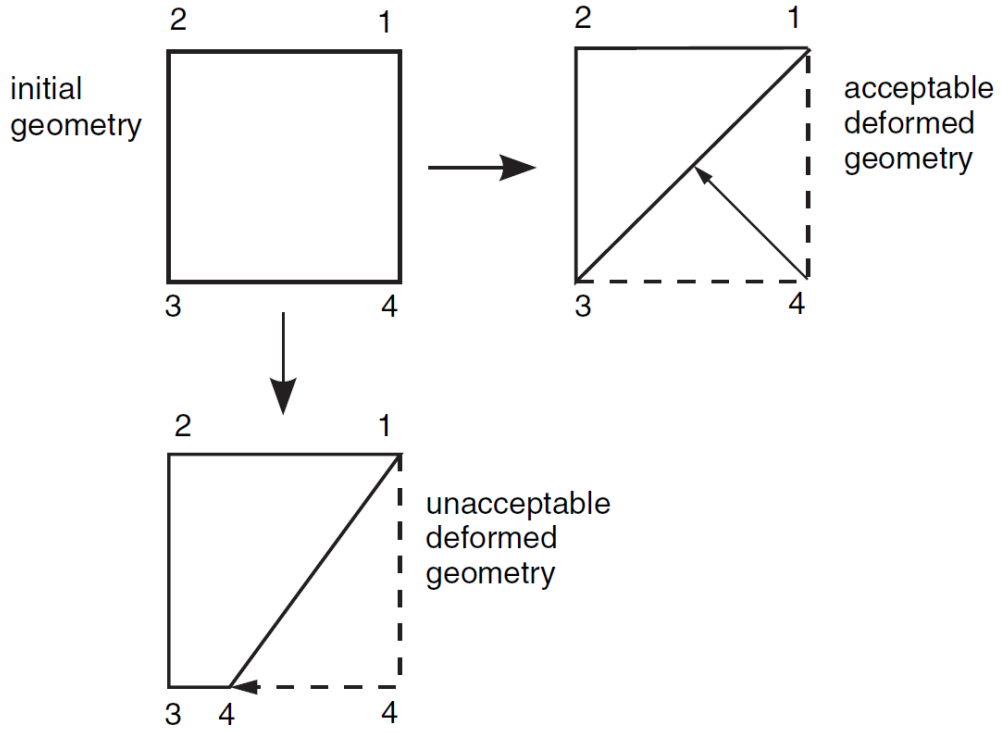

Figure 3-1: Acceptable and unacceptable zone deformation (from FLAC manual, 2016)

3.2.2.5 Automatic Rezoning

Earthquake loading may cause excessive deformation in the soil. FLAC numerical analysis accommodates large deformation. However, the zones have to meet a certain aspect ratio through the analysis. Large deformation causes distortion of zones and creates runtime "bad geometry" errors before converging to the solution. Refining the density of zones or remeshing in order to capture the physical change in the model due to large deformations is crucial in such numerical analysis (Borouchaki et al., 2005, Erhart, 2006; Han et al., 2008).

Rezoning is performed in three stages. First, the excessive deformation is identified in order to trigger the remeshing region. Secondly a new mesh is formulated in order to accommodate the physical deformation on the model. Thirdly the properties and stress parameters of old grid will be transferred to the new grid system (Peterson, 1998).

There are various methods of rezoning discussed in the literature such as mapping transformation, node insertion and connection and a regular grid overlay approach (Mackerle, 2001). In FLAC, zone mapping in volume and interpolation at a point remeshing method is used to reorganize the deformed zone and maintain the geometry within its aspect ratio. FLAC remeshing not only maintains the aspect ratio of the zone within limit, but also transfers the parameters of the old mesh such as stress, velocity and displacement to the new rezoned mesh with minimum loss in accuracy. It is performed by transferring those stress values to the overlaid subzone set in to the regular quadrilateral zone. The stresses corresponding to the new zones are calculated from the overlapping subzones against new subzones from the weighted average depends on the overlaps (FLAC Manual, 2016).

In FLAC, there are two ways of applying and measuring the model quantities. Material properties or stress components are specified as zone quantities within the finite volume, and kinematic quantities such as acceleration, velocity or displacements are specified as grid point quantities at the nodes.

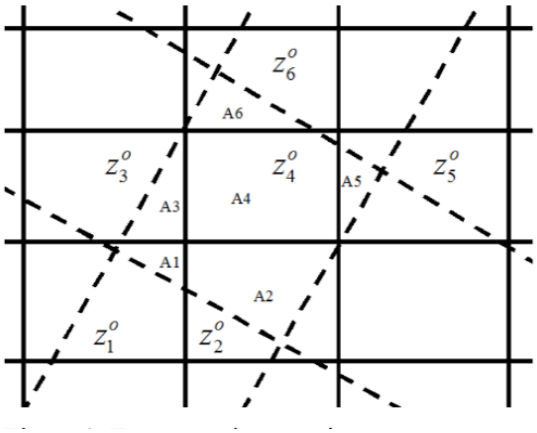

Figure 3-2: Zone quantity mapping (From FLAC Manual, 2016)

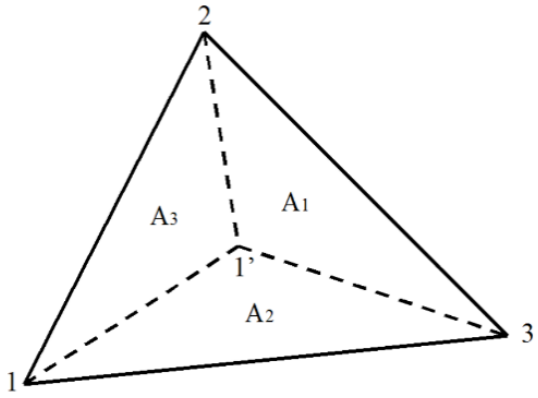

Figure 3-3: Grid-point quantity interpolation (From FLAC Manual, 2016)

Figure 3-2 and Figure 3-3 shows an example of mesh in solid line and re-meshed zones in dashed line. Upon distortion of zones due to excessive deformation, the zone quantities are averaged as follows,

$$z^N = \frac{\sum_{i=1}^{6} A_i z_i^0}{\sum_{i=1}^{6} A_i}$$

Where z^N is the value of continuous zone quantity in the new grid; z_i^0 is the value of zone quantity in the old grid; A_i is the overlapping area or the volume with unit thickness between old and new grid. Similarly, the grid point quantities are calculated with reference to the old grid points by interpolation from triangular subzones where the new grid points located among old grid points a follow.

$$g^N = \frac{A_1 g_1^0 + A_2 g_2^0 + A_3 g_3^0}{A_1 + A_2 + A_3}$$

Where g^N is the new grid point value; g_i^0 is the value of vertices of old grid point where the new grid points located in; A_i is the weighted area of subzone triangle depends on the overlaps (FLAC Manual, 2016).

3.2.3 Dynamic motion

In order to perform dynamic analysis, seismic motion history for dynamic loading conditions is specified. Depending on the type of earthquake motion record either outcrop motion or ground motion, deconvolution and scaling process may be required in order to convert the given motion history to bedrock acceleration time history. The deconvolution process can be done from 1-dimensional Shake equivalent linear analysis in order to get rock motion history. Artificial time histories generated to match the design spectra of the seismic site class A corresponding to the specific site, shall be directly used as input rock motion to the FLAC 2-D model. In the analysis of the Orleans valley profile, the artificial time histories are developed from response spectra of the seismic site class A (rock) and applied directly as input base rock motion.

3.2.3.1 Cut-off frequency and Filtering

The earthquake motion records are generally obtained in the form of acceleration history, and are typically sampled at 25 – 100 Hz. The input to FLAC is the velocity history which is obtained by integrating the acceleration time history. The process of converting the acceleration time history into the velocity history is preceded by filtering the frequency content and baseline correction. Filtering is done to remove those motion frequency components that have little to no influence on the seismic response. Typically, frequencies exceeding 10~15Hz do not affect the seismic response and the cut-off frequency is often set at 20 Hz. Including higher frequency motions do not improve the accuracy of the predictions but will significantly extend the run time.

3.2.3.2 Baseline correction

The baseline correction is the process to mitigate the systematic error caused by the fact that earthquake motion data will begin to record in the seismograph only upon triggering the threshold acceleration. Motions preceding the triggering stage will not be recorded and this may cause a compounding error in velocity and displacement increments. As a result, the displacement of the ground from the 2^{nd} integration of acceleration history will not be zero which exhibits residual displacement in the model even after the motion being stopped. This effect remains as an error unless corrected through bassline correction (FLAC Manual, 2016). Baseline correction is one of the important steps prior to applying the motion history to the model. Conceptually, at the end of an earthquake, the ground will rest at its original position and the displacement should be zero, unless there has been lateral movement. Residual displacement at the end of motion happens due to some other reasons

as well. Earthquake motion being recorded in a certain time interval Δt (0.02 sec) with the recording frequency of $\frac{1}{\Delta t}$ (50Hz). Motion in-between the recording time interval will get lost from the recorded motion history and this may also lead to residual displacement at the end of motion. In addition, the earthquake motion can be represented by a combination of various simple harmonic motions with different frequencies and amplitudes. Fourier spectra is the plot between those frequencies and amplitude. In Fourier spectra, after a certain frequency which is called as cut-off frequency, the amplitude becomes relatively small to contribute damage to soil deposit. So, the cut off frequency is used for numerical efficiency, and motion at frequencies higher than the cut-off frequencies will be eliminated. To correct it, the Fourier spectra or the set of frequencies and amplitude formed the motion history will be re-adjusted by adding low frequency wave to the original motion history in order to bring the final displacement to zero.

3.3 HYPERBOLIC MATERIAL MODEL

The true stress-strain behavior of soil is complicated, and it depends on various factors. A hyperbolic model is a convenient, and sufficiently simple, approximation of the soil response. Duncan & Chang (1970) originally proposed the hyperbolic model to characterize soil behavior. Duncan-Chan model addresses the nonlinear mechanical behavior of soil and captures stress state dependency, and modulus degradation. Duncan and Chang evaluated the stress-strain data in $\gamma/\tau \ vs \ \gamma$ space (Figure 3-4) to demonstrate that soil behavior can be approximated as hyperbolic (hyperbolic stress-strain curve would transform as a linear relationship in the modified space). However, the model does not represent the exact field conditions and is an approximation. Field geometry is incorporated

into the numerical model, and the analysis assumes soil behavior can be represented by a hyperbolic relationship. Modulus reduction and damping characteristics control the response in such analysis.

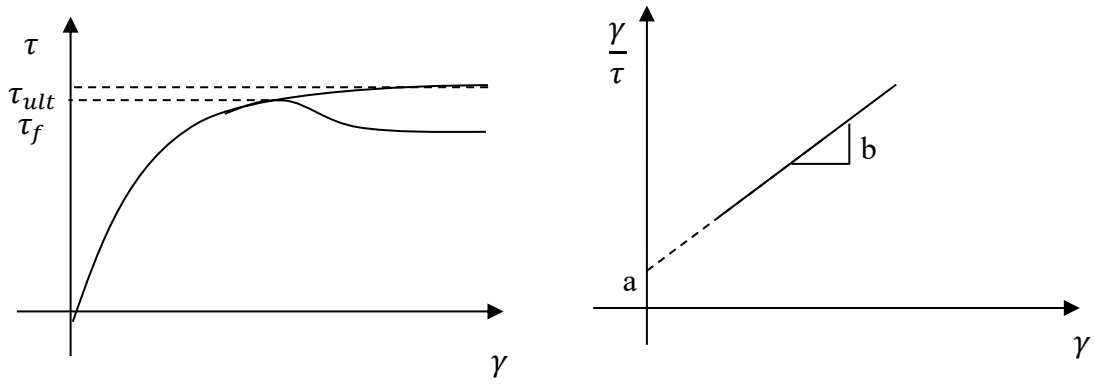

Figure 3-4: Relationship of shear stress vs shear strain (left); Relationship of shear strain/shear stress vs shear strain.

3.3.1 Modulus reduction

The nature of the stress-strain curve can be represented by the initial shear modulus (G_{max}) and the degradation of the modulus with strain. Shear modulus is the ratio between shear stress and shear strain, and may be defined at an instant (tangent modulus, G_t) or with respect to the initial state (secant modulus G_s). The secant modulus is used in numerical analysis to minimize numerical instabilities as soil reaches failure or when it strains softens. Given by $\tau = G_s\gamma$ by considering the limits of the relationship in the transformed space of $\gamma/\tau \ vs\ \gamma$, the following relationship can be derived.

Shear modulus is the ratio of between shear stress and shear strain and it is given by $\tau = G_s\gamma$. From the relationship of $\frac{\gamma}{\tau}\ and\ \gamma$, the following relationship is derived.

$$\frac{G}{G_{max}} = \frac{1}{1 + \frac{G_{max}}{\tau_{ult}}\gamma} = \frac{1}{1 + K\gamma}$$

Where K is the ratio between the maximum shear modulus and ultimate shear strength which is a constant for a selected soil type at a given initial state under ideal conditions. Modulus reduction ratio varies depending on the type of soil and its environmental loading conditions as shown in Table 3-1 (Kramer, 1996) is that modified from Dobry & Vucetic, 1987.

Table 3-1 : Variation of Modulus reduction ratio depends on type of soil and its environmental loading conditions (Kramer, 1996; modified after Dobry and Vucetic, 1987)

Increasing Factor	G/G_{max}
Confining Pressure, σ'_m	Increase with σ'_m; effect decrease with increasing PI
Void ratio, e	Increase with e
Geologic age, t_g	May increase with t_g
Cementation, c	May increase with c
Over consolidation ratio, OCR	Not affected
Plasticity Index, PI	Increase with PI
Cyclic Strain, γ_c	Decrease with γ_c
Strain rate, $\dot{\gamma}$	G increases with $\dot{\gamma}$ but G/G_{max}probably not affected if G and G_{max} are measure at same $\dot{\gamma}$.
Number of Loading Cycles, N	Decrease after N cycles of large γ_c(G_{max} measured before N cycles) for clays; for sands, can increase (under drained conditions) or decrease (under undrained conditions)

3.3.2 Damping

The shape of the modulus reduction curve alone captures the monotonic loading response. However, the damping characteristics are an important consideration under cyclic loading. Damping may be expressed in different forms, the simplest being the viscous damping where the damping force $F_D = C.\dot{x}$ leading to the commonly recognized Newton's second law equation $[M]\{\ddot{x}\} + [C]\{\dot{x}\} + [K]\{x\} = \{F(t)\}$. Damping characteristics are highly material dependent, and to some extent loading frequency dependent. Two forms of damping may be considered in numerical analysis.

3.3.2.1 Rayleigh Damping

Rayleigh damping is formulated with mass and frequency proportional parts and it is given by $C = \alpha M + \beta K$. Here α and β are mass proportional and stiffness proportional damping constants. Stiffness proportional damping influences the time step in FLAC calculation. Mass proportional damping reduces the time step in the calculation. For geological models, damping is in the range of 2% to 5 % of critical damping at small to moderate strains.

The critical damping ratio at any angular frequency of the system ω is expressed as $\xi = (\alpha/\omega + \beta\omega)/2$. In this formulation, $\xi_{min} = (\alpha\beta)^{\frac{1}{2}}$ and $\omega_{min} = (\alpha/\beta)^{\frac{1}{2}}$. $\beta = 0$ leads to $\xi = \frac{\alpha}{2\omega}$ (exponential relationship) and $\alpha = 0$ leads to $\xi = \frac{\beta\omega}{2}$ (linear relationship). Figure 3-5 shows normalized critical damping ratio vs angular frequency variations.

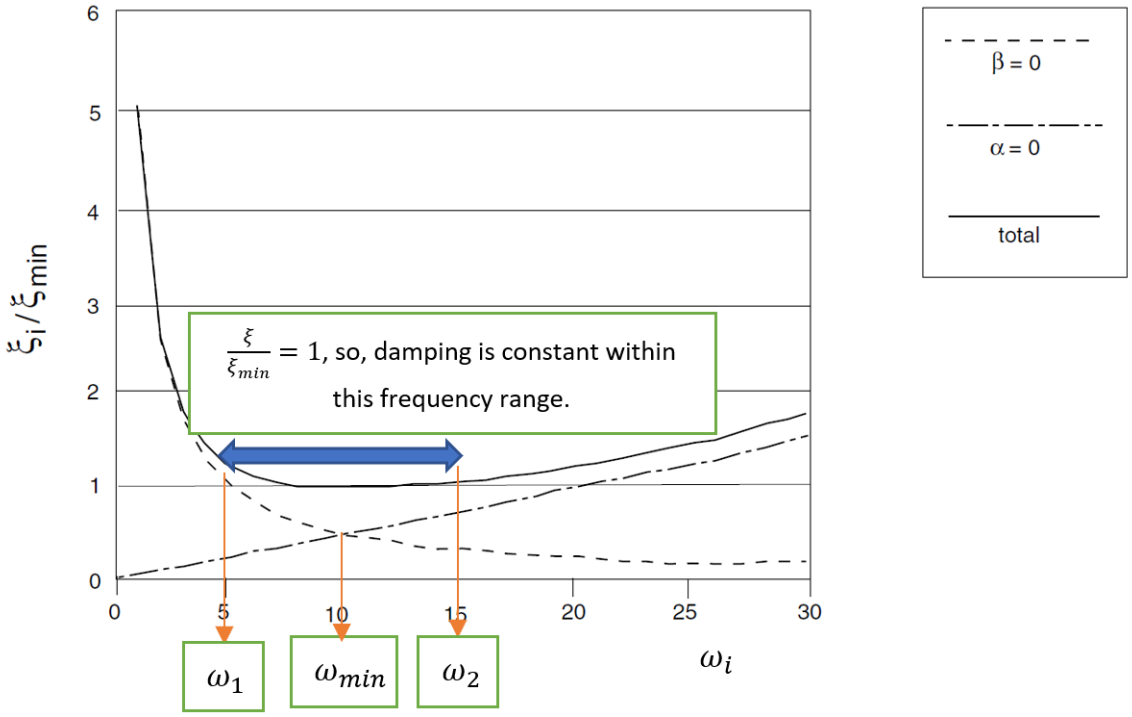

Figure 3-5: Variation of normalized critical damping ratio with angular frequency (FLAC Manual, 2016)

As shown in the Figure 3-5, cumulative damping from mass and frequency components is essentially a constant within the angular frequency range from $\omega_1 to\ \omega_2$ where $3\omega_1 = \omega_2$. For example, if $\omega_{min} = 10\ rad/s$, then $\omega_1 = \frac{10}{2} = 5\ rad/s$ and $\omega_2 = 3 \times \frac{10}{2} = 15$ rad/ s. So, the damping ratio is constant within the frequency range of $5\ rad/s\ to\ 15\ rad/s$. As mentioned above, the Rayleigh damping is frequency independent for a range of frequencies. If the highest predominant frequency (ω_2) is three times greater than lowest predominant frequency (ω_1) then, it will be within that 3:1 "frequency independent range" of spectrum. Rayleigh damping is defined in FLAC by specifying the minimum frequency $f_{min} = \omega_{min}/2\pi$ and will capture most of the important frequencies.

Predominant frequencies can be found to be the combined effort of input frequencies and the natural mode/frequency of the system. Minimum frequency can be found in a way that the maximum and minimum frequencies lie within the 3:1 range to get frequency independent damping ratio. To determine the predominant frequency, a preliminary run can be performed under undamped conditions and the predominant frequency can be found from the history of velocity or displacement (FLAC Manual, 2016).

However, defining the model with Raleigh damping may not be suitable for dynamic problems if the range of input frequency varies widely. Due to the frequency dependency and influence of time step in FLAC Rayleigh damping is not suitable for dynamic analysis because earthquake loading contains a wide range of frequency content. a hysteretic damping model is recommended for dynamic analysis in FLAC.

3.3.2.2 Hysteretic damping

Hysteretic damping is the strain dependent damping ratio and secant modulus function. In hysteretic damping, damping force is independent of frequency. So, the time step is not affected by hysteretic damping. Hysteretic damping is derived from S-shaped shear modulus reduction factor ($G/G_{\max}$) vs logarithm of cyclic strain curve represented by a cubic equation with zero slope at both low strain and high strain, and has the form, $M_s = s^2(3 - 2s)$. Here $s = \frac{L_2 - L}{L_2 - L_1}$ and $L = log_{10}(\gamma)$. L_1 and L_2 are the extreme values of logarithmic strain where tangent slope becomes zero. Hysteretic damping parameters L_1=-3 and L_2=1 means that the S-shaped curve will extend from a lower cyclic strain of 0.001% to and upper cyclic strain of 10%. Default values of L_1=-3.156 and L_2=1.904 produces a

curve that provide a reasonable match to the shear modulus reduction curve and damping ratio curve for clay material and values of L_1=-3.325 and L_2=0.823 match to the sand. For the rock, the values of L_1=-3 and L_2=3 gives a better matching as same as defined by Idriss, 1992.

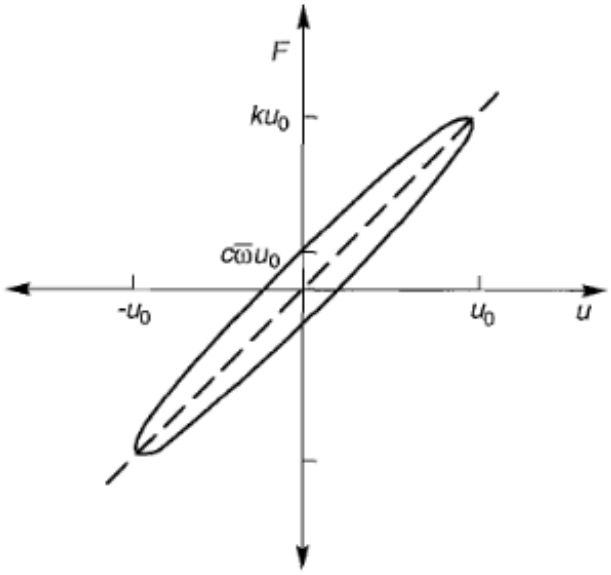

Figure 3-6: Force displacement hysteretic loop

The use of hysteretic damping is intended to account for the various ways of energy loss such as friction, heat generation, plastic yielding etc. All these are lumped together and represented by hysteretic damping to simplify the analysis. Integrating the force-displacement hysteresis loop (Figure 3-6) will give total energy dissipation of $W_D = \int_{t_0}^{t_0+2\pi/\omega} F.\frac{du}{dt}dt = \pi c\omega u^2$ and strain energy of $W_s = \frac{1}{2}ku^2$. From there the damping ratio $\xi = \frac{W_D}{4\pi W_s}$.

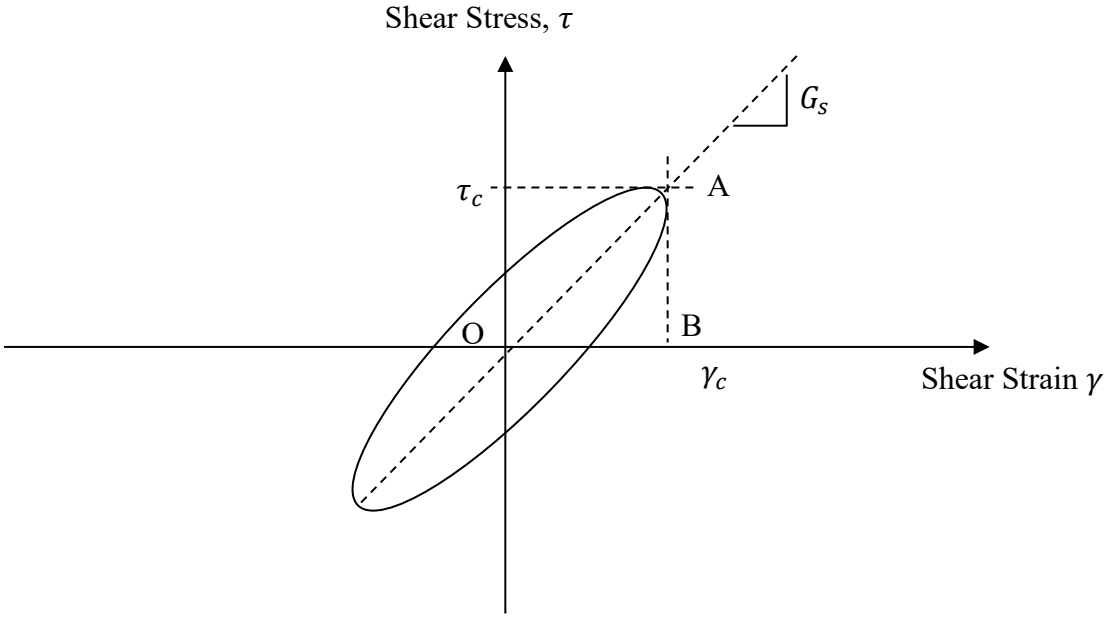

Figure 3-7: Shear stress vs Shear strain hysteretic loop

Damping is calculated from the area of the loop from cyclic shear stress vs cyclic shear strain graph shown in Figure 3-7.

$$\xi = \frac{1}{2\pi} . \frac{(A_{loop})}{G_s {\gamma_c}^2}$$

According to this equation for damping ratio, damping increases with increase in the area of the $\tau - \gamma$ loop (A_{loop}). In the other words, damping ratio increases with increasing shear strain. Variation of damping ratio depending on the type of soil and its environmental loading conditions as tabulated below (Kramer, 1996, modified from Dobry & Vucetic, 1987).

Table 3-2: Variation of damping ratio depends on type of soil and its environmental loading conditions (Kramer, 1996; modified after Dobry & Vucetic, 1987)

Increasing Factor	Damping ratio, ξ
Confining Pressure, σ'_m	Decreases with σ'_m; effect decrease with increasing PI
Void ratio, e	Decrease with e
Geologic age, t_g	Decrease with t_g
Cementation, c	May decrease with c
Over consolidation ratio, OCR	Not affected
Plasticity Index, PI	Decrease with PI
Cyclic Strain, γ_c	Increase with γ_c
Strain rate, $\dot{\gamma}$	Stay constant or may increase with $\dot{\gamma}$.
Number of Loading Cycles, N	Not significant for moderate γ_c and N.

3.3.3 Boundary conditions

It is critical to define appropriate boundary conditions in dynamic analysis to ensure the results are relevant to the real site. In reality, the site is located in an infinitely large soil medium. Defining the boundary as fixed may cause reflection of outward propagating waves back into the model. In reality, the boundary will not bounce back the entire wave in to the model unless the wave hits on a rigid surface or the soil layer have a higher impedance ratio. If the boundary is defined as rigid, then the outgoing waves bounce back and energy dissipation will not happen. Defining a large model may reduce the issue of

outgoing waves bouncing back in to the model back. But this will make the analysis more time consuming and complicated.

In addition, the predefined rigid base motion controls the motion of the base grids as a constant displacement boundary (FLAC Manual, 2016). So, the reflected waves reach at the base completely bouncing back into the model. Even though the impedance contrast between soil and rock is large in most cases, it's not infinitely large to define the boundary as rigid base. The rigid boundary condition in dynamic analysis will not represent the actual field conditions.

So, FLAC defines a compliant base (or quiet boundary) where the half of the energy is absorbed and radiates the other half energy back in to the model for equilibrium. It is a viscous boundary scheme developed by Lysmer & Kuhlemeyer (1969) where two sets of dashpots are attached independently to the mesh in the normal and shear directions to absorb energy. The stress absorbed by the dashpot is given by $\sigma_s = \rho C_s v_{su}$ where ρ-density, $C_s -$ shear wave velocity of the base material and $v_{su} -$ particle velocity of upward propagating motion in the shear direction. These viscous dashpots of the quiet boundary are defined at the base of the model to absorb the energy and prevent the downward propagating waves to reflect back in to the model.

In order to allow the base boundary to move freely, the acceleration history is converted into velocity history and applied as stress waves at the base with the factor of two in order to compensate for the absorbing viscous dashpots at the quiet boundary. So, the stress conversion from velocity history formed according to $\sigma_s = 2\rho C_s v_{su}$. This is the reason

the recorded acceleration history which is the superposition of upward and downward reflected motion will not match with the input acceleration record (Mejia & Dawson, 2016).

Sides of the model defined as a free field boundary. The side boundary grid motion should be independently moving during the wave propagation vertically. Free field condition ensures the independent motion of side boundary grids as well as non-reflecting behavior. To achieve this, viscous dashpots are attached (same as quiet boundary) and the unbalance forces transferred to the main grids. Also, these dashpots absorb energy only if the side boundary grid motion is different from the free field condition. This difference of side boundary motion may cause due to the presence of any structures or due to the radiation of waves from the surface. In addition, the free field condition ensures no distortion of wave energy in the side boundary and simulate the actual site condition in the model.

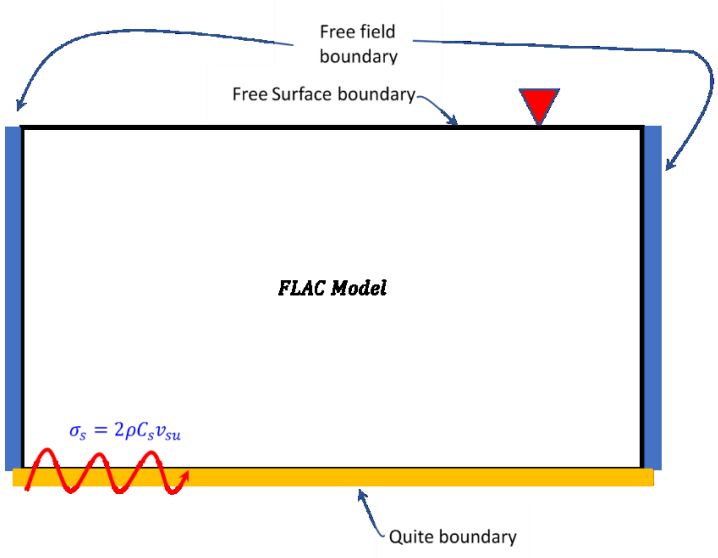

Figure 3-8: Schematic diagram of FLAC model showing boundary condition for dynamic analysis

Finally, the top surface is defined as free surface with no other boundary conditions attached. The upward propagating shear waves reflect completely back to the model with the 180° phase transformation (and doubled amplitude) in the real case. Figure 3-8 shows an illustration of the boundary conditions adopted to the FLAC 2-D model for seismic analysis.

3.4 EARTHQUAKE WAVES

Epicentral distance and the depth to the focal point of the earthquake are far away from the local site. So, the generated earthquake waves travel a long distance before reaching the local site, and as result will reach the local site bedrock soil interface vertically. This is due to the natural variation of soil properties and wave refraction through it. The incoming seismic wave approaches the local site vertically with an amplitude of E_n on rock as shown in Figure 3-9.

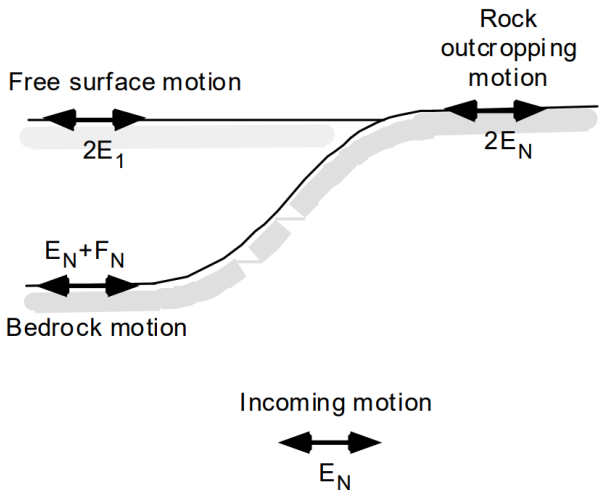

Figure 3-9: Amplitude of motions in different segments of model - image from Equivalent-linear Earthquake site Response Analysis, EERA manual of layered soil deposit (Bardet et al., 2000)

Earthquake motions may be recorded either on soil (ground surface) or rock outcrop. Free surface motion is the motion recorded at the ground surface after the wave passing through multiple layers. Soil layers naturally formed with various static and dynamic parameters and geological shapes where the incoming seismic wave amplitude E_n get modified as E_1 when it reaches to the ground surface. For the compatibility requirement of zero shear stress condition at the free surface, the amplitude doubles $(2E_1)$ due to the complete reflection and $180°$ phase shift at the ground surface.

Similarly, the amplitude will double at rock to comply with the zero-shear stress condition at free surface. So, the amplitude of the outcrop motion will have double of the amplitude of incident wave $2E_n$.

However, the bedrock motion below the soil not necessarily same as the incoming motion, E_n because the actual bedrock motion is going to be a result of superposition of both incoming (E_n) and reflected waves (F_n) that transmitted from above top layers. So, the amplitude of the bedrock motion becomes $(E_n + F_n)$.

In numerical analysis, the base model is limited with a certain depth. So, the reflected wave F_n gets doubled as at the top free surface. Also, the applied motion also doubles in order to comply with the zero-shear stress condition. So, the resultant amplitude becomes as $2(E_n + F_n)$ which is not same as the real case. This issue has been resolved by defining the base model as quiet boundary (also named as viscous boundary) where two viscous dashpots independently attached to absorb the half of the energy.

3.4.1 Artificial time history

Time history of earthquake shaking is a critical input in seismic analysis. Seismic analysis using artificially generated earthquake time histories are common (Atkinson & Beresner, 1998; Gangsig & Ohseop, 2016) because the real earthquake records are not always available for the selected site under the required seismic conditions. It is difficult to obtain real records at the base level corresponding to the target earthquake magnitude and epicentral distance. Even though deconvolution techniques are used to convert the ground motion in to bedrock motion, still there are uncertainty because of the static and dynamic properties used for each layer, and the magnitude and epicentral distance of the earthquakes.

However, National Building Code of Canada (NBCC) provisions on the seismic analysis provides a set of recommendations on the response spectrum with 2475-year return period for sites in Canada. These spectral acceleration values can be determined with respect to the seismic site classification of local site. Even though it is a complicated process, multiple combination of artificial time histories may be generated from the response spectra for the seismic analysis. In this numerical analysis, artificial time histories are generated from the design spectrum that follows the frequency range from 0.1Hz up to 20Hz (0.05s to 10s) as specified in NBCC2015.

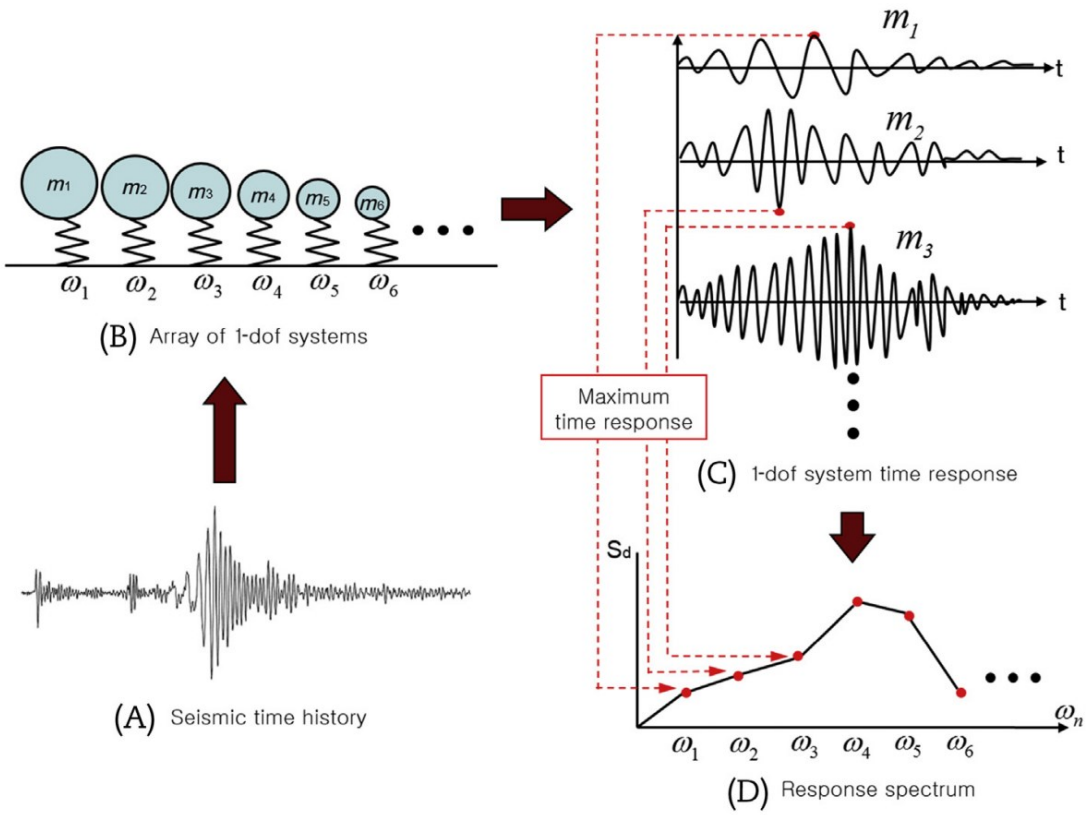

Figure 3-10: Basic concept of formulating response spectrum (Gangsig and Ohseop, 2016)

Deriving a response spectrum from time history is simple and straightforward. The theoretical maximum response of a series of a single degree of freedom (SDOF) system with different natural frequencies, plotted against the frequency of the SDOF system is defined as response spectra. But the backward calculation of obtaining a time history from a response spectrum is a complicated process. Unlike the single response spectra for a given time history, there are many time histories can be generated from a response spectrum. Software tools from the literature are used to generate spectrum compatible time histories that are input to the numerical analysis.

3.4.2 Seismic input to FLAC

Dynamic input motion can be given in one of four ways to the model: acceleration history, velocity history, stress (pressure) history or force history. Also, the input motion can be applied in the x-z direction to the model or normal-shear direction to the model boundary. In this model, the acceleration history is transformed to velocity history and converted as a stress field and applied at the base model. Directly applying the acceleration time history as input motion to the model will restrict the model boundary to vibrate according to the pre-defined way. But the quiet boundary must be able to move freely to absorb incoming waves in order to represent the actual field condition. This requires the acceleration-time history be transformed in to stress-time history and given as input stress field at the base model. The input stress-time history specifies the upward propagating wave motion into the FLAC model.

Lysmer and Kuhlemeyer (1969) expressed various possibilities to express an appropriate boundary condition analytically and came up with the expressions of normal and shear stresses.

$$\sigma_s = b\sigma C_s v_s$$

$$\sigma_n = a\rho C_n v_n$$

Here $\sigma_s$and σ_n are shear and normal stress, ρ is mass density, C_s and C_n are s and p wave propagation velocity through medium, v_s and v_n are input shear and normal particle velocity that comes from the earthquake motion by integrating the acceleration history, shear wave (S) velocity and primary (P) wave velocity of a medium can be calculated from its material properties of shear modulus G and bulk modulus K using the formula of $C_s =$

$\sqrt{G/\rho}$ and $C_p = \sqrt{\frac{K+4G/3}{\rho}}$. a and b are the dimensionless parameters that depend on the wave absorption or reflection at the boundary. For perfect absorbing or non-reflecting condition, a=b=1 (Georges et al., 2011). In this study, only vertically propagating shear wave is considered. There will not be any incident primary waves will be applied as input motion to the model. So, rest of the chapter only focus on the input shear stress on the model.

If the boundary condition where the stress history being applied (usually at the base of the model) is not defined as absorbing boundary, then the reflecting wave will get amplified due to doubling of its amplitude. In order to represent actual site response, the bottom boundary is modelled as a quiet (absorbing) boundary.

3.4.3 NBCC 2015 Classification of the site

Design spectrum $S(T)$ corresponding to local site classes are specified in the National building code of Canada (NBCC 2015). Volume 1 section B 4.1.8.4, classifies sites based on the average shear wave velocity $(\bar{V}_{s,30})$ in the top 30m below the foundation level.

$$V_{s,30} = \frac{\sum h_i}{\sum \frac{h_i}{v_i}}$$

In addition to shear wave velocity, corresponding average standard penetration resistance $(\bar{N}_{60})$ and soil undrained shear strength $(\bar{S}_u)$ may be used if shear wave velocity data are not available. The peak ground acceleration (PGA), peak ground Velocity (PGV) and the 5% damped spectral response acceleration values $S_a(T)$ are specified for the reference site class (Class C). Design spectral acceleration values $S(T)$ corresponding to periods T of 0.2

s, 0.5s, 1.0s, 2.0s, 5.0s and 10.0s will be determined as $F(T)S_a(T)$ based on the pre-defined peak ground acceleration (PGA) values and spectral acceleration for the selected site will determined through interpolation with respect to the peak ground accelerations (PGA). These recommendations are given based on a 2% probability of exceedance in 50-year period (2475-year return period).

For the Orleans Site, according to NBCC- 2015 Vo 1 Seismic Provision Division B 4.1.8.4,

$$V_{s,30} = \frac{\sum h_i}{\sum \frac{h_i}{v_i}} = \frac{30}{\frac{2}{130} + \frac{1}{100} + \frac{7}{103} + \frac{10}{110} + \frac{10}{118}} = 112\ m/s$$

From NBCC 2015 seismic provisions, table 4.1.8.4-A, the site classification for seismic site response for $V_{s,30} < 180\ m/s$ is site class E. Corresponding spectral values are estimated by interpolating those PGA values and reference site class spectral values as shown in Table 3-3 and Table 3-4 for both site class E and site class A respectively.

Table 3-3 : Estimated spectral amplitudes corresponding to site class E with reference to the site class C

Site: Ottawa (Orleans)			
Spectral Acceleration	S_a for Site Class C	F(T) for Site Class E	S_a for Site Class E
$S_a(0.2)$	0.474	1.045	0.495
$S_a(0.5)$	0.252	1.473	0.371
$S_a(1.0)$	0.124	1.732	0.215
$S_a(2.0)$	0.058	1.912	0.111
$S_a(5.0)$	0.015	2.133	0.032
$S_a(10.0)$	0.0056	1.995	0.011
PGA	0.304	0.974	0.296
PGV	0.208	1.473	0.306

Table 3-4: Estimated spectral amplitudes corresponding to site class A

Site: Ottawa (Orleans)			
Spectral Acceleration	S_a for Site Class C	F(T) for Site Class A	S_a for Site Class A
$S_a(0.2)$	0.474	0.69	0.327
$S_a(0.5)$	0.252	0.57	0.144
$S_a(1.0)$	0.124	0.57	0.071
$S_a(2.0)$	0.058	0.58	0.034
$S_a(5.0)$	0.015	0.61	0.0092
$S_a(10.0)$	0.0056	0.67	0.0038
PGA	0.304	0.9	0.274
PGV	0.208	0.62	0.129

3.4.4 Selection of Ground Motion

In addition to using artificial earthquake history generated from the design spectra prescribed by the building code, analysis using actual earthquake motions would add confidence in the assessment. Real earthquakes will contain actual variations of shaking intensities at different frequencies expected in the seismic motions at the site during an earthquake. But it is not always possible to get an appropriate recorded motion matching the magnitude and distance of the earthquake. So, the recorded earthquake motions also have to be scaled in order to match the expected spectra at the site; There are various methods of scaling an earthquake to match local sites, such as frequency domain methods and time domain methods (Farzad et al., 2004) in the literature. Both frequency domain and time domain spectral matching produce realistic acceleration records (Atik & Abrahamson, 2010) that enables the response spectra of input acceleration to match with the target response spectra generated from the seismic code of practice. Target response spectra formulated based on the probabilistic hazard analysis for a certain return period. NBCC recommends the target design spectra depending on the location and seismic soil class with 2% exceedance in 50 year which means the probability of occurring an earthquake is one in 2475 years.

3.4.4.1 Val-des-Bois Earthquake

Val des Bois earthquake is the strongest earthquake to hit the Ottawa region in almost 200 years. This earthquake occurred on June 23rd 2010 at 13:41 EDT and the magnitude was recorded as 5.0. The epicentre was located near the town of Val-des-Bois, about 55 km North-East of Ottawa. The earthquake was at 10km depth and the vibration traveled far

and felt by some cities near US border, and even in Kentucky. It lasted for 10 to 30 seconds depending on the site conditions, and caused damage to some properties, including the collapse of a Quebec Road, a bridge collapse on highway 307 near Bowman, another bridge collapse in highway 105 in Gracefield, two landslides, residential and commercial property damages. Power failure in the areas around the epicenter and an emergency call center in Gracefield for three days are some of the impacts that reflect the severity of the Val-des-Bois earthquake.

Ground shaking during Val-des-Bois earthquake has been recorded at many stations within Quebec, Eastern Ontario and beyond the US border. The bedrock motion (site class A) recorded at station code ST012 (Lat: 45.3942 and Lon: -75.7167), which is located at distance of 13.5 miles from Orleans Valley is the closest recording to the site considered in this analysis. Two components of this motion were selected and scaled to match the design response spectrum of the local site according to NBCC-2015. The scaled Val-des-Bois earthquake in both north-south and east-west motions applied to the model individually to see the response and compare against the artificial earthquake responses.

3.4.4.2 Scaling and Spectral Mapping

In the past, recorded time histories were scaled to match the peak ground acceleration alone without regard to the individual frequency components. Such scaling, while numerically simpler may not be a proper representation of the motions expected at the site. Generating the input acceleration from a real earthquake is performed in two steps in this study; amplitude scaling and spectral matching. Amplitude scaling is a time domain scaling method that is performed by factoring the actual earthquake motion data in order to match

the highest spectral amplitude (typically in the period range of 0.1s to 1s) of the input motion to the highest spectral value in the target design spectrum. This gives a spectrum with similar maximum amplitude, but without any correspondence to frequency content. The next stage of the spectral matching is done in the frequency domain by adjusting the frequency content of the motion history in order to align with target spectrum for a range of spectral periods with minimum variance. But the spectral mapping involves modification in the original frequency content in order to produce a perfect match of ground motion spectrum and design spectrum. However, the intensity of earthquake and its characteristics will be still retained as it is even after it scaled in frequency domain.

Each of these components represent a drawback in the recorded motions. Amplitude of acceleration varies with distance to the epicenter where the earthquake is originated. The scaling of amplitude in order to match with the target design spectra of the local site will represent an earthquake with a certain epicentral distance. Similarly, the frequency scaling of earthquake record can be justified in the basis of magnitude of earthquake. Larger magnitudes earthquakes contain relatively long period motions. The correction of the frequency content can thus be considered an accounting of the magnitude of the earthquake. Thus, the combination of both amplitude and frequency scaling of real earthquake in order to match with the target spectrum represent an earthquake with a certain epicentral distance and magnitude. The use of scaled real earthquakes by complying to target design spectrum through scaling enables the seismic analysis to expected to represent a more realistic loading scenario that captures the details of real earthquakes with inbuilt with natural variations.

Originally the spectral matching method was proposed by Lilhandand & Tseng (1987, 1988) where the time domain modifications made in time history to match the corresponding spectrum with the design spectrum. Further, it is developed by many researchers with computerized algorithm as optimization problem (Abrahamson, 1992; Hancock et al., 2006; Atik & Abrahamson [2010].

3.4.4.3 Period range of target spectra

The target spectrum of the real earthquake required to be satisfied the design spectrum over the range of period from T_{min} to T_{max} that result inelastic response of the structure (Tremblay et al., 2015). Lower limit of the period (T_{min}) represents the highest vibration mode that accommodates 90% of the structural mass in vibration or 20% of the fundamental period ($0.2T_1$) of the structure whichever is smaller. Upper limit of the period (T_{max}) defined as two times the fundamental period ($2T_1$) of the structure. But the upper limit should not be less than 1.5 sec period as the major part of the energy of any earthquake falls within that period. This range of upper and lower limit applicable for structures with natural period within 3~5 sec (Tremblay et al., 2015). Larger frequency ranges are covered in the analysis in the research conducted which satisfy the above requirements.

3.5 ANALYSIS AND INTERPRETATION OF SEISMIC RESPONSE

FLAC analysis is validated by comparing the response acceleration recorded at the ground surface in both FLAC 2D and the widely used equivalent linear "SHAKE" analysis. A model with a horizontal layer is created and its response under in FLAC and SHAKE are

compared. The SHAKE implementation used in the study is the commercially available software ProSHAKE.

Response spectrum is the widely used plot to compare the earthquake motions in frequency domain. Response spectrum directly illustrates not only the amount of amplification but also the dominant frequencies of the soil deposit. Upon validating the FLAC model, the results obtained from nonlinear profile will be analyzed based on the response stresses and accelerations. Cyclic stress ratio (CSR) simply represents the severity of earthquake and the potential for liquefaction or large deformations.

3.5.1 Spectral ratio method

The intensity of earthquake shaking at different locations within the soil deposit is obtained from the analysis. This is an indicator of the acceleration, and the resulting stress increments at the specific location. The relative magnitude of this "load" with respect to the "capacity" of the soil at that location will determine whether there will be failure. Even if there will be no failure, it is of interest to identify the influence of motions at different frequencies and how much they amplified (or attenuated).

Amplification of motion at specific periods is evaluated using the spectral ratio method. It's a frequency dependent method of evaluating the amplification of seismic motion in soil layers, and is defined as the ratio of the spectral ordinate at a given period to that on the input motion at the same period. Soft sites have larger amplification with respect to the bedrock motion at long periods, and stiff sites at short periods. Spectral amplification method also illustrates the dominant frequency that corresponds to the largest amplification.

Soil deposit undergoes complex loading path because of the wide range of frequency contents in the incoming seismic waves. These various combinations of frequencies with corresponding amplitudes composes the seismic wave in the time domain. The response of soil layers is sensitive to input frequency since larger motions are triggered when the frequency of the incoming wave matches the natural frequency of the soil. Considering the soil deposit as a whole structure, the dominant frequency in the earthquake motion results higher amplification when the seismic wave approaches to ground surface. So, rather than analyzing the earthquake in the time domain, the frequency domain analysis is a simplest way of representing the seismic amplification corresponds to the frequency content. Spectral characteristics are the best and preferred method of analyzing the response of seismic amplification and the intensity of shaking rather than considering accelerations (Housner, 1965).

3.5.1.1 Dominant Ground Period

Dominant ground period associated with the particular site is defined in the spectral amplification plot. Dominant ground period is the component of the earthquake motion that is amplified the most at the particular site. The response spectrum is a combination of responses of a set of single degree of freedom systems with a wide set of frequencies. Natural frequency of a single degree of system that matches with the dominant frequency will get higher resonance for the given earthquake motion. The dominant frequency component not only depends on the natural frequency of the soil deposit but also the amplitude of incoming seismic wave on that particular frequency. Combined effect of both frequency component and amplitudes triggers the soil deposit in different levels depending

on its properties. Mostly the dominant frequency or the period will be very close to the natural frequency of the entire soil deposit. So, the predominant frequencies are the associated with the individual subsoil structure (Kanai et al., 1966) and thus the geology of the subsoil will significantly change not only the amplification but also the predominant frequency corresponds to the higher amplification.

3.5.1.2 Natural frequency of soil deposit

Homogeneous planer soil layer with depth of H and shear wave velocity of v_s will have the nth frequency of $\omega_n = \frac{v_s(\pi/2 + n\pi)}{H}$ and the nth period of $T_n = \left(\frac{1}{1+2n}\right)\frac{4H}{v_s}$ (Kramer, 1996). The fundamental period will be at $n = 0$ and its value will be $T_0 = \frac{4H}{v_s}$. The highest amplification of an incoming earthquake motion will happen towards the fundamental period. This fundamental period can be approximated from the representative shear wave velocity of entire soil deposit. However, the amplitude of other higher order frequency components may also play an important role in amplification. Mostly, relatively higher amplitude frequency component adjacent to the fundamental period of the soil deposit will get amplified during the earthquake motion.

3.5.2 Shake Analysis

Shake analysis is a widely used one dimensional seismic analysis tool (Schnabel et al., 1972) to evaluate the local site effects. The 1-D analysis model implies that soil layers are horizontal and seismic waves propagate vertically. Non-linear soil behavior is incorporated using a modulus reduction curve, and there is an abundance of information in the literature

about this method. Shake has implemented the wave propagation solutions proposed by Kanai (1951), Roesset & Whitman (1969) and Tsai & Housner (1970) and modified it for use in personal computers. A Microsoft windows version, commercially available under the name ProShake, which is widely used by geotechnical designers and researchers around the world, is used in this study.

Shake analysis requires the earthquake motion (time history) as an input. The local site is represented as layers of soil, and the unit weight, the initial shear modulus and damping, and modulus reduction and damping curves as function of strains are prescribed for each layer. The values of density (ρ), maximum shear modulus (G_{max}), modulus reduction G/G_{max} and damping ratio (ξ) for each layer for the selected site are obtained from the literature. Generated artificial time histories from the design spectra for the Orleans site region is given as input and the results are analysed in the frequency domain.

CHAPTER 4

ANALYSIS AND RESULTS OF NUMERICAL WORKS

4.1 INTRODUCTION

A numerical study was carried out to assess the effects of 2-dimensional soil profile on seismic amplification. Two cross sections of a site in the Orleans suburb of Ottawa were considered in the modelling process. FLAC 8.0 finite difference code (Itasca, 2019) was used and the effects of geology and bedrock inclination on seismic amplification, and maximum ground motions due to incoming NBCC 2015 compatible bedrock motions were evaluated.

The concave shaped rock profiles are modelled using regional bedrock type, and the soil deposit is divided in to several layers. The soil properties of the layers were modelled with a gradual variation with depth as reported in the literature (Motazedian & Hunter, 2014). Both recorded bedrock motions and artificially generated earthquake records were used to simulate input ground shaking. Recorded time histories were scaled to roughly match the anticipated target spectrum at the site, and the artificial ground shaking records were generated based on the NBCC 2015 design spectra. Artificial earthquake records were produced for site class A of rock and used directly as incoming motion at the base of the model.

The recorded motion was obtained from the earthquake record of the 2010 Val-des-Bois event in the same seismic zone, but adjusted for shaking intensity. The real earthquake records in two horizontal orthogonal directions (North-South and East-West) were collected from station OT012 which was the nearest station to the Orleans site at 13.5 miles.

The raw records were scaled in order to roughly match the design spectrum of the Orleans site. As the OT012 station is located on rock, the scaled motion can directly be used as input to the model. The response of the model due to artificially generated spectra matching motions (NBCC 2015) is compared to scaled Val-des-Bois motions representing the design earthquake.

The characteristics of the seismic site response were evaluated and compared using the maximum horizontal acceleration, maximum shear stress and the cyclic stress ratio (CSR) of selected elements at different depths. The cyclic stress ratio (CSR), in geotechnical practice, is defined as the ratio of maximum shear stress to the initial effective vertical stress if the loading is constant stress amplitude harmonic wave. The shear stresses vary with time during an earthquake, and a factor of 0.65 proposed by Seed & Idriss (1971) has been used to compute the CSR values from the time history. The proper value of the reduction factor is somewhat dependent on the earthquake, and varies between about 0.55 to 0.75. The value chosen is appropriate for the region, and since the purpose of this analysis is the comparison of bedrock geology it technically has no influence on the conclusions.

4.2 GEOLOGY OF THE ORLEANS VALLEY

The seismicity of Ottawa is influenced by the Western Quebec Seismic Zone. In terms of seismic risk, Ottawa is considered to be the third largest earthquake risk prone city in Canada following Vancouver and Montreal. This is based on earthquake hazard level and the population which would be affected due to an earthquake (Adams et al., 2002). Ottawa

area contains soft soil sediments underlain by Paleozoic sedimentary rock formation (Harrison & MacDonald, 1980).

The selected basin in the Orleans neighbourhood of Ottawa is approximately 5km long and 3.5km wide and its geographical location is shown in Figure 4-1 and Figure 4-2 shows a contour map of elevation in this region. It is a narrow valley with about 100m thick deposit of Leda clay. The entire valley is underlain by bedrock and the top 2m is assumed to be weather soils or backfill, and the bottom 4m, just above the bedrock, an alluvial deposit consistent with the typical geological profile of Ottawa. The Leda clay in between these two layers has been divided into 10 layers to properly represent the density and shear wave velocity changes. Both density and shear modulus gradually increase with depth in this material. Soil layering and soil parameters are assigned to match the regional soil properties typical of the Orleans region. The cross-sectional details of the 2-D profile of the valley along sections A-B and C-D, shown in Figure 4-3 (Khaheshi Banab 2010), were modelled in FLAC. As seen in Figure 4-3, section A-B has a fairly steep soil-bedrock interface slope, compared to section C-D.

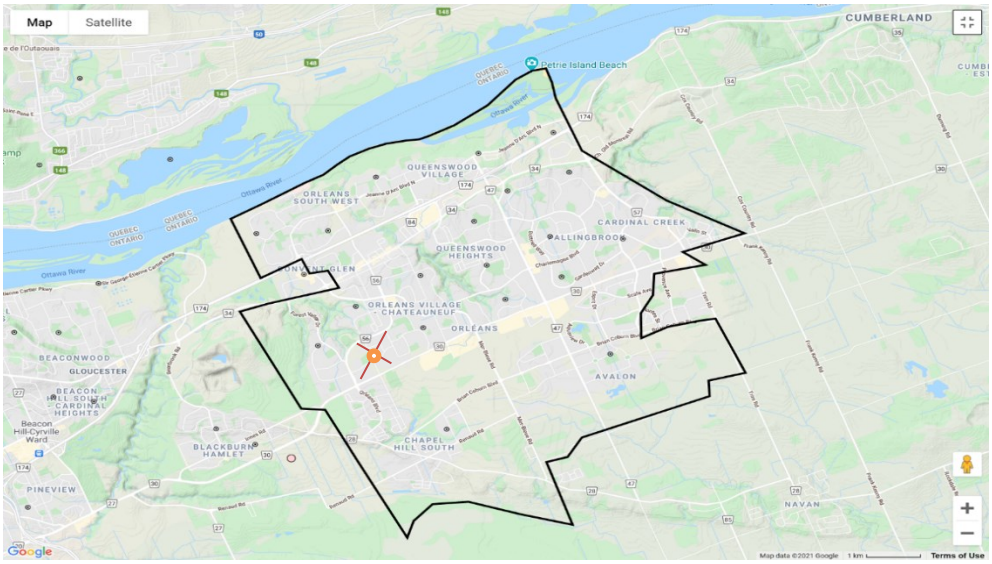

Figure 4-1: Location of Orleans, Ottawa (Google Image)

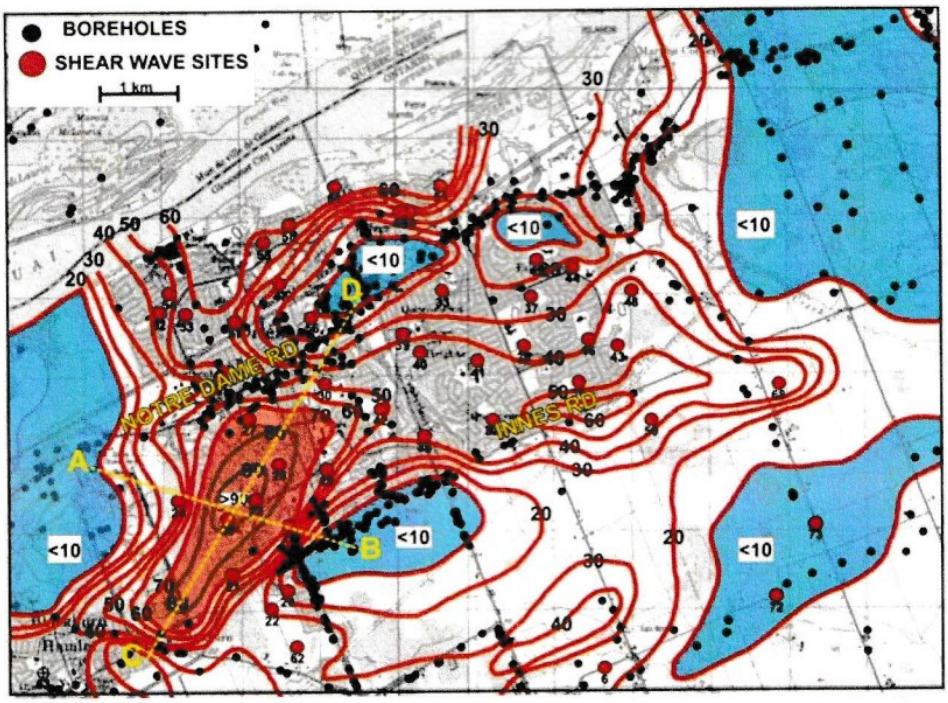

Figure 4-2: Plan view of the Orleans region showing the location of section A-B and C-D (after Kaheshi 2010)

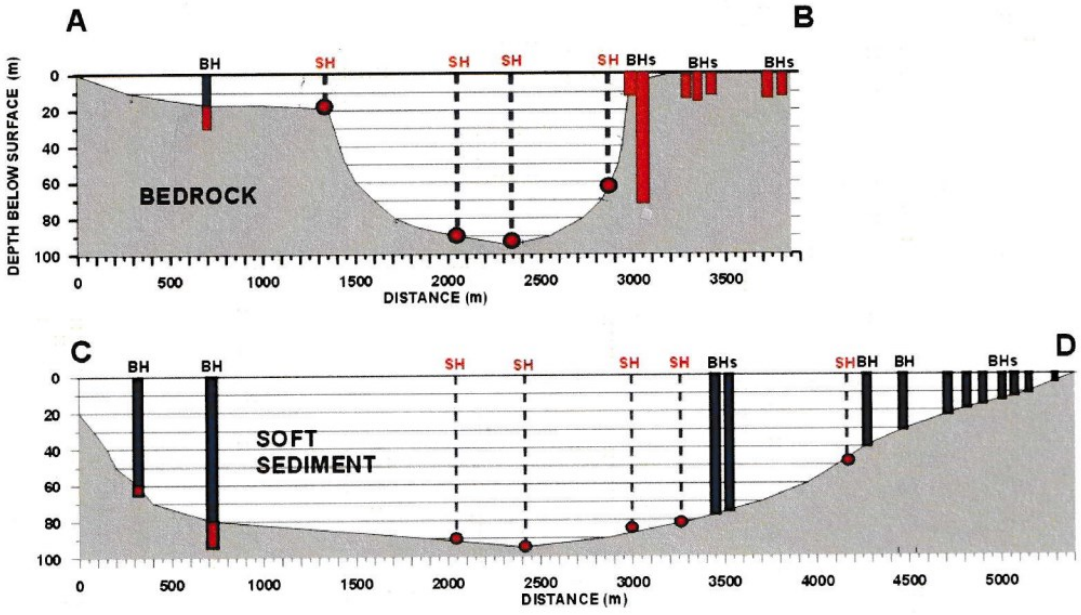

Figure 4-3: Transverse and longitudinal cross section of the Orleans valley with a vertical exaggeration of ~10:1 (after Kaheshi 2010)

4.2.1 Influence of geometry of rock during dynamic motion

Typically, site response analysis in practice is conducted by assuming a horizontal soil – bedrock interface subjected to vertically propagating seismic waves (which implies normal incidence). The geometry of the soil and rock layers influences wave reflection and refraction characteristics. Concave bedrock, such as the one in the Orléans profile, implies non-normal incidence at the soil-rock interface, and will focus wave refraction towards the center of the basin which may cause high amplifications at the center. In contrast, if the bedrock is convex shaped, then the refracted waves will spread over a wider range and the intensity of the shaking at the site will be relatively smaller.

4.2.2 Simultaneous propagation of compression and shear waves due to nonlinear profile

Prasanna & Sivathayalan (2021) demonstrated through numerical analysis that even a small deviation in the soil bedrock interface from the horizontal plane may lead to significant changes in the seismic shaking in the soil deposit. As explained in Chapter 2, this generally leads to non-normal incidence and the resulting particle motions along and perpendicular to the interface are responsible for this complexity (as opposed to particle movement along the interface only when the interface is horizontal and the wave propagation is vertical). The incoming seismic waves, and those reflected on the ground surface, or on the bedrock cause complex loading on the soil elements in both vertical and horizontal directions. Applied stress field would include both shear and normal stresses unlike the typically assumed scenario of shear loading only. The net increment of shear stresses is due to both

the effects of shear wave (changing the shear stress) as well as compressional waves (changing the normal stresses), and the maximum shear stress can be determined from a Mohr circle.

Initially the entire system is in static equilibrium under gravitational forces. The relative values of the horizontal and vertical stresses ($\sigma_x = \sigma_h;\ \sigma_z = \sigma_v$) depend on material properties, primarily the Poisson's ratio, which determines Ko. Under the initial equilibrium state, there will be zero shear stress on the horizontal x-y plane if the ground surface is horizontal. The maximum shear stress is half of the difference between the vertical and horizontal stresses in this case. If the ground surface is inclined and not horizontal, there will be an initial static shear stress on the horizontal plane. Similarly, static shear stresses can be present on the horizontal plane if the soil layers are inclined and have different material properties (unit weight, K_o). Stresses due to compressional and shear waves are superimposed onto this initial condition during an earthquake. As a result, the particles may start rolling.

This rolling or Raleigh wave effect can increase the normal and shear stresses in two ways with components $\Delta\tau_{xz,S}$ (s-wave induced) and $\Delta\tau_{xz,P}$ (p-wave induced). Similarly, the normal stress increments due to P and S waves on the vertical and horizontal normal stresses can be represented by ($\Delta\sigma_z,\ \Delta\sigma_x$), where $\Delta\sigma_z = (\Delta\sigma_{z,S} + \Delta\sigma_{z,P})$ and $\Delta\sigma_x = (\Delta\sigma_{x,S} + \Delta\sigma_{x,P})$. Since seismic shaking is time dependent, the principal stress and its direction will continuously rotate depending on the initial stresses and the magnitude of vertical and horizontal normal and shear stress increments.

The variation of local site geology highly impacts the horizontal motion compared to the vertical motion (Borchert, 1970). Horizontal motions cause extensive damage to both soil

deposit as well as structures above. This research study focusses on the actual shear stress increment in the horizontal x-z plane caused by the wave reflection and refraction due to the non-linearity in the soil bedrock profile. So, the increase in shear stress $\Delta\tau_{xz}$ due to the excitation of particles in the x-z plane which due to both shear waves $\Delta\tau_{xz,S}$ and compressional wave $\Delta\tau_{xz,P}$ in the x-z plane will be considered for the analysis. This combined effect of shear and compressional wave on the shear stress magnitude in x-z plane is expected to vary considerably compared to the simpler horizontally layered soil model.

Considering the Mohr circle at static equilibrium

$$\sigma_{1,3} = \left(\frac{\sigma_x + \sigma_z}{2}\right) \pm \sqrt{\left(\frac{\sigma_x - \sigma_z}{2}\right)^2 + {\tau_{xz}}^2}$$

$$\tau_{max} = \sqrt{\left(\frac{\sigma_x - \sigma_z}{2}\right)^2 + {\tau_{xz}}^2}$$

If the soil layers are assumed to be perfectly horizontal, then $\tau_{xy} = 0$, $\sigma_1 = \sigma_z$ and $\sigma_3 = \sigma_x$ and $\tau_{max} = (\sigma_v - \sigma_h)/2$.

As shown in Figure 4-4 Mohr circle, additional stresses are superimposed during cyclic loading, and due to shear waves, $\tau_{xz} \rightarrow \tau_{xz} \pm \Delta\tau_{xz}$ and due to compressional waves $\sigma_x \rightarrow \sigma_x \pm \Delta\sigma_x$ and $\sigma_z \rightarrow \sigma_z \pm \Delta\sigma_z$.

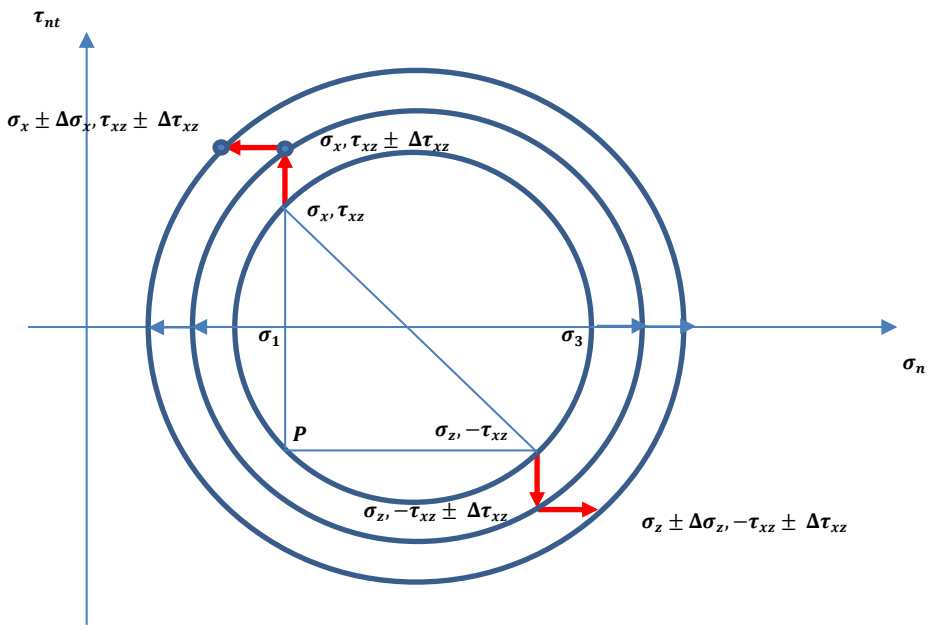

Figure 4-4: Representation of stress increment on Mohr circle

$$\sigma_{1,3} = \left(\frac{(\sigma_x + \Delta\sigma_x) + (\sigma_z + \Delta\sigma_z)}{2}\right) \pm \sqrt{\left(\frac{(\sigma_x + \Delta\sigma_x) - (\sigma_z + \Delta\sigma_z)}{2}\right)^2 + (\tau_{xz} + \Delta\tau_{xz})^2}$$

$$\tau_{max} = \sqrt{\left(\frac{(\sigma_x + \Delta\sigma_x) - (\sigma_z + \Delta\sigma_z)}{2}\right)^2 + (\tau_{xz} + \Delta\tau_{xz})^2}$$

4.2.3 Site amplification

Site amplification of seismic motion depends on many factors: the mechanical properties of soil and rock and the intensity and frequency components of input motion. Impedance contrast between two layers cause to amplification or attenuation of the incoming waves. Density and shear wave velocity of the rock/soil influences the amount of shear wave reflection or refraction depending on the impedance ratio, $z = (\rho v)_{rock}/(\rho v)_{soil}$, which

is often called the impedance contrast. Generally, the factor ρv is higher for rock compared to soil. So, most of the incoming earthquake shaking will refract into the soil layers. But the waves reflected at a hard soil layer or the ground surface will travel through soil downwards and reach the soil-rock interface. If the impedance ratio between rock and soil is high, then the reflection of the downward propagating wave at the soil-rock also will be high. This is normally referred to as the wave trapping phenomenon within soil layers. If the impedance contrast is not high, the rock will also absorb the energy due to wave refraction into the rock, which helps to attenuate the motion. If the peak acceleration of the rock motions is higher than a saturation point then the soil will not amplify or respond to the motion in proportion. This may cause peak soil acceleration to be lesser than the rock. If the seismic wave travels through a stiff layer to a soft layer, the wave gets amplified and the amount of amplification is proportional to the impedance contrast. The potential for resonance depending on the natural frequency of the soil layer with respect to the frequencies present in the earthquake wave will also decide on how the soil deposit would respond. Further, the characteristics of the material, such as non-linearity, elasto-plasticity, soil-rock interfaces would also influence the amplification (Bard & Bouchon 1980a, 1980b, 1985). Given these, the Orleans valley area is identified as a suitable location to study the effects of amplification. The impedance contrast in this region is quite high and the bedrock is shaped like a narrow valley with about 94m thick soft-clay at the middle.

4.3 MODEL INFORMATION

The Orleans Valley model is created as 2-dimensional concaved bedrock with soil deposit. The site characteristics are obtained from the literature. Previous site survey outcomes

indicate that the Orleans valley contains a fairly deep soft Leda clay deposit. The top two meters of the soil is fill materials with the shear wave velocity around 130 m/s and density 1500kg/m^3. Leda clay underlies the top soils, and has a shear wave velocity of 100m/s and density 1600 kg/m^3 at shallow layers; but both density and modulus increase, somewhat linearly, up to the bedrock level. Assuming a linear increment of both shear wave velocity (Motazedian & Hunter 2010) and density is justifiable because of the increased overburden pressure along with the depth. The shear wave velocity and density of bedrock are taken to be 2400 m/s and 2200 kg/m^3 respectively A thin layer of alluvial deposit is typical just above the bedrock layer, and its properties have been assumed to be Vs = 220 m/s and density 1800 kg/m^3. These values, summarized in Table 4-1, are consistent with the characteristics of reported for the Ottawa region. As the soil behavior would be undrained during earthquakes because of the rapid loading condition within a short duration due to seismic motion, the ground water table assumed to be at ground level to simulate the critical loading condition.

Table 4-1: Model properties: Variation of density and shear wave velocity

Depth	Soil Material	Shear wave velocity (m/s)	Density (kg/m3)
0~2	Top Soil: Fill Material	130	1500
2~3	Clay: Leda Clay 1	100	1600
3~90	Clay: Leda Clay 2	100 + 0.8(z-3)	$1600+\frac{[1800-1600]}{[90-3]}$(z-3)
90~Rock	Alluvial-Material: Dense	220	1800
Rock	Rock	2400	2200

In this study, 2-dimensional bedrock profile of two sections; section A-B and section C-D have been analyzed under the seismic loading condition. In addition to the actual site profile of both sections, a 2-dimensional model with a horizontal bedrock was also created. In the horizontal layer model, the bedrock assumed to be at same level as the lowest level of the valley deposit, and these results were used as the baseline representing current practice. Section C-D was modelled with a 5.5km wide grid, and A-B modelled with a 4km wide grid. The horizontal bed-rock model extended to the width of the section C-D model. In the all three cases, the same soil properties were assigned as a function of depth in order to visualize the influence of geological variation in soil rock interface. Table 4-2 summarizes the properties of the soil layers and the bedrock.

Table 4-2: Dimensional model layers and corresponding model input parameters of static and dynamic Properties of Orleans Valley

Table in FLAC	Material	Depth (m)	Density (kg/ m^3)		Shear Wave Velocity (m/s)		Shear Modulus (MPa)	Bulk Modulus (MPa)
Layer-1	Fill	0-2	_	1500	_	130	25	66
Layer-2	Leda Clay-1	2-3	_	1600	_	100	16	42
Layer-3	Leda Clay-2	3-10	1600+([1800-1600])/ ([90-3]) (z-3)	1608	100 + 0.8(z-3)	103	17	44
Layer-4	Leda Clay-3	10-20		1628		110	20	51
Layer-5	Leda Clay-4	20-30		1651		118	23	60
Layer-6	Leda Clay-5	30-40		1674		126	26	69
Layer-7	Leda Clay-6	40-50		1697		134	30	79
Layer-8	Leda Clay-7	50-60		1720		142	34	90
Layer-9	Leda Clay-8	60-70		1743		150	39	102
Layer-10	Leda Clay-9	70-80		1766		158	44	114
Layer-11	Leda Clay-10	80-90		1789		166	49	128
Layer-12	Alluvial Deposit	90-100	_	1800	_	220	87	227
Layer-13	Rock	>100	_	2200	_	2400	12,672	33,047

4.3.1 Section C-D model profile

Section C-D of the ground profile was characterized by 5550 meters long × 100 meters deep domain as shown in Figure 4-5. Further, extending the model boundaries laterally would normally be preferred to avoid boundary transition effects, but it would have increased the run time significantly, and required extrapolation of the bedrock profile data. Given the time constraints, a decision was made not to extend the boundaries any further. As noted previously, a damping boundary condition was used along the vertical edges to absorb the energy and avoid reflections, and it is considered an appropriate optimization. The soil rock interface is shaped concave down towards middle of the section where there is a narrow roughly flat bottom for a short span of about 500 meters. The slope of the concave profile has a fairly smooth boundary that gradually reaches the low point and again reach back to the ground surface. The rock outcrops on the right side of the model.

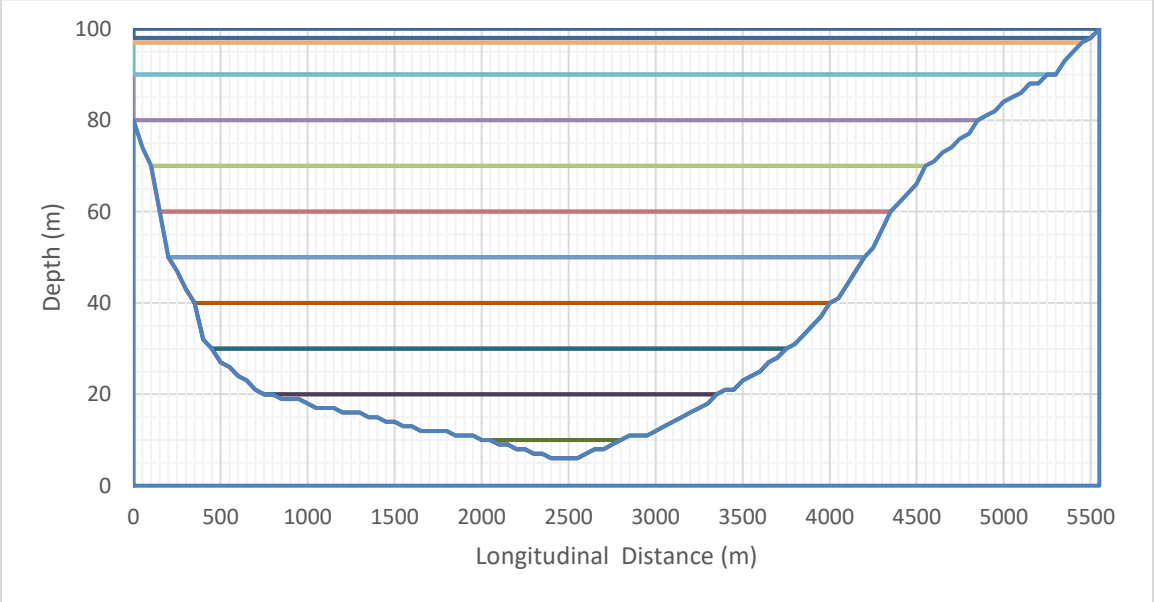

Figure 4-5: Model profile - Section C-D

4.3.2 Section A-B model profile

Similar to Section C-D, section A-B also has a concave profile, but with much steeped slopes (Figure 4-6). The lowest point has a short roughly flat section at the middle of the profile, but unlike in Section C-D, there is about 1000m long essentially flat section at about 20m depth on the right side. The entire section is 4000-meter-long and the middle of the section reach to the lowest point at 94m depth as same as section C-D.

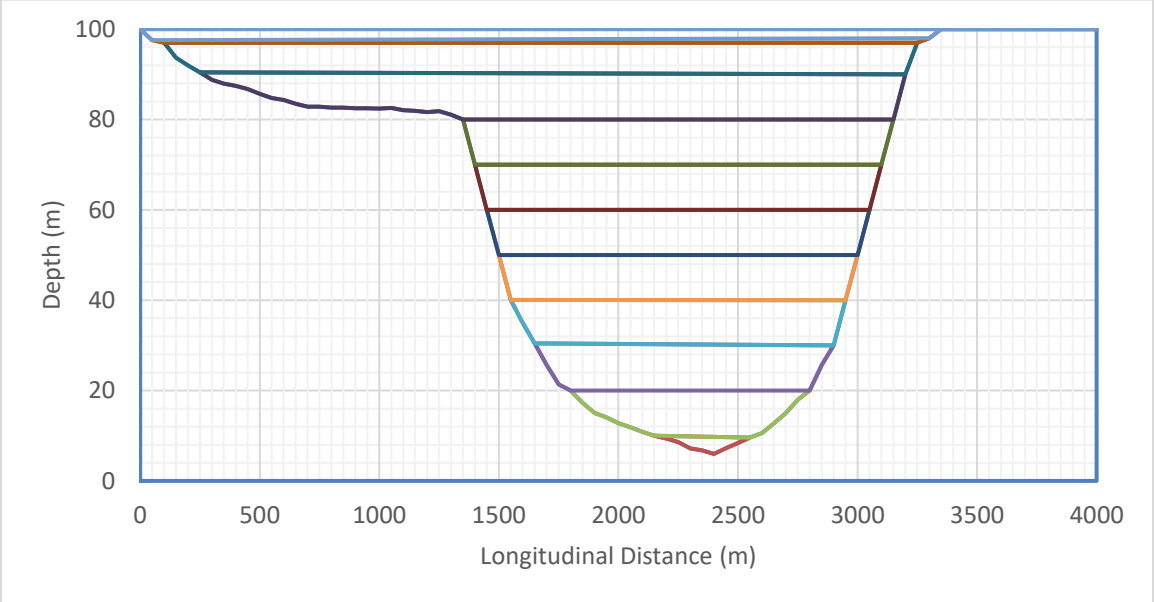

Figure 4-6: Model profile - Section A-B

Both sides of the section A-B contain the rock outcropped to the ground surface, and due to the flat profile at about 20m depth, and the overall shorter width, the inclination of the soil-rock interface is much steeper at certain depths. In order to avoid numerical instabilities, the maximum inclination of the soil-rock interface was limited to about 1V: 5H maximum. As a result, the model width is slightly wider than the actual width of Section

A-B in-situ which has inclination as steep as 1V:3H on the right side. The primary difference between the model sections A-B and C-D is thus the steeply sloping soil-bedrock interface in A-B, as high as 1V: 5H in A-B compared to 1V: 25H in C-D.

4.4 ARTIFICIAL EARTHQUAKES

Seismic analysis with the aid of artificial earthquakes generated from design spectrum for the specific site is commonly used by many researchers (Strenk & Wartman, 2011). It is due to the lack of sufficient real earthquake records for the selected site at the required shaking intensities. Generation of artificial earthquakes provides an opportunity to have multiple earthquake time history records with desired overall characteristics. The actual ground motions, shaking intensities and peak ground acceleration may vary somewhat among these records, that are used as input for the site-specific analysis.

Artificial earthquake records are generally generated to match a specified response spectrum. Even though there is only one response spectrum for an acceleration time history, the reverse is not a single solution. Multiple acceleration time histories may be produced from a given response spectrum. The response spectra of generated time histories are only an approximate match to the initial design spectrum. This permits the generation of a number of time history records that have similar characteristics on the frequency domain.

4.4.1 Input motion - Earthquake Time History #1 to #6

Six artificial time history records that are compatible with the NBCC 2015 target design spectrum for the Orleans location were generated using the SSQuake software at Carleton

University. Given the latitude and longitude of the site, the software retrieves the NBCC design spectrum for the site and generates motions that match the NBCC2015 seismic provisions. These spectral values correspond to a 2475-year shaking event (i.e., an event with a 2% chance of exceedance in 50-years). The algorithm originally developed by Vanmarke et al. (1976) is used by the software to generate the spectrum compatible time histories. The duration of the earthquake shaking was limited to 20 seconds and data points were produced at 0.02 second interval, which means the frequency of up to 50Hz is captured in the motion. The design spectrum is produced for seismic site class A ("Hard rock") and the artificial earthquakes is thus considered to be representative of the incoming bedrock motion, and applied at the base of the model without any scaling or deconvolution process.

4.4.1.1 Spectral accelerations & time history

The design spectrum for the Orleans site is compared with the computed response spectra (5% damping) in Figure 4-6. A relatively close overall match is noted, even though the larger difference exists at certain periods. Earthquake shaking is uncertain by nature, and these variations are not a concern. The time histories of motion of the six artificially generated earthquakes are shown in Figure 4-8 to Figure 4-13. The peak ground acceleration in all six earthquakes is 0.280g even though the actual shaking record is different among the motions.

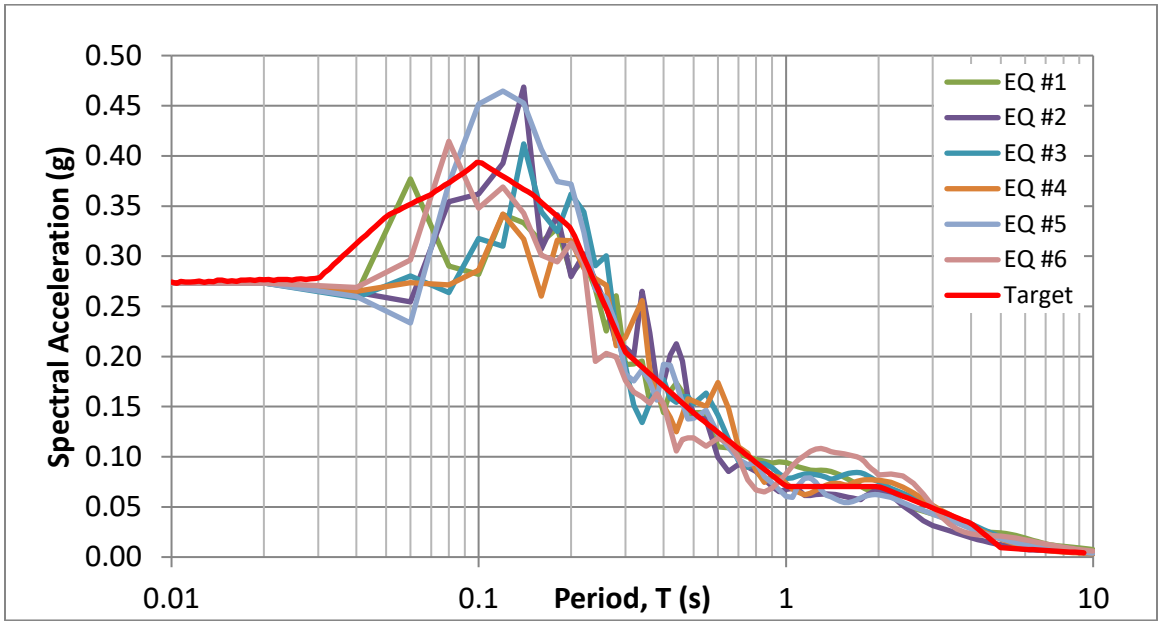

Figure 4-7: Response spectrum of six artificial earthquakes and target design spectrum

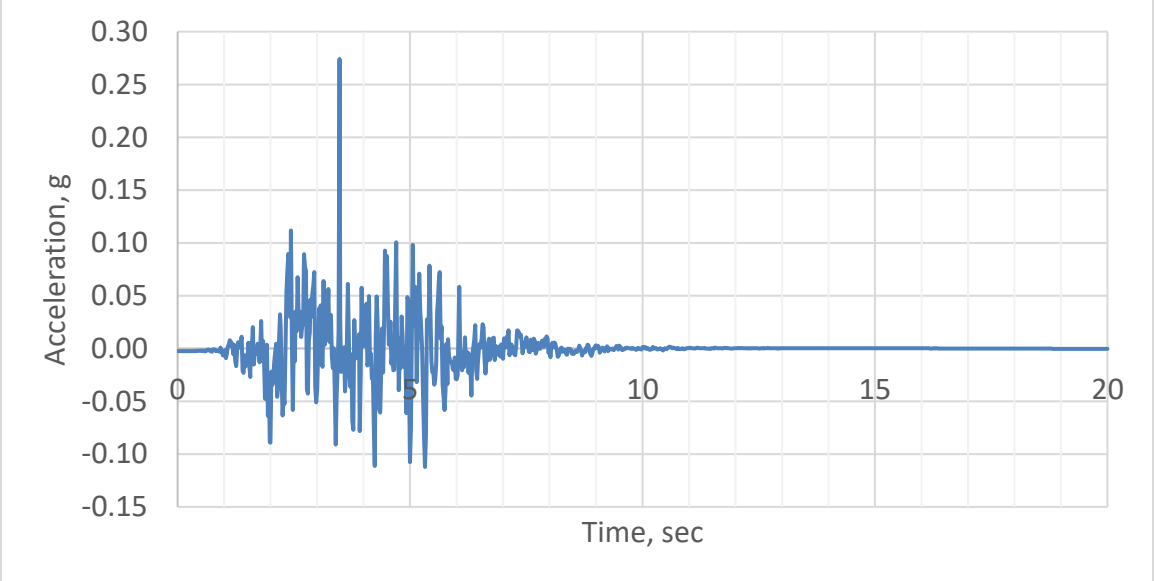

Figure 4-8: Acceleration vs time history of artificial earthquake #1

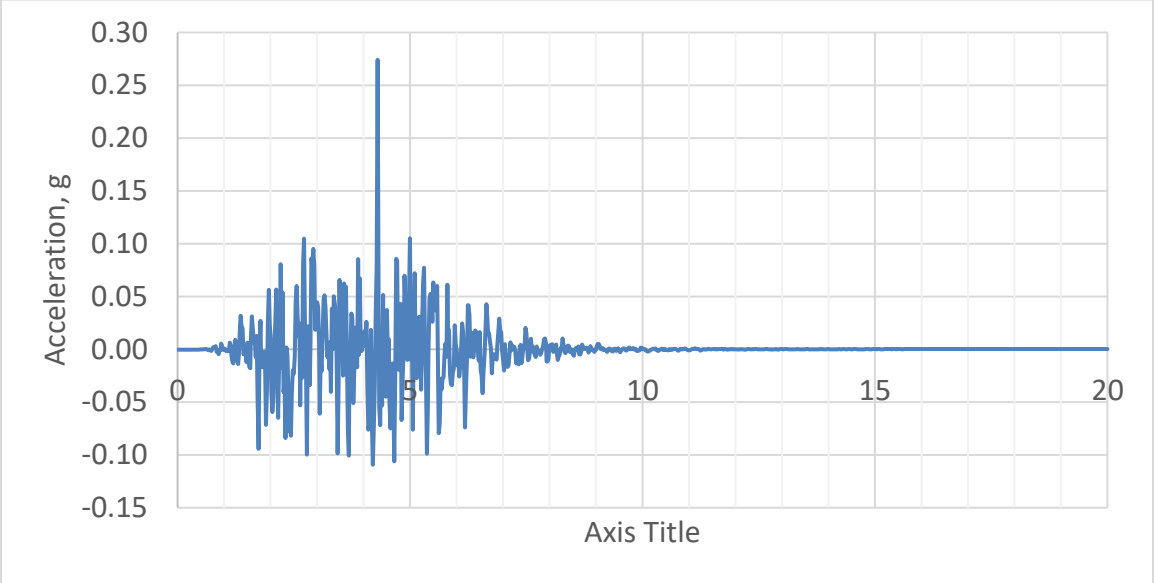

Figure 4-9: Acceleration vs time history of artificial earthquake #2

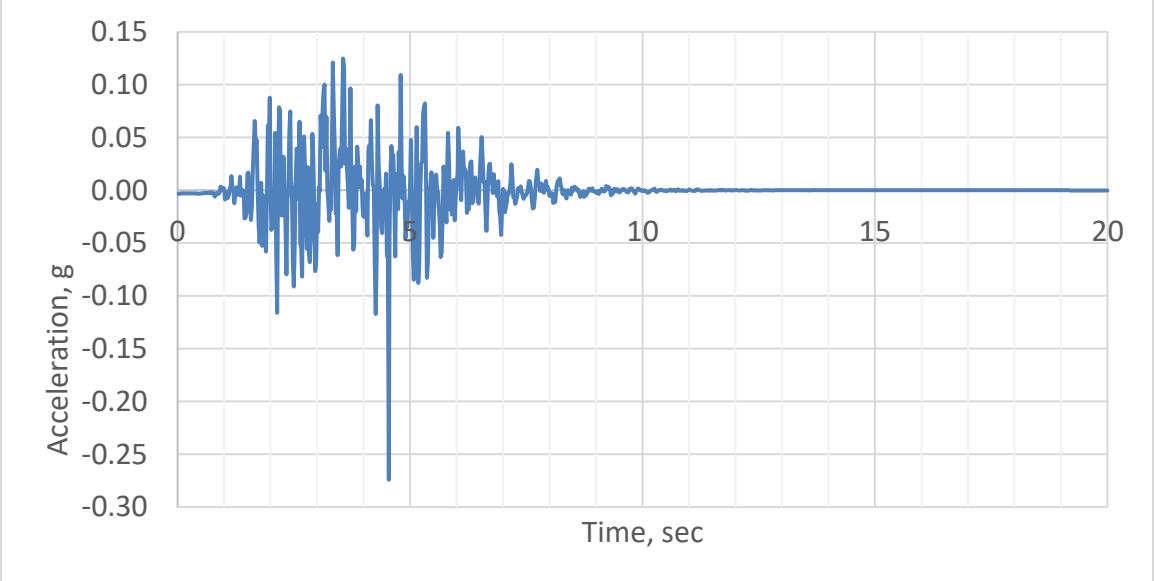

Figure 4-10: Acceleration vs time history of artificial earthquake #3

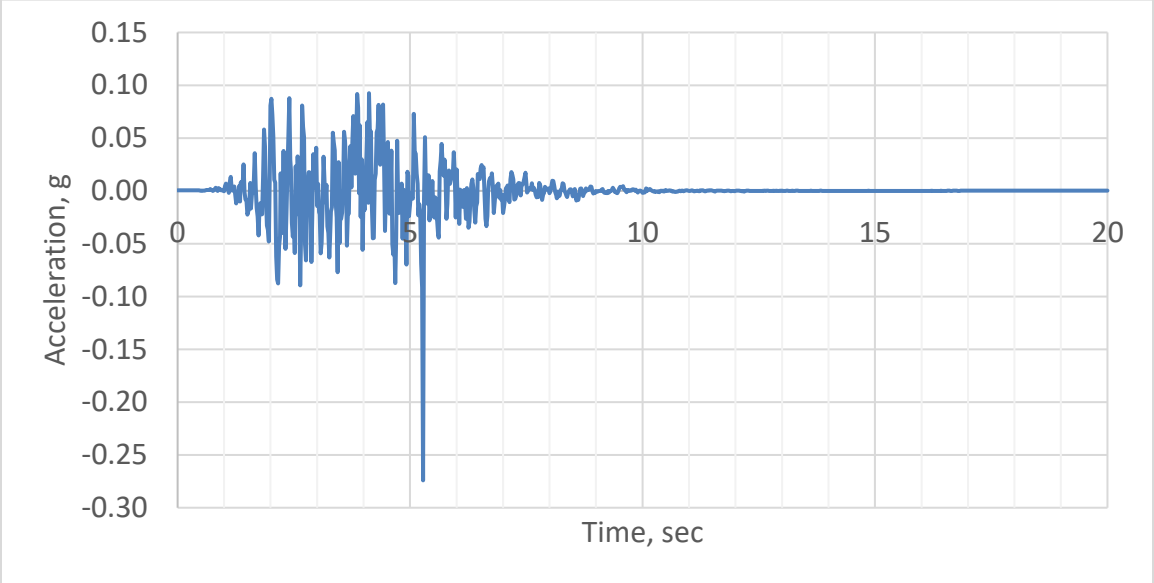

Figure 4-11: Acceleration vs time history of artificial earthquake #4

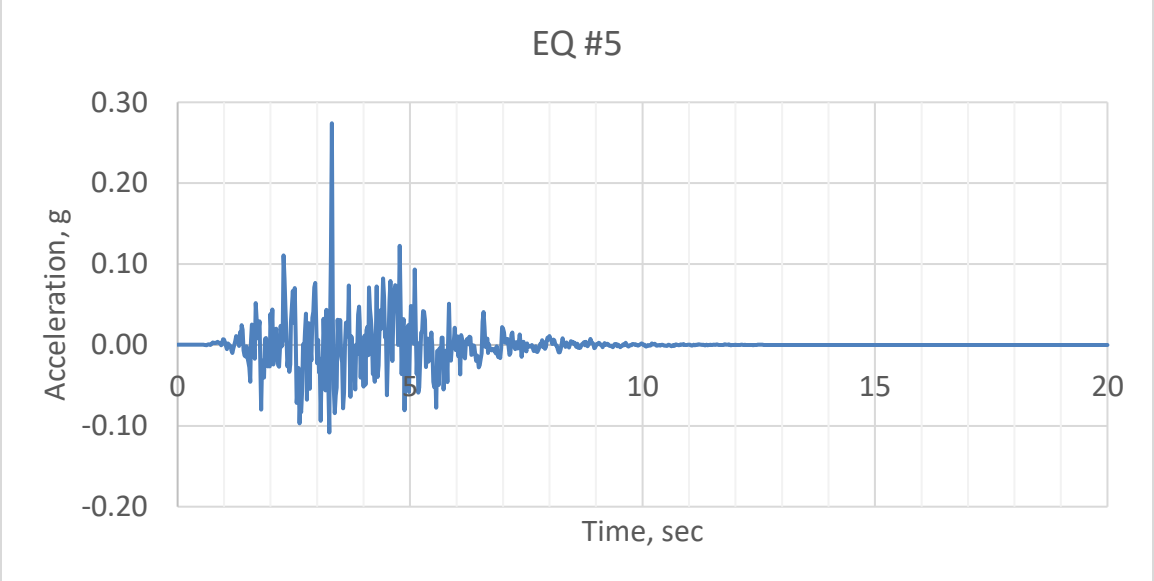

Figure 4-12: Acceleration vs time history of artificial earthquake #5

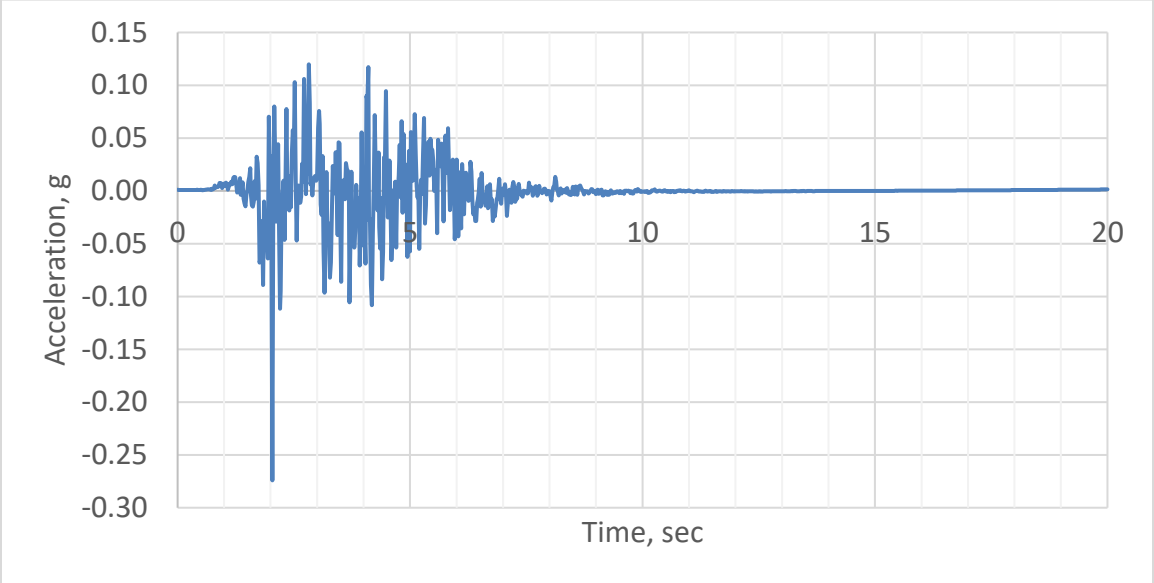

Figure 4-13: Acceleration vs time history of artificial earthquake #6

4.5 Real Earthquake Time History

The use of recorded earthquake records in the same seismic environment is preferable since it would represent both the variation of intensity and frequency content which are functions of the regional geology. The artificial earthquakes are produced to match the design spectrum specified by the code of practice, but no single real earthquake would follow the design spectrum. Thus, while artificial records match the intensity of shaking in terms of peak ground acceleration and spectral ordinates at specific periods, overall, they would represent a higher energy content than natural earthquakes. But it is difficult, if not almost impossible, to get earthquake shaking records that match both the epicentral distance and the earthquake magnitude. The earthquake records with characteristics that are closest to the desired target are selected and then scaled to match the anticipated loading prior to being used as input in geotechnical analysis.

4.5.1 The Val-De-Bois Earthquake

The June 23, 2010 Val-des-Bois earthquake in the Western Quebec Seismic zone caused the strongest ground shaking in the Ottawa region in the past 200 years. Yet the shaking intensity is well below the design shaking levels prescribed in NBCC 2015. The earthquake occurred at a depth of 22km, and the epicentre at latitude $45.88\ °N$ and longitude $75.48\ °W$ is about 55km North East of Ottawa. Even though the earthquake was felt across the region and in parts of North Eastern United states, there was very little damage in Ottawa (NRC Geofacts, 2010). The ground shaking was recorded at many sites (Seismotoolbox database), and Station ST012 located at $45.3942\ °N$ and longitude $75.7167\ °W$ is the closest location to the Orleans Valley at a distance of about 20km.

The earthquake shaking may be recorded on ground or rock outcrops, and both on-soil and on-rock motions were available at stations around the site for the Val-des-Bois earthquake. The advantage of outcrop motions is that they will closely match with the incoming base motion in terms of frequency content compared to ground motions recorded on soil sites. On that basis, the selected recording station is located on the rock outcrop and it is expected that the incoming motion would have with similar characteristics.

Val-des-Bois earthquake motion is recorded along three orthogonal directions, two horizontal (North-South & East-West) and the Vertical direction. However, in this study, the vertically propagating shear wave is focused on the concaved geology of Orleans

Valley. So, the East-West and North-South motions of Val-des-Bois earthquake at Station ST012 are used as two separate input motions in the analysis (Figure 4-14 and Figure 4-15). The actual peak ground acceleration recorded at Station ST012 during the earthquake was 0.032g N-S and 0.033g E-W, and the highest response spectral acceleration about 0.10g at a period value of 0.1s for E-W, and 0.12s for N-S as shown in Figure 4-16. These shaking intensities are well below the target shaking during the design event corresponding to NBCC 2015 (which has PGA of about 0.28g, and Sa (0.1) at 0.40g. Thus, the downloaded time history records have to be "scaled" prior to use in the analysis if the objective is to assess the response under design motions matching NBCC 2015.

Time history of recorded motions from the Val-des-Bois, both E-W and N-S are 60s long in duration and sampled at 100Hz. Relatively strong shaking occurs only for a much shorter duration; the bracketed duration of acceleration exceeding 0.01g is less than 10 seconds in both N-S and E-W motions. However, the entire recorded motion was used in the analysis for consistency.

4.5.1.1 Summary of acceleration history

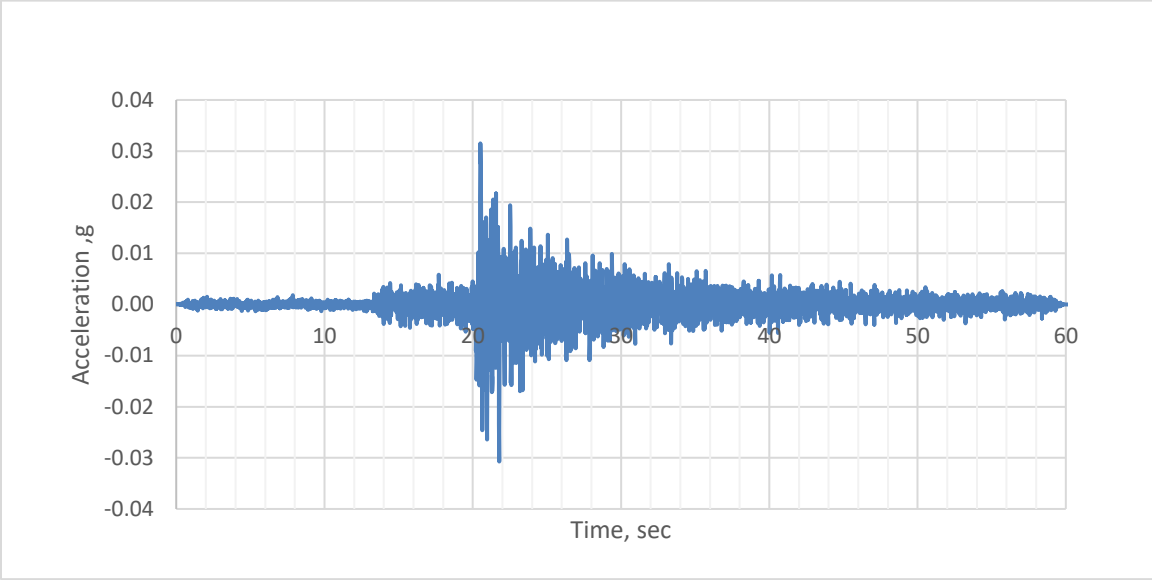

Figure 4-14: ST012 East-West directional motion time history (from SeismoToolbox, 2021)

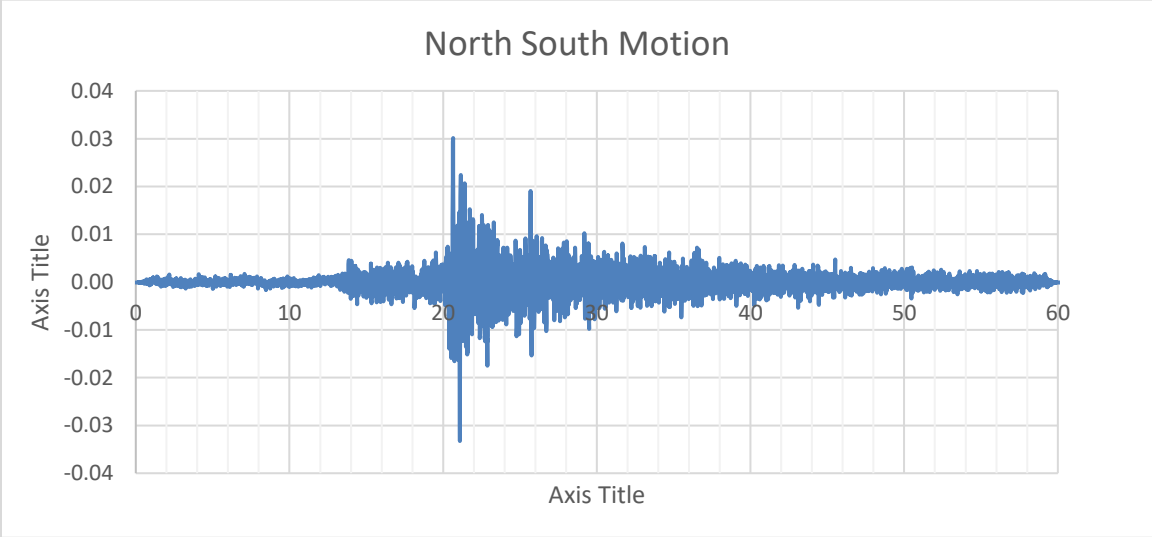

Figure 4-15: ST012 North-South directional motion time history (from SeismoToolbox, 2021)

4.5.1.2 Summary of spectral accelerations

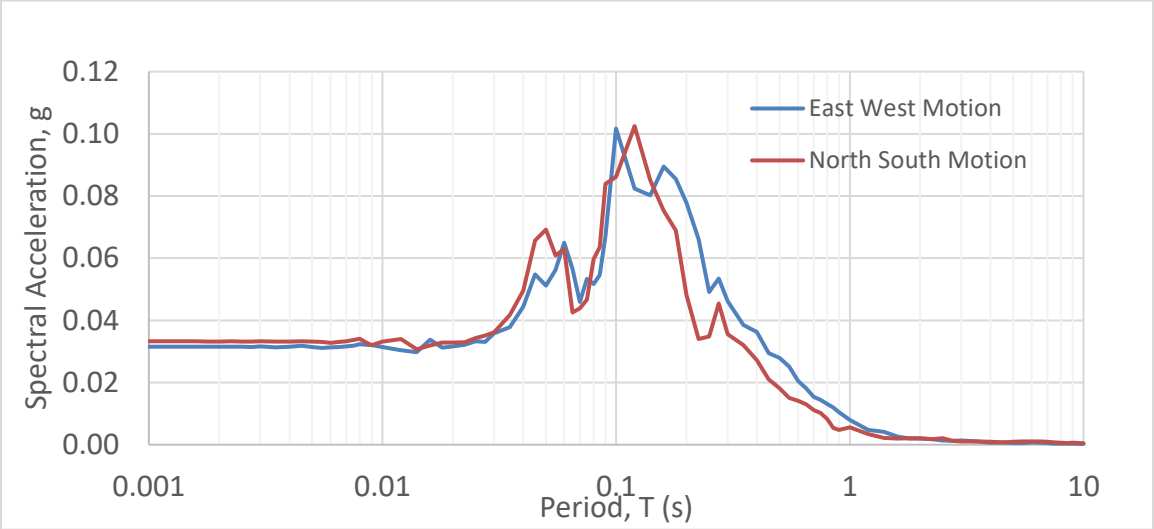

Figure 4-16: Spectral acceleration of the recorded motions at Station ST012

4.5.1.3 Amplitude scaled motion

Typical geotechnical practice is to scale to match the peak acceleration. Such an approach is very elementary and misses the fact that peak acceleration corresponds to very high frequencies (e.g., 100 Hz) but the behaviour to a larger extent is controlled by the strength of the motions at typically in the 1 – 10 Hz (or 0.2 to 20 Hz if a more accurate representation is preferred) range. An improved scaling method that considers the overall response spectral ordinates is used in this research.

First, the design spectrum according to NBCC2015 code of practice is taken as the target spectrum. Then a scaling factor is evaluated in order to match the selected earthquake spectrum with the target design spectrum. Both N-S and E-W motions of Val-des-Bois earthquake treated separately and from the mean value, a scaling factor, S_F is selected. The

selection of a scaling factor is crucial as it regulates the entire spectral plot of the real earthquake to match with the target design spectrum. Two methods can be used to compare the appropriate scaling factor such as peak spectral ratio method and average spectral ratio method: (1) Scaling factor based on the ratio of peak spectral ordinate in the design spectrum, (2) Scaling factor based on an average of the spectral ordinates in a representative period range.

Ratio of peak spectral accelerations, $\left(\frac{S(T),peak}{S_{br}(T),peak}\right)$ for both motions is about 3.8. If using this scaling, it leads to lower spectral accelerations compared to the target design spectral accelerations at other periods. But the scaling factor based on the ratio of average spectral accelerations showed reasonable match of most of the spectral data. As a result, scaling factor calculated by considering average spectral ratio of actual motion and target design motion, $avg\left(\frac{S(T)}{S_{br}(T)}\right)$ within the selected period range. A period range of 0.05 to 0.5s selected for the E-W motion as the spectral plot is widely spread within this range. But, only a short period range of 0.1 to 0.2 s is selected for the scaling factor of N-S motion as the spectral plot shows sudden drops outside this period range. The average spectral ratio for E-W motion is $\left(\frac{S(T)}{S_{br}(T)}\right) = 5.02$ and the amplitude scaling factor of $S_F = 5$ is selected. The average spectral ratio for N-S motion is $\left(\frac{S(T)}{S_{br}(T)}\right) = 4.30$ and the amplitude scaling factor of $S_F = 4.5$ is selected. Figure 4.17 and Figure 4.18 shows the spectral amplitude scaled motions.

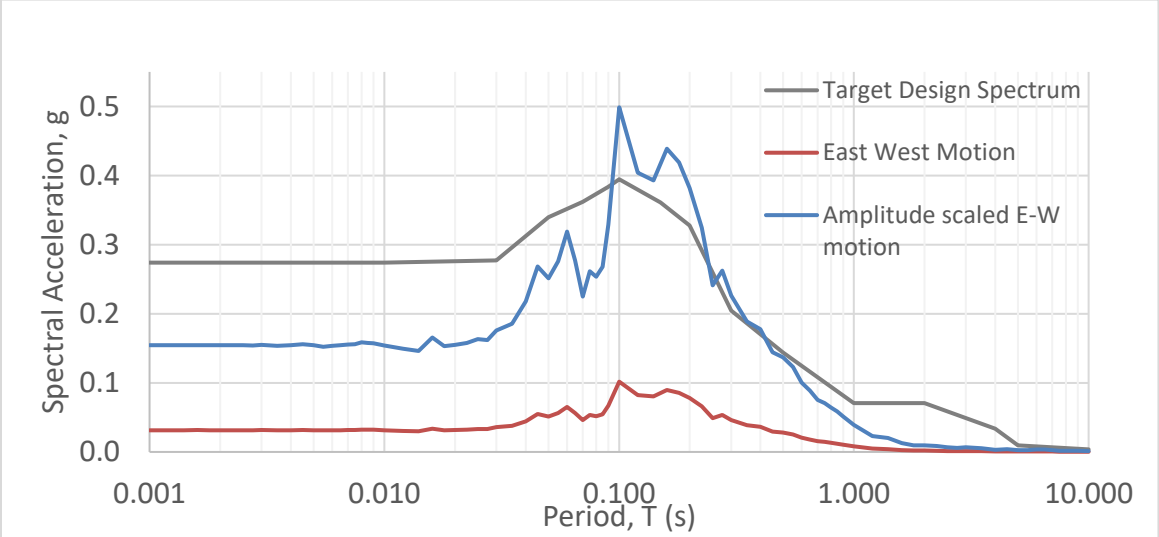

Figure 4-17: Comparison of original and amplitude scaled response Spectrum of ST012 East-West motion against target design spectral amplitudes.

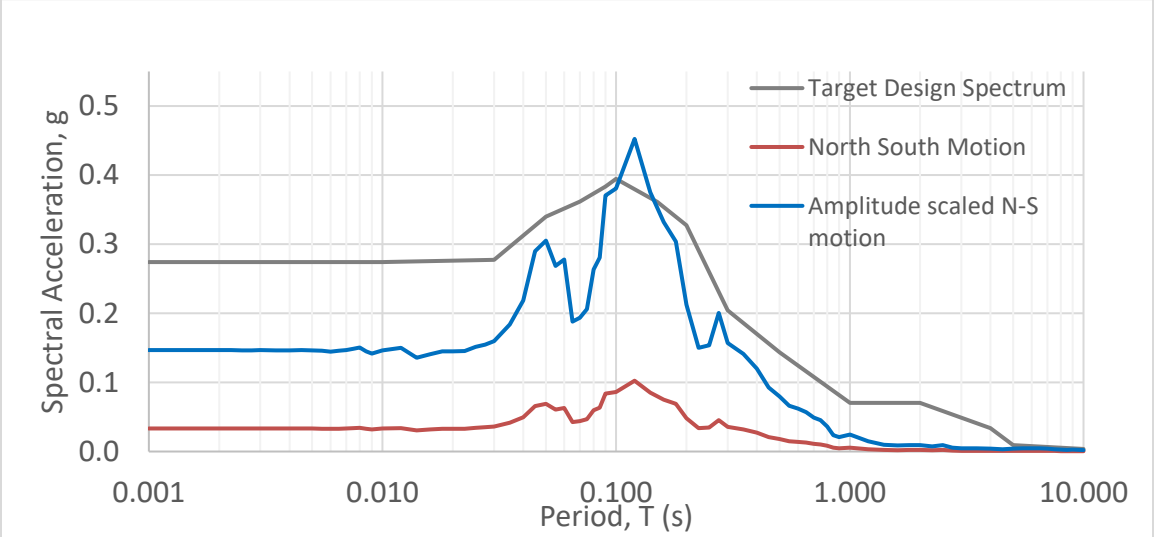

Figure 4-18: Comparison of original and amplitude scaled response Spectrum of Val-des-Bois North-South motion against target design spectral amplitudes

4.5.1.4 Both amplitude and frequency scaled motion

The spectral amplitude scaled E-W motion showed a good match within the period range of interest (from 0.1sec to 1sec). But for the N-S motion, there was a shift in the spectral shape in the period axis direction. In order to enhance the match, frequency scaling factor is introduced based on the ratio of predominant periods where the time step changed from 0.01sec to 0.012 in order to scale the frequency content. The time step between data points was multiplied by 1.2 so that the spectrum shifts towards long period. After this scaling, the spectral ordinates of the motion matched better with the design spectrum at the period range of interest, and yielded the time history. The response of the scaled motions used as input to the analysis are shown in Figure 4.17 and Figure 4.19.

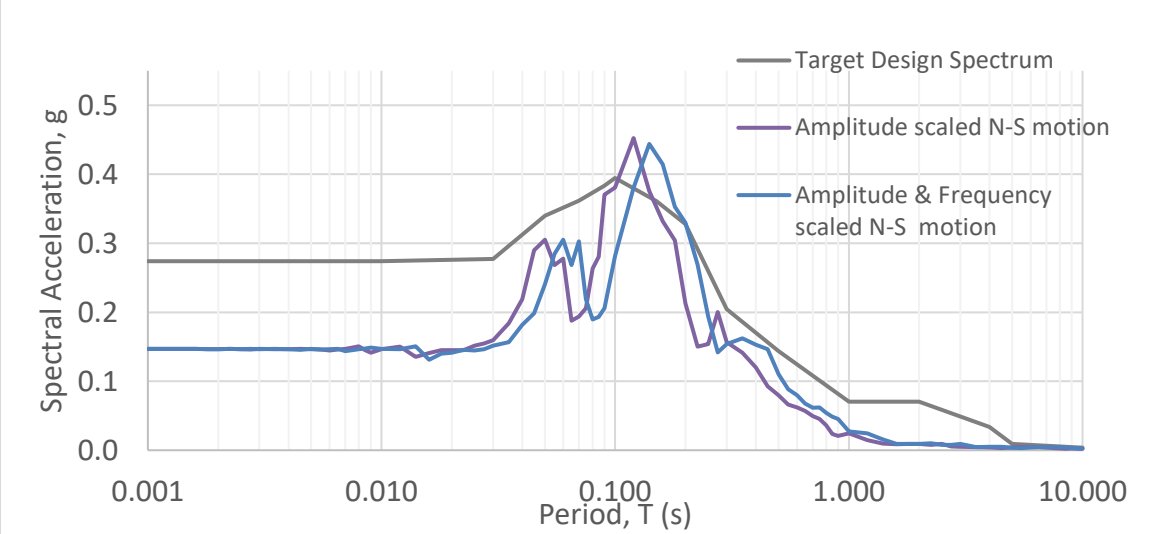

Figure 4-19: Amplitude and frequency scaled spectral accelerations of Val-des-Bois North-South motion

4.6 Dynamic Properties - Modulus reduction & damping

Technically, soil behavior is elastic at very small strains, and subsequently elasto-plastic. But, a proper elasto-plastic dynamic analysis is complex, and beyond the scope of this research. Further, it does not necessarily imply improved results since the uncertainty in the models, and the required input parameters increase significantly. As a result, the typical practice is to model the soil behavior as nonlinear elastic.

The nonlinear behavior of soils is captured using modulus reduction and damping curves in practice. This is referred as the equivalent linear dynamic analysis, and a hysteric damping model is used in FLAC to capture this response. A family of curves that are dependent on strain for a given material have been proposed in the literature for various types of soils, such as gravels, sands, and clays. The clay curves are based on the plasticity index, but concerns have been expressed that the values in the literature for clay are not appropriate for Leda clay due to its high sensitivity. Therefore, it is appropriate to use Leda clay specific modulus reduction and damping curves (Theenathayarl, 2015, Thavakumaran 2017).

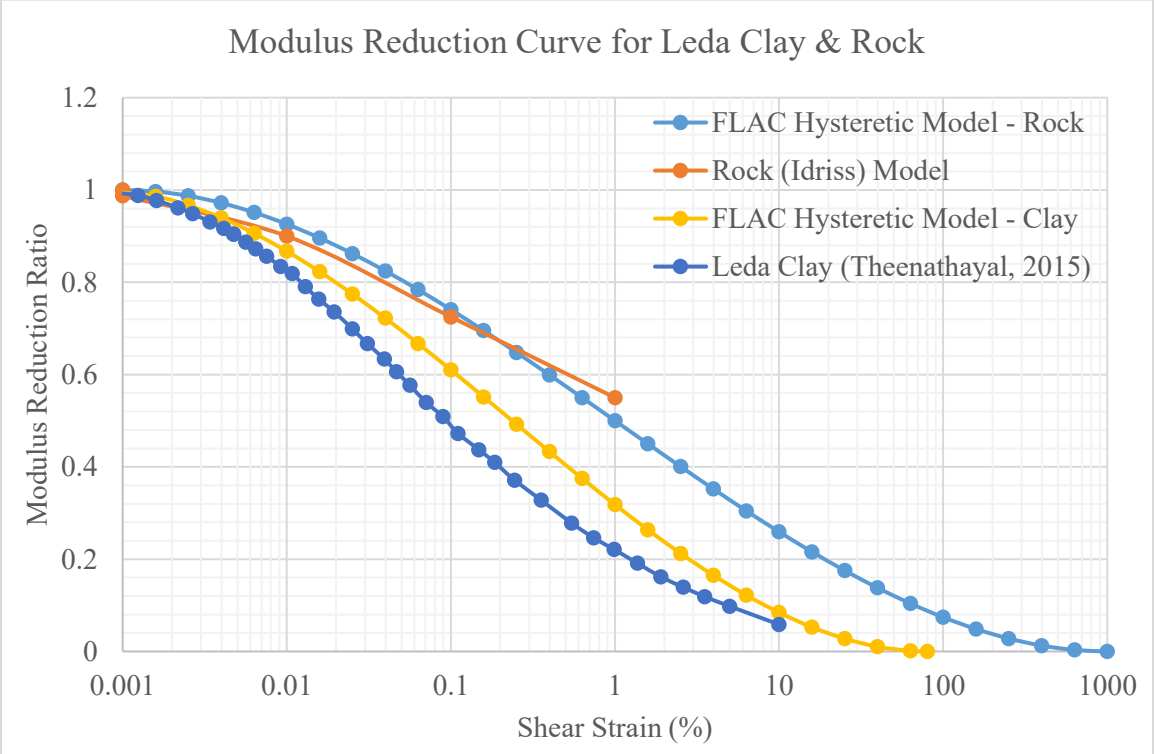

Figure 4-20: Assumed modulus reduction and damping properties of Leda clay and rock material in Orleans region

Figure 4.20 shows the modulus reduction curves used to represent the soil and bedrock in the analysis. FLAC controls the shape of the modulus reduction curve by using two parameters, L1 and L2. The values of $L_1 = -3$ and $L_2 = 3$ in the hysteretic damping model yielded a curve that closely matches the modulus reduction curve defined for rock by Idriss (1992). For the Leda clay, the modulus reduction curve proposed by Theenathayal (2015) is taken as the reference, it is approximated in the hysteretic damping model with $L_1 = -3{,}156$ and $L_2 = 1.904$.

The modulus remains constant at its initial value, G_{max} within the linear elastic range ($\gamma < \gamma_L$). There is no reduction in modulus during this range (i.e., modulus reduction curve is flat). The magnitude of γ_L depends on the material, and is typically between 0.001% and 0.01%. Technically the bedrock response is also nonlinear, but due to the high stiffness of the rock the loading causes fairly small strains in the bedrock. Therefore, the modulus of the bedrock may not undergo much reduction in the modulus in these problems. This has been assessed by comparing the response of a model with constant shear modulus in the bedrock with another model with nonlinear bedrock. In both cases the soil model was kept the same (nonlinear, and characterized by modulus reduction and damping). The site response was then assessed by applying the time history of the six artificial earthquakes at the base of the model, and comparing the response in terms of the average responses between the two cases. Figure 4-21 compares the horizontal acceleration response, and Figure 4-22 the horizontal displacement response. It was noted that both elastic rock and the hysterically damped nonlinear rock gave essentially similar results. Further, the shear strains calculated from the horizontal displacements are shown in Figure 4-23. The strain values are noticed to be very small within the region of rock, generally between $1 \times 10^{-5}\%$ to $1 \times 10^{-4}\%$. This indicates that both models gave the same response since the deformation within the bedrock is limited to the elastic range. An elastic model is less complex, and results in faster runtimes. Therefore, the bedrock was modelled as elastic, and without any hysteric damping, in the subsequent analysis to minimize the runtime.

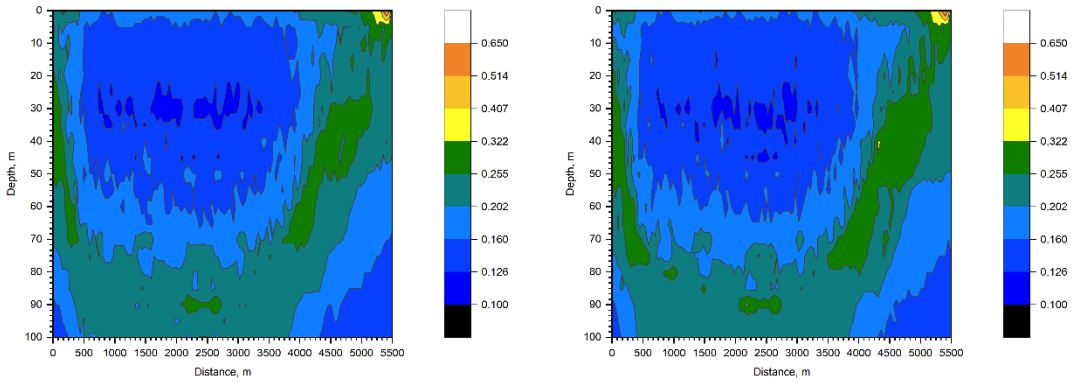

Figure 4-21: Comparison of average maximum horizontal acceleration response for the six artificial earthquakes on the mild steep section of Orleans Valley with and without modulus reduction and damping for rock (Left figure - no modulus reduction/ damping assigned for rock)

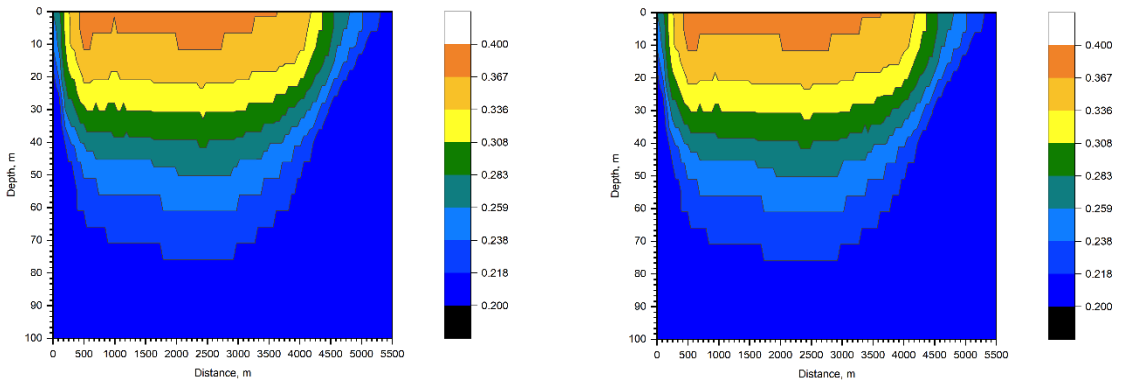

Figure 4-22: Comparison of average maximum horizontal displacement response for the six artificial earthquakes on the mild steep section of Orleans Valley with and without modulus reduction and damping for rock (Left figure - no modulus reduction/ damping assigned for rock)

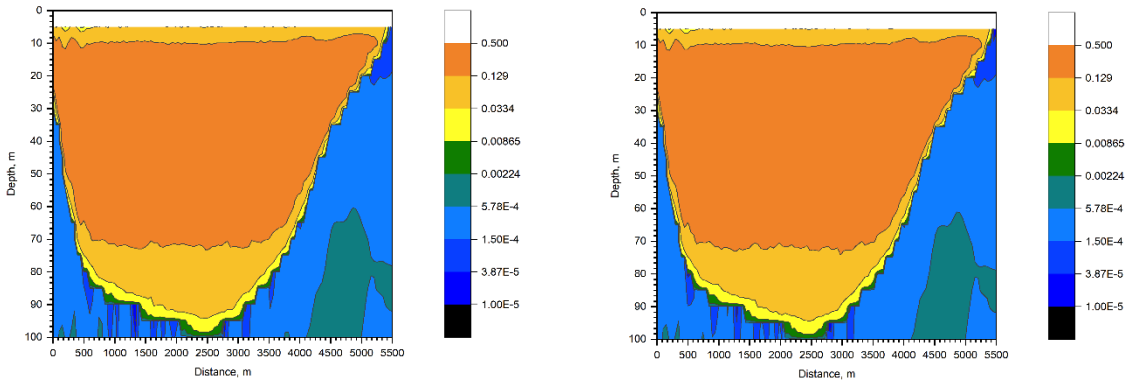

Figure 4-23: Comparison of average shear strain for the six artificial earthquakes on the mild steep section of Orleans Valley with and without modulus reduction and damping for rock (Left figure - no modulus reduction/ damping assigned for rock)

4.7 Validation of the FLAC Model

A "SHAKE" analysis (Schnabel et al., 1972; Idriss & Sun, 1992) is typically used in research and engineering practice to quantify the response of a local site subjected to seismic loading. SHAKE analysis is a simple one-dimensional equivalent linear consideration whereas a two-dimensional FLAC analysis is the consideration in this research to understand the basin effects. However, a FLAC model with horizontal bedrock (and soil layering) represents a configuration similar to SHAKE.

The results obtained from a 2-dimensional horizontal bedrock model in FLAC was compared with 1-dimensional equivalent linear shake in order to validate the FLAC model and to establish trust in the numerical solutions obtained from FLAC.

Even though both analyses are considering the response of vertically propagating shear waves in a horizontally layered soil deposit, differences exist between these two applications. The shake analysis is conducted in frequency domain and FLAC analysis in time domain. Shake analysis determines amplification transfer functions produced in frequency domain and the results are then converted in to time domain. The finite different method in FLAC directly considers the motion in time domain and converges to solution through multiple iterations in time domain.

4.7.1 FLAC 2D horizontal bedrock Profile

A 2D horizontal bedrock profile is created and analyzed with artificial earthquake as input in order to validate the model outcomes against the 1-dimensional shake analysis. Bedrock is assumed to be flat at the same level as the lowest elevation of concave bedrock profile (94m below GL). The results from the FLAC analysis are shown in Figure 4-24 and Figure 4-25. Essentially constant response across the horizontal layers is observed. Minor fluctuations noted are a result of the numerical approximations, and overall, these results are representative of 1-D wave propagation. Even though only plots of the determined maximum horizontal acceleration and the induced cyclic stress ratio are shown for brevity, the variation in other parameters showed similar characteristics.

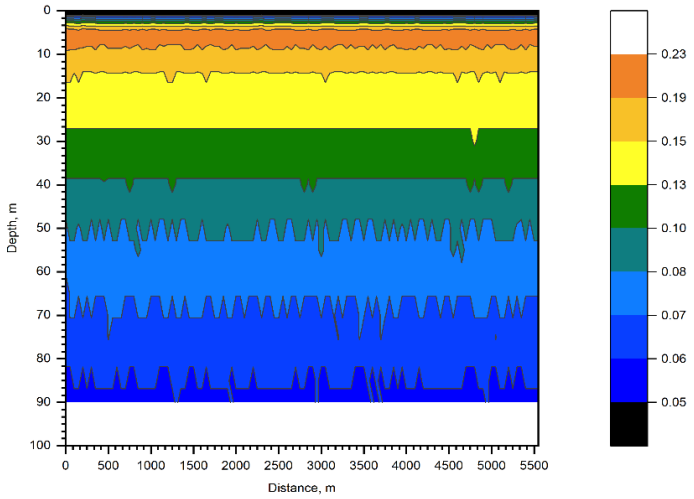

Figure 4-24: Variation of Average CSR of six artificial earthquake records on the 2-D Horizontal Bedrock Model

From the analysis, the cyclic stress ratio shows larger values at shallow layers and reduces with depth. The maximum CSR was about 0.23 and occurred in the top clay layer at a depth of about 4m from the ground surface. It reduced to 0.1 at about 40m from GL. The cyclic stress ratio values are computed from the measured maximum cyclic stress (88kPa at 5m from GL to 42kPa at 40m from GL) using the Seed & Idriss (1971) formulation as noted earlier.

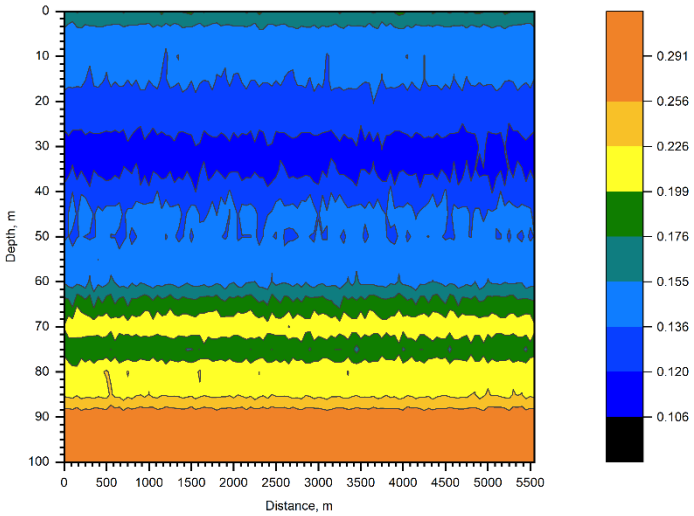

Figure 4-25: Variation of Average Horizontal Acceleration (Max) of six artificial earthquake records on the 2-D Horizontal Bedrock Model

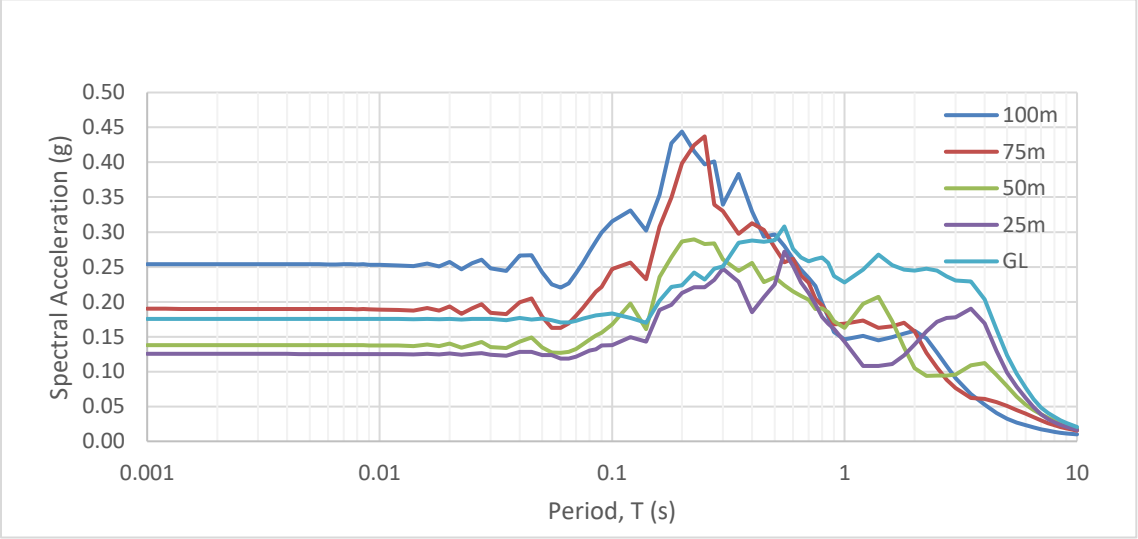

Figure 4-26: Response Spectrum of acceleration at different elevations recorded from FLAC Analysis - Average response of 6 artificial earthquakes

The peak ground acceleration of all artificial earthquakes is equal to $0.274g$. Figure 4-25 shows the average of peak accelerations recorded in the six analyses, and Figure 4-26 a comparison of the average response spectra of the acceleration at select depth. As seen in Figure 4-25, the peak acceleration response was higher at the bedrock region; The values recorded within this region varied from a high $0.291g$ and starts to reduce from 94m onwards where the soil layer begins. The acceleration values dropped to $0.226g$ at 70m depth and there was some attenuation subsequently to about 30m which was followed by a small level of amplification. Even though the value of acceleration increases and reduces in the middle layers, the earthquake gets attenuated within the top 70m up to the ground surface and the average value of the maximum acceleration observed near the ground surface is close to $0.2g$. It is noted that these comments are with reference to the peak ground acceleration, which is characteristic of high frequencies. The spectral acceleration might amplify at some particular range of periods, and those aspects will be discussed in the latter sections.

4.7.2 ProShake 1D profile

The commercially available ProSHAKE software was used to conduct the 'SHAKE' analysis. A 1-dimensional shake model is created where the bedrock is kept at 94m from GL which matches the bedrock location in the FLAC 2D horizontal bedrock model. The FLAC model includes a 6m thick bedrock in the grid, but bedrock was indicated as a semi-infinite interface in SHAKE analysis to be consistent with typical practice. The response

was analyzed with the same six earthquakes motions as in FLAC. An illustration of the 1-D ProSHAKE model is shown in Figure 4-27.

Model parameters used are the same as in the FLAC model for each corresponding layer. Consistent with the FLAC hysteretic damping model, the modulus reduction and damping ratio of the Leda Clay used as the input parameter of the soil model. The outcome from the Shake analysis compared with FLAC 2D correctional bedrock model in order to validate the results. Spectral accelerations recorded at elevations of 25m, 50m, 75m and 100m from the ground level in ProSHAKE analysis shown in Figure 4-28.

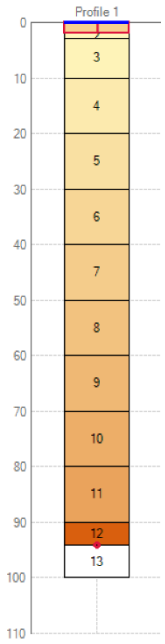

Figure 4-27: One dimensional ProShake Model

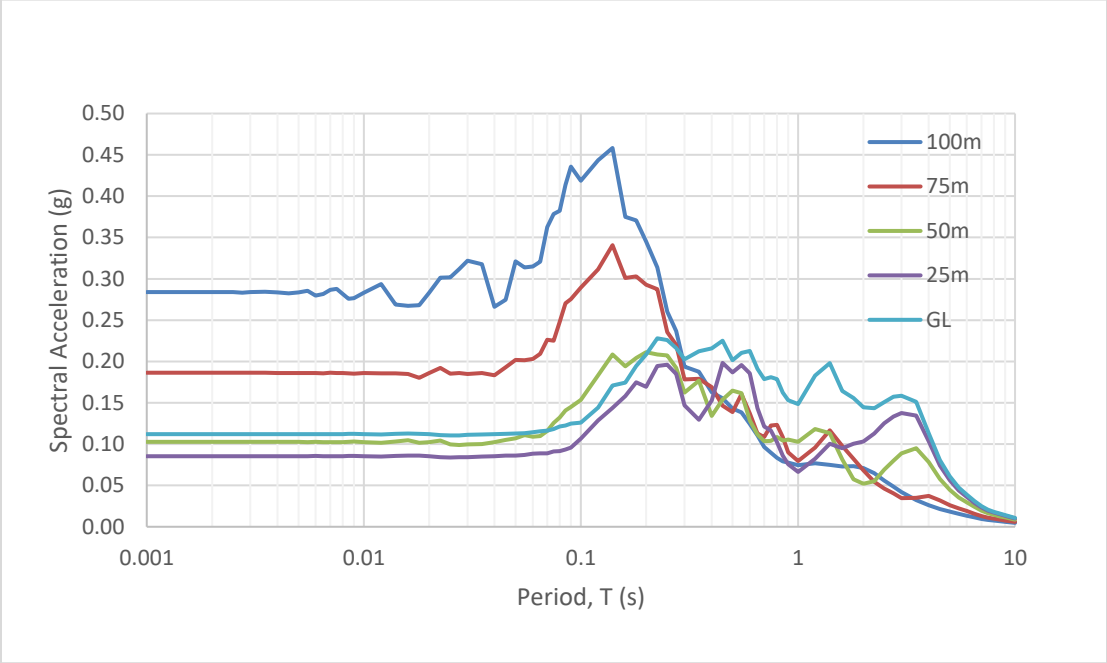

Figure 4-28: Response Spectrum of acceleration at different elevations recorded from ProShake Analysis - Average response of 6 artificial earthquakes

4.7.3 Comparison of the effect of Artificial earthquake on both FLAC and ProShake

In spite of the different techniques used in shake and FLAC analysis the results obtained are relatively consistent. The match was much better at lower layers compared to near the ground surface. The spectral acceleration taken at elevations of 100m, 75m, 50m, 25m and at the ground level were directly compared, and Table 4.3 shows the peak ground acceleration at each depth. A close match is observed in peaks and low points of the spectral acceleration plot at depth, but the FLAC values are about 30% ~35% higher than the Shake

analysis in the upper layers -in the top 50m. Fig. 4.29(a) shows a comparison of the average response at ground level, and 4.29(b) at 100m depth.

Table 4-3: Comparison of peak ground acceleration between Shake 1-D analysis and FLAC 2-D flat model analysis.

Elevation	Peak Ground Acceleration – Shake 1-D Analysis (g)	Peak Ground Acceleration – FLAC 2-D Analysis (g)
100m	0.284	0.254
75m	0.187	0.190
50m	0.103	0.138
25m	0.086	0.125
GL(0m)	0.112	0.175

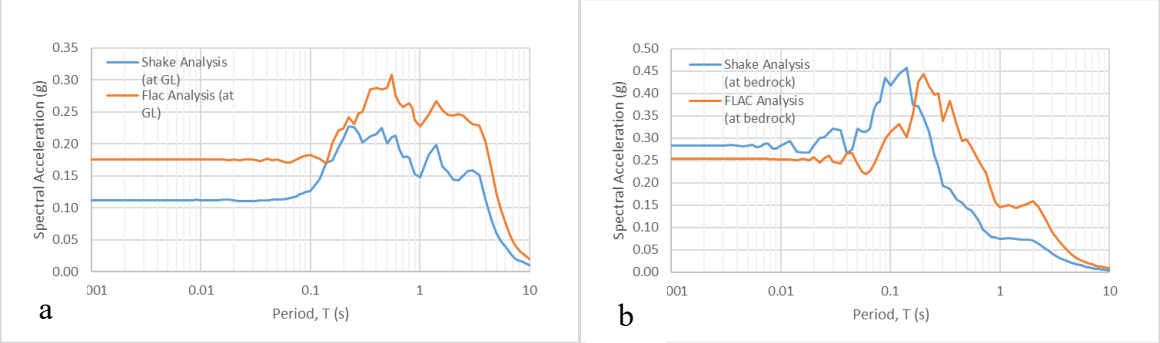

Figure 4-29: Response Spectrum of acceleration at bedrock & GL from ProShake 1-D and FLAC

As seen in the Figure 4-29 (a & b), the spectral acceleration of both ProShake and FLAC for the horizontal bedrock and soil layering profile shows a similar pattern but with an offset of about 0.05g on average. The differences are much smaller at a depth of 100m.

These types of differences have been observed in the literature by other researchers who used FLAC for the numerical analysis (Strenk & Wartman, 2011; Prasanna, 2020). The differences on account of the time domain analysis in FLAC and frequency domain analysis in ProShake, and the different implementations of the damping characteristics are citied as contributors for the variation between the two analyses. However, the similar peaks and relatively low variation in the spectral plot given the confidence on the FLAC model.

4.8 Interpretation of 2D FLAC Analysis

Seismic response of a 2-dimensional profile such as Orleans profile shows various responses in different location. This is expected given the vast domain considered in the analysis (up to 5.5km long, and 100 m deep profile). Further, the bedrock profile changes continuously, and thus the depth of soil layer which is related to the natural frequency of the model also varies from location to location. In addition, the wave reflection and refraction also play an important role in amplification or attenuation.

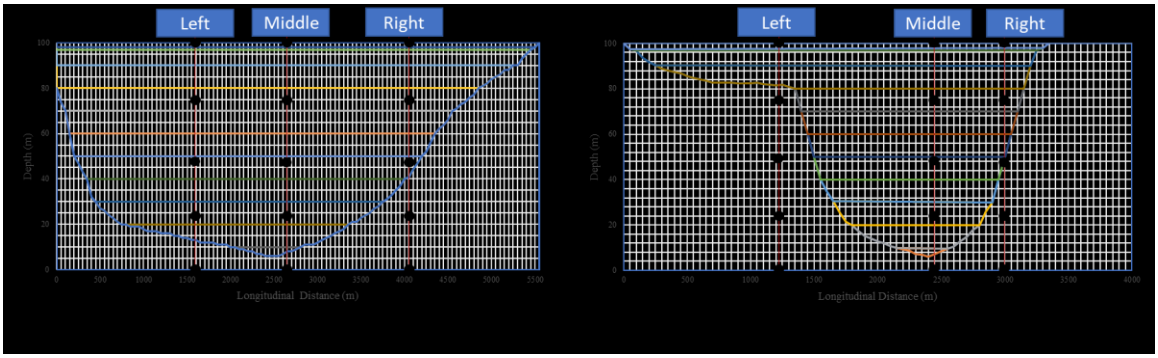

Figure 4-30: Locations of zones selected in section C-D and section A-B for the comparison of seismic responses

In order to manage the volume of data, and the runtime for each analysis, the output from the FLAC numerical analysis was considered at five different elevations, and at each elevation at three locations which were equally spaced within that layer as shown in Figure 4-30 (a & b). The first location selected within first quarter ("left"), second is in the middle ("middle") and the third section lies within the third quarter ("right"). The five different elevations taken into consideration are 100m, 75m, 50m, 25m and the ground level.

The results obtained for sections A-B and C-D are discussed below in terms of the response spectral ratio of the recorded horizontal acceleration to the applied ground motion among various zones. It is noted that there is not much amplification or attenuation observed within 0.1s to 1.1s period range particularly below 40m layers to rock surface. At period values less than 0.1s and greater than 1.1s the response spectrum shows attenuation of the incoming motion. This effect can be caused due to two major factors. First the confined boundary of rock at both sides of the soil deposit may restrain the excessive movement of the soil deposit. Second is the overburden pressure coming from the top soil layers provide

additional confinement below soil layers from large amplification. The large amplification observed at the top layers of 20 to 40m soil deposit that shows about 2~3 times the applied motion within 5 to 1Hz and 4~8 times the applied motion observed within 1Hz to 0.1Hz range.

4.8.1 Spectral Acceleration - Section C-D

As noted previously, the response was considered at three locations at each elevation. The left section in first quarter of the section C-D has the bedrock at 85m from GL and inclined at slope of about 1:100. The middle section has the bedrock at 94m from GL and the bedrock is concaved down and become horizontal for a short span before it concaves upwards. The right section location selected in the third quarter have the bedrock at 50m from GL inclined at slope of about 1:20.

The averages of the spectral acceleration values at the left, middle and right sections are shown in Figure 4-31, Figure 4-32 and Figure 4-33 respectively. As illustrated the figures, the spectral amplitudes are the highest in the period range of 0.2s~3s. The figures representing the left, middle and the right zones shows the peak ground acceleration as amplified from the base of the model towards middle of the model (at 50m from GL) and then attenuated towards 25m and again amplified to the same spectral value as observed at 75m when it reached GL. Comparing to the base input motion, the peak ground accelerations got attenuated.

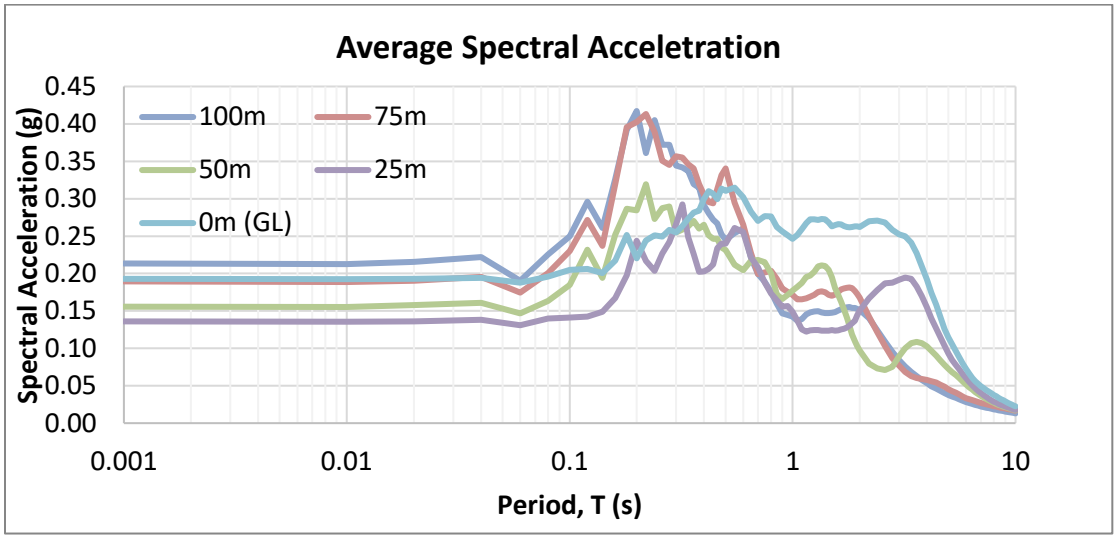

Figure 4-31: Average Spectral Acceleration - Left zone of section C-D

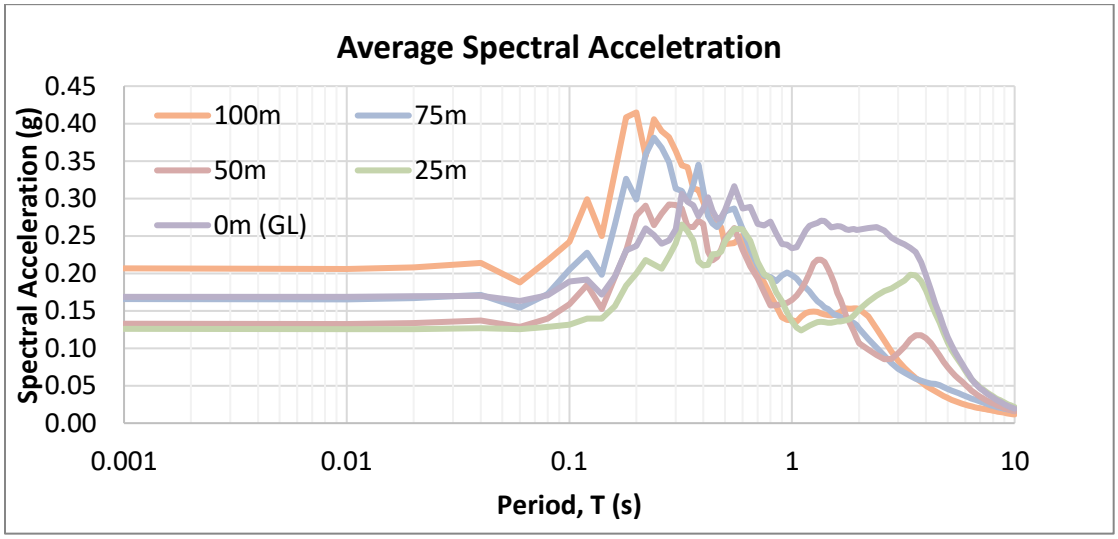

Figure 4-32: Average Spectral Acceleration- Middle zone of section C-D

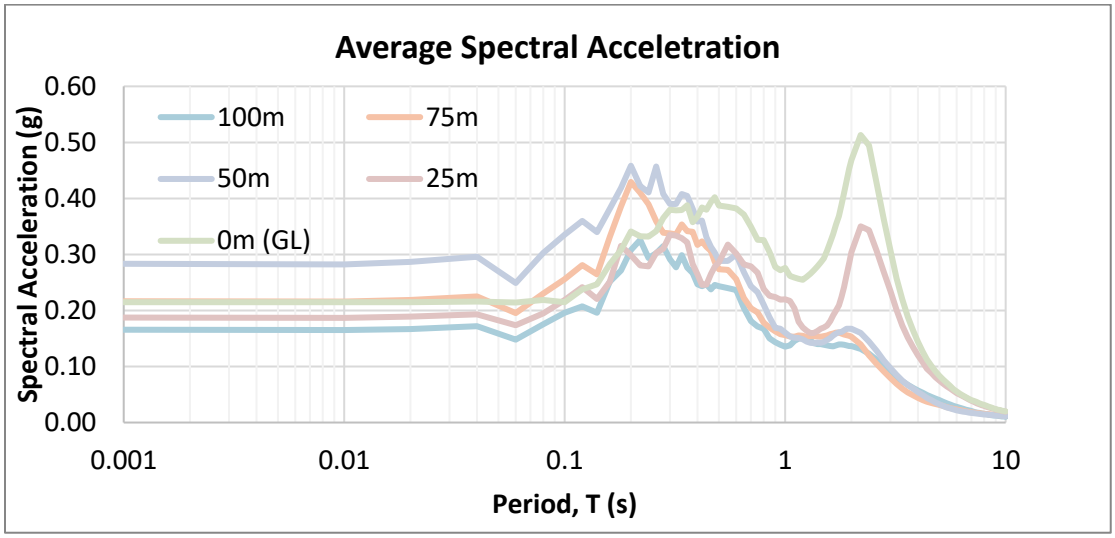

Figure 4-33: Average Spectral Acceleration- right zone of section C-D

Spectral amplification corresponding to its frequency content can be well represented through the spectral ratio parameter, which is the ratio of the spectral ordinate at the target location to the spectral ordinate of the input motion.

4.8.2 Spectral Ratio - Section C-D

Spectral ratio plots clearly show the amplification or attenuation of response spectrum at each period level with respect to the response spectra of the input motion. The calculated spectra ratio of the three zones discussed in the previous section are shown in Figure 4-34, Figure 4-35 and Figure 4-36. As illustrated in these figures of spectral ratio, the peak ground acceleration observed in the base of the model is 50~60% of the peak acceleration of the incoming motion. As explained in the previous chapter, the input acceleration history is converted as stress field and applied at the base of the model as shear stress to represent

the vertically propagating shear wave condition. By doing this, the motion of the zones and grid points of the model is allowed to vibrate freely to represent the actual field condition. As a result, the recorded base acceleration histories are not required to match exactly as the input acceleration because the recorded base acceleration will be the superposition of resultant input and reflected earthquake wave. This difference is clearly observed in the peak acceleration observed in spectral ratio plot where the base model has the ratio less than 1. However, the spectral amplitude in the range of 1s~10s shows higher spectral ratio and particularly the peak of up to 8 time the input spectral acceleration values are recorded at period values in the range of 2.5 to 3.5s range.

The ratio of peak acceleration was essentially one or less than one at all locations indicating there was no amplification in terms of the peak ground acceleration. This is anticipated since the layer is fairly deep and thus would have a relatively large fundamental period. Using the $4H/V_s$ approximation the fundamental period of this would be about 2 seconds. This also explains the large amplifications noted at the long period range values, especially around 2 to 4s period range.

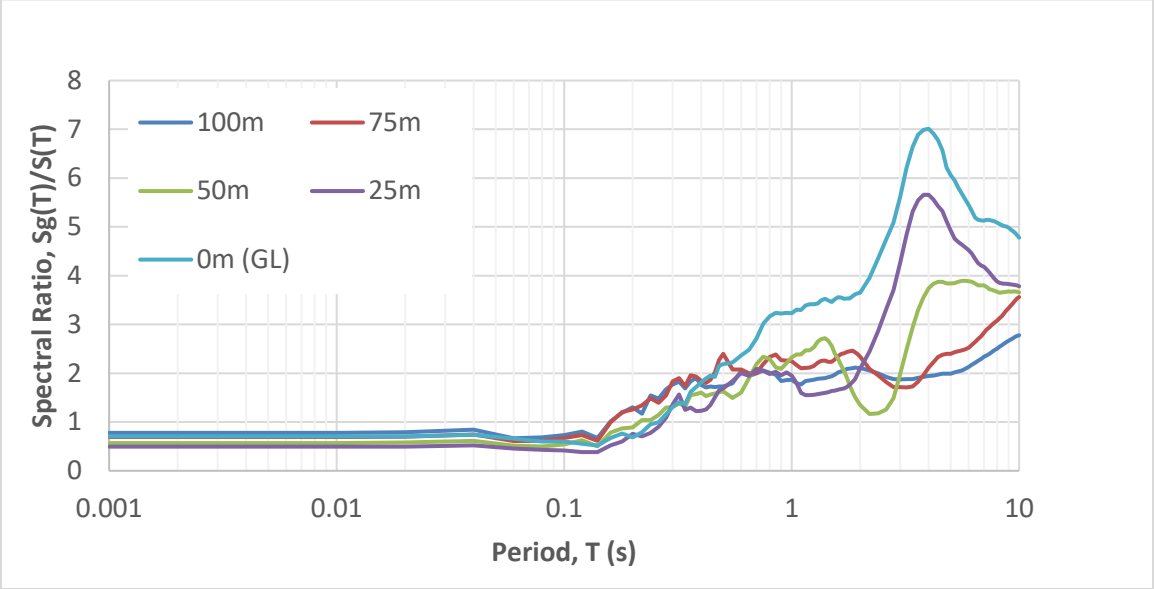

Figure 4-34: Spectral Ratio, Sg(T)/S(T) – Left zone of section C-D

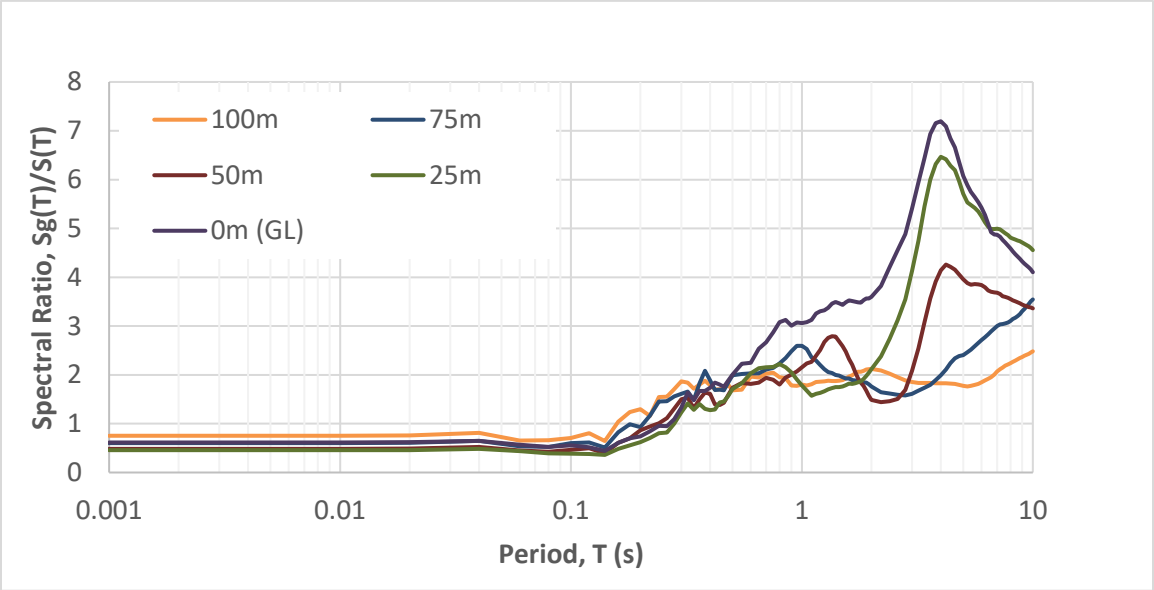

Figure 4-35: Spectral Ratio, Sg(T)/S(T) – Middle zone of section C-D

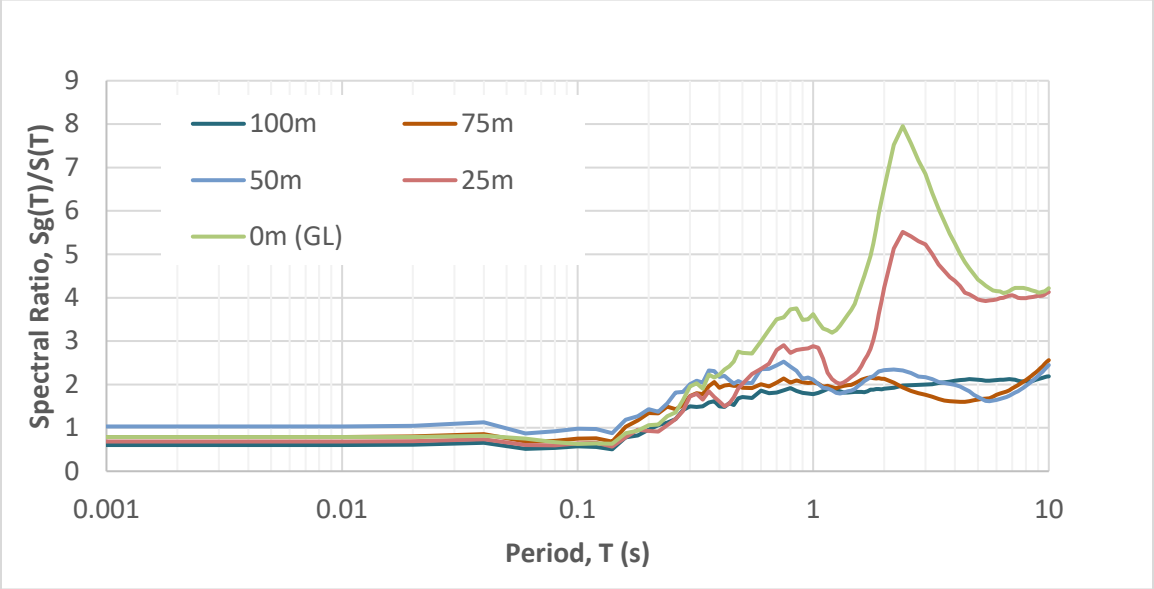

Figure 4-36: Spectral Ratio, Sg(T)/S(T) – Right zone of section C-D

4.8.3 Spectral Acceleration - Section A-B

Similar to section C-D, three locations along the longitudinal span are selected for the spectral analysis to assess the response within section A-B. Response spectra are generated from the response acceleration time history recorded in each of these three locations at five different elevations as discussed earlier (100m -base of the model, 75m, 50m, 25m and 0m -ground level) are shown in Figure 4-37, Figure 4-38 and Figure 4-39.

The bedrock location of the left zone is at 20m concave downwards with a slope of 1:200, for the middle zone the rock at 80m fairly flat and for the right zone the rock is at 50m from the ground level with the slope of 1:5.

The amplitudes of higher spectral accelerations observed in this case are similar to the observations in the section C-D in that the strongest spectral amplitudes are observed in

the period range of 0.2s~3s. However, the peak ground acceleration in all three locations shows amplification compared to the base spectral values. It is also observed that the amplification increases when the wave reaches towards ground surface, and higher spectral values are recorded at the ground level. This observation stands different from the one observed in section C-D where the wave in the first quarter and third quarter amplified and attenuated, and again amplified when it reaches ground surface. However, the middle zone of section C-D attenuated compared to the base acceleration.

Again, the spectral ratios of each of these spectral plots against the input motion will represent the actual frequency of motion where the amplification or attenuation happens within the model and permits an assessment of the site characteristics.

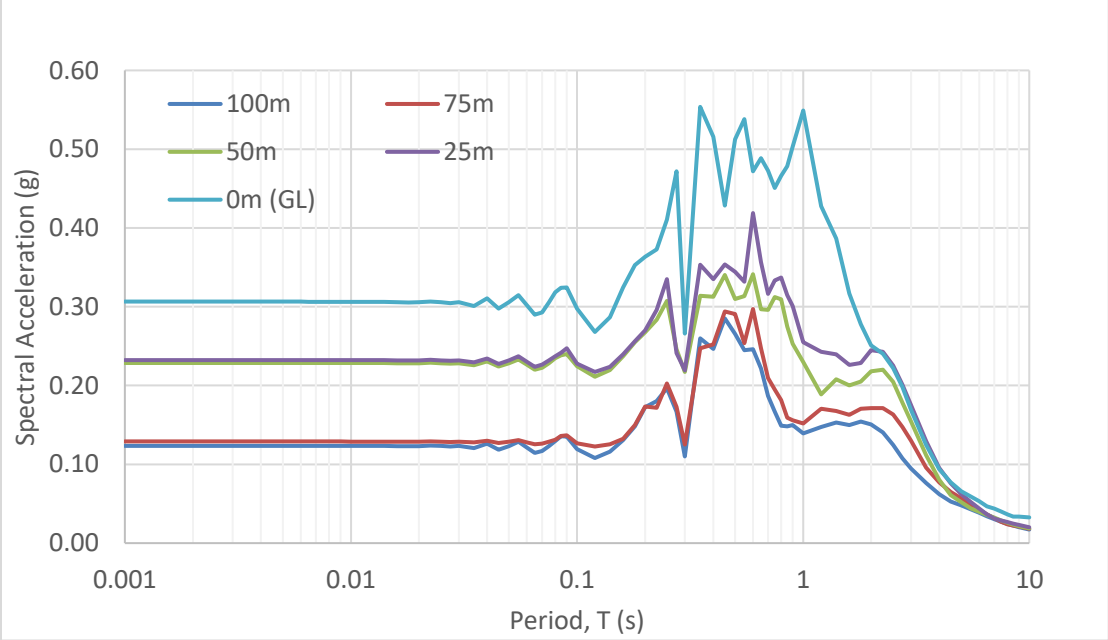

Figure 4-37: Spectral Acceleration – Left zone of section A-B

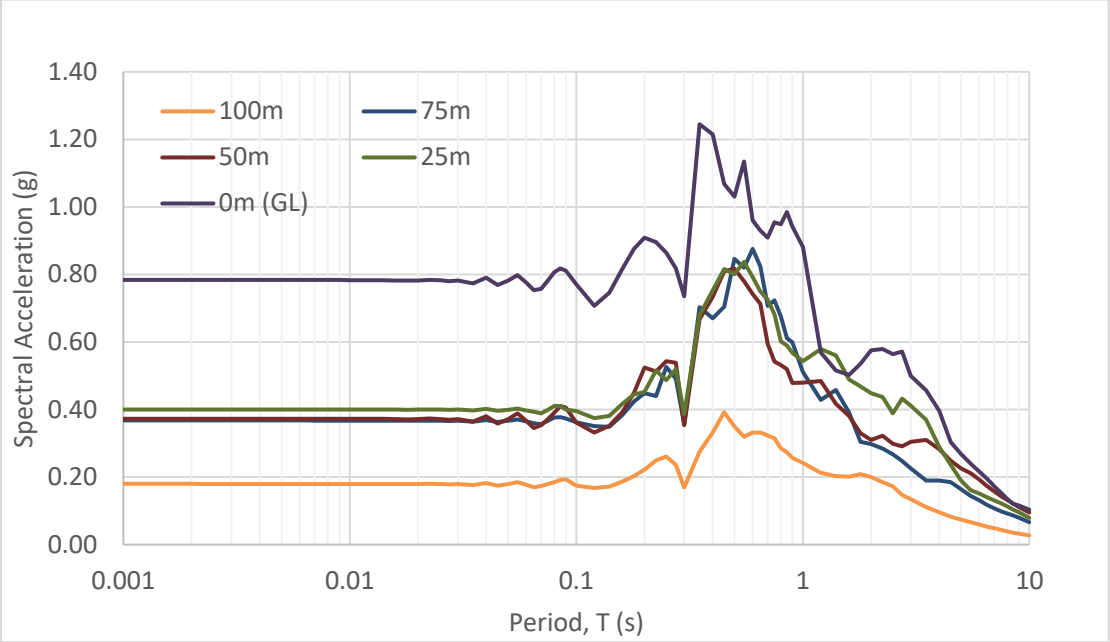

Figure 4-38: Spectral Acceleration - Middle zone of section A-B

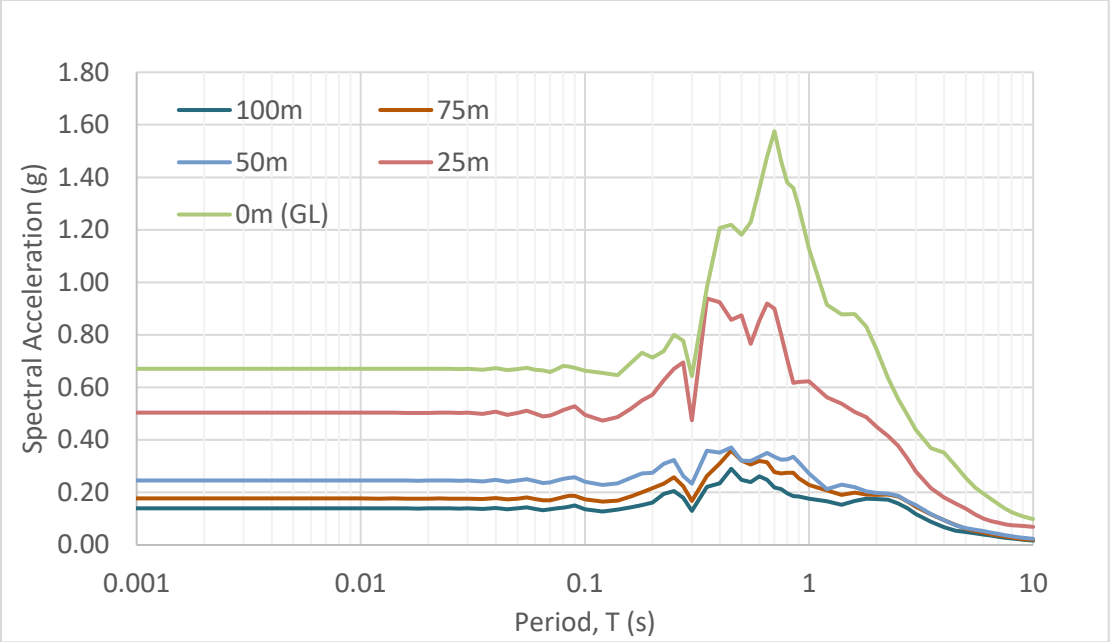

Figure 4-39: Spectral Acceleration – Right zone of section A-B

4.8.4 Spectral Ratio – Section A-B

Similar to the section C-D, the peak accelerations of each section at the base are not same as the input acceleration. Peak accelerations observed at the base is about 45~55% of the input peak acceleration. As explained, this might be due to the superposition of input motion and reflected motions. The calculated spectra ratio of the three zones with five different elevations are shown in Figure 4-40, Figure 4-41 and Figure 4-42. Again, the spectral ratios are about or less than one up to a period of about 0.3s, and then they increase rapidly to reach a peak at a period of about 1s. Following some reduction in amplification ratio beyond one second (in some case) the ratios again increase significantly towards 10s period. Section AB shows that quite a long range of frequencies get amplified where spectral amplification observed from 0.3s onwards up to 10s. The first peak spectral amplification of up to 18 observed around the period of 1s and second peak amplification observed up to 22 around the period 10s. The strong amplification of the 10s motion is not typically observed in simple one-dimensional analysis. It was not present in the 2-D analysis of section C-D either. The highest value of the spectral ratio, i.e., the amplification, is quite large in section A-B compared to the peak spectral ratio observed in section C-D. Also, the amplification gets reduced after the period of 1s in section C-D where the section C-D shows another peak even more amplification than the first at 10s. These observations might be due to the geological effect of section A-B and section C-D where the section C-D is a fairly smooth concave shape compared to the section A-B which has a very steep

rock-soil interface. As a result, more focusing the earthquake energy towards the soil deposit at the center of the valley, and large number of reflections on the soil-rock interface.

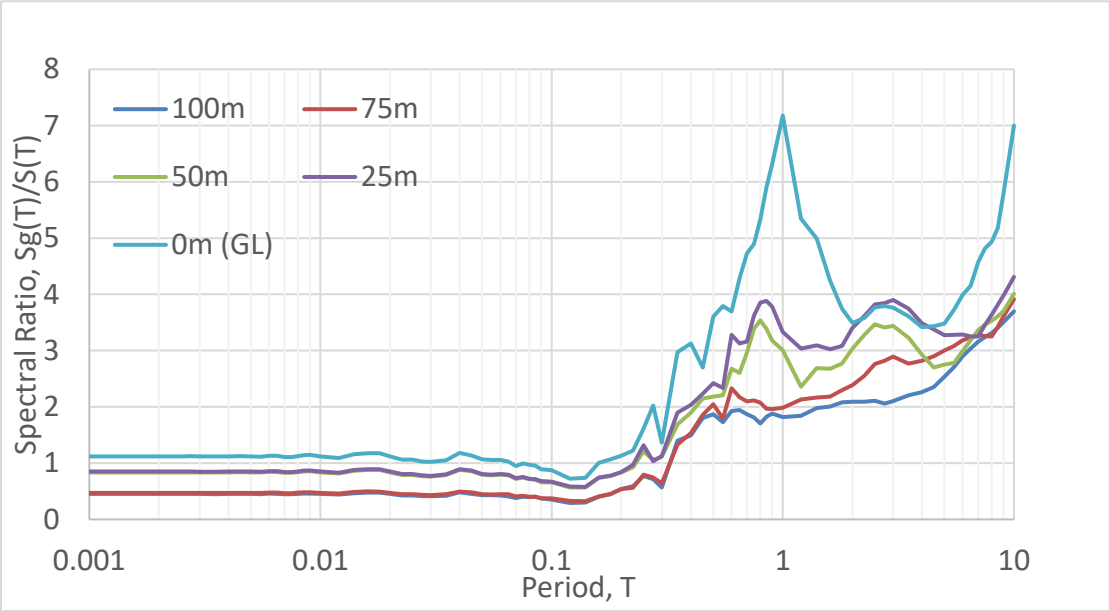

Figure 4-40: Spectral Ratio, Sg(T)/S(T) – Left zone of section A-B

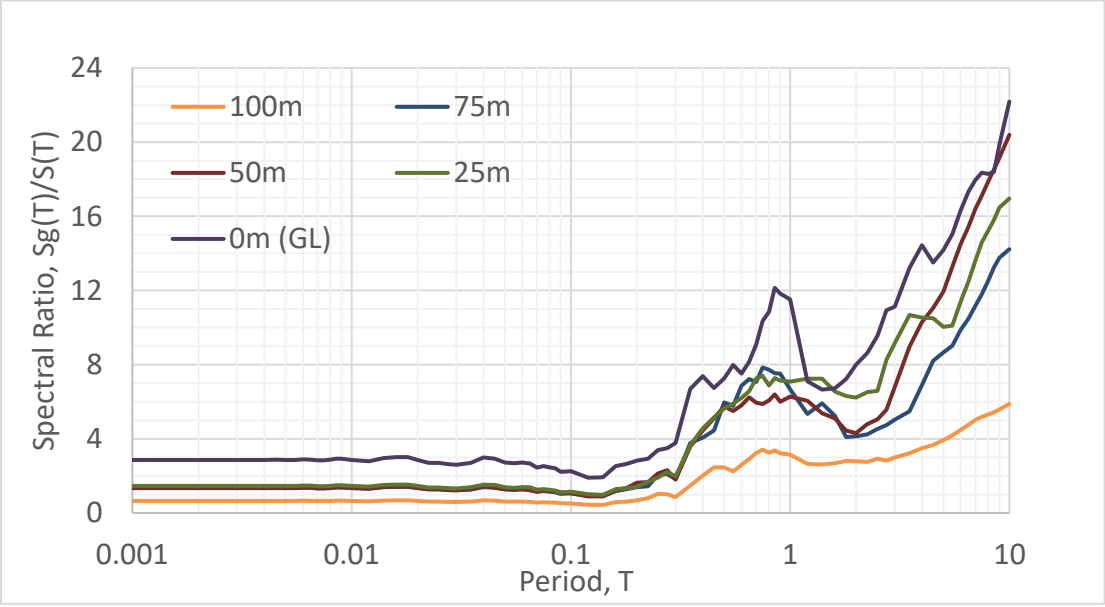

Figure 4-41: Spectral Ratio, Sg(T)/S(T) – Middle zone of section A-B

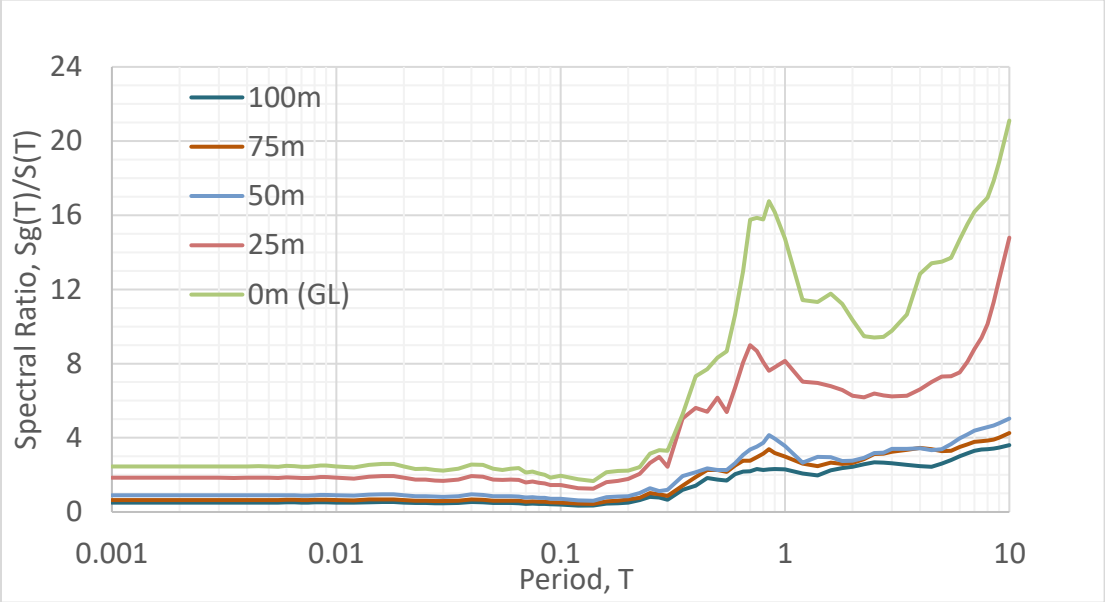

Figure 4-42: Spectral Ratio, Sg(T)/S(T) – Right zone of section A-B

4.8.5 Maximum Horizontal Acceleration

The maximum horizontal acceleration within the soil deposit throughout the motion of earthquake is filtered for each zone and illustrated in the images below. Variation is section C-D is shown in Figure 4-43, and that in section A-B in Figure 4-44. The zones representing the rock are excluded as the primary interest is on the soil deposit. In both sections there is a possibly a small portion of numerical inaccuracies that can be observed at a small region where the accelerations show sudden high amplitudes compared to the adjacent zones.

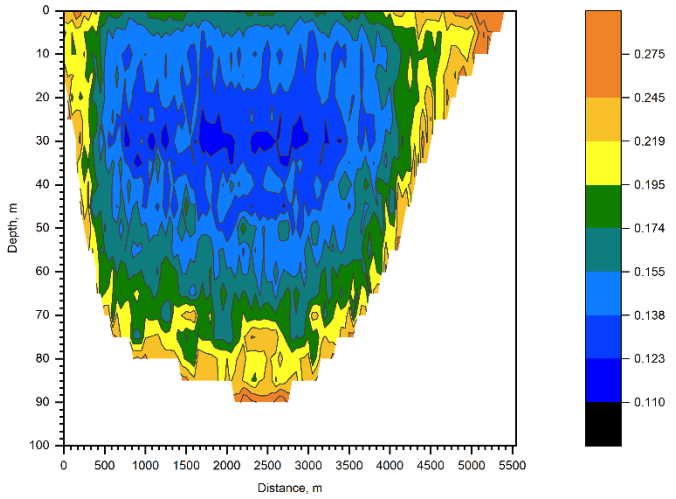

Figure 4-43: Variation of Peak horizontal acceleration of six artificial earthquake records on the Orleans profile of Section C-D

Those unrealistic spikes are deemed numerical artifact, and have not been considered in assessing the implications of the results. This would give a better picture of variations of the peak horizontal accelerations, and it is noted that the magnitudes range from about 0.11g to 0.275g for the section C-D, but the range varies from 0.22g to 1.22g for section AB. The high values in section A-B, the peak horizontal accelerations exceeding about 0.6g are at the zones located near the rock soil interface. The peak horizontal acceleration and it reduces towards the center of the valley deposit. For section C-D, the soil-rock interface acceleration varies from 0.219g to 0.275g and it reduces towards the center to 0.11g. For section A-B, the soil-rock interface acceleration values range from 0.64g to 1.22g and it reduces to 0.22g at the center.

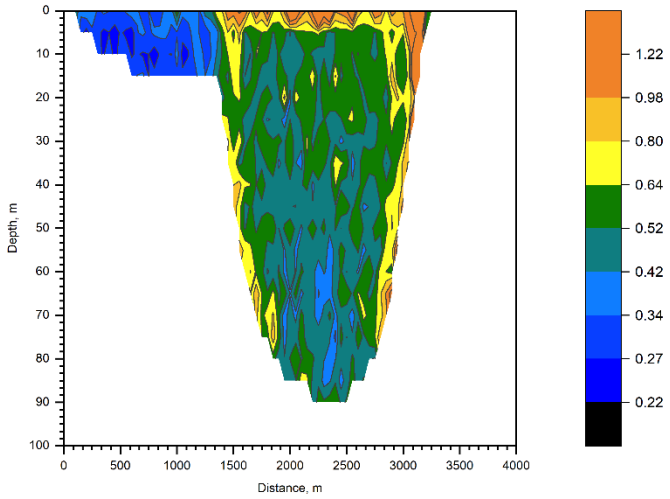

Figure 4-44: Variation of Peak horizontal acceleration of six artificial earthquake records on the Orleans profile of Section A-B

Generally, the peak horizontal accelerations recorded in in the section C-D are lesser than the input peak horizontal acceleration of 0.274g except the boundaries of soil-rock interface. However, the boundary elements showed almost similar amplitude of acceleration of 0.275g compared to the input peak acceleration.

But, in contrast to this section A-B shows larger amplification on the maximum peak acceleration except at the center of the valley and few zones near ground level. A possible reason for such drastic differences is postulated to be the shape of the valley. In analysis with horizontal profiles the reflected waves would go back to the base at 100m depth before reflecting back. In the case of section C-D some of the reflected waves would hit the rock at shallower depths, and in the case of section A-B, most of the reflections are not going down to the base. They reflect within the valley deposit, back and forth, and get stagnant

there. This is a worst-case scenario of the wave trapping phenomena, and as a result, higher amplifications obtained in section A-B are realistic.

4.8.6 Absolute value of Shear Stress Increment

In typical seismic analysis, the maximum shear stress increment corresponds to the maximum horizontal acceleration, since the seismic loading is presumed to only apply shear stresses on the horizontal plane. But, in the 2-D analysis undertaken in this study, the soil elements are subjected to both normal stress changes, and a shear stress changes on the horizontal plane. Thus, the maximum shear stress increment will not correspond to the shear stress increment on the horizontal plane.

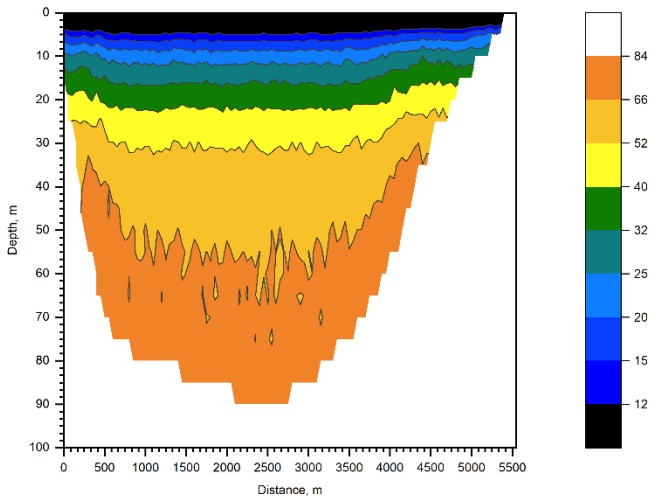

Figure 4-45: Variation of Average Shear Stress Increment (abs value) of six artificial earthquake records on the Orleans profile of Section C-D

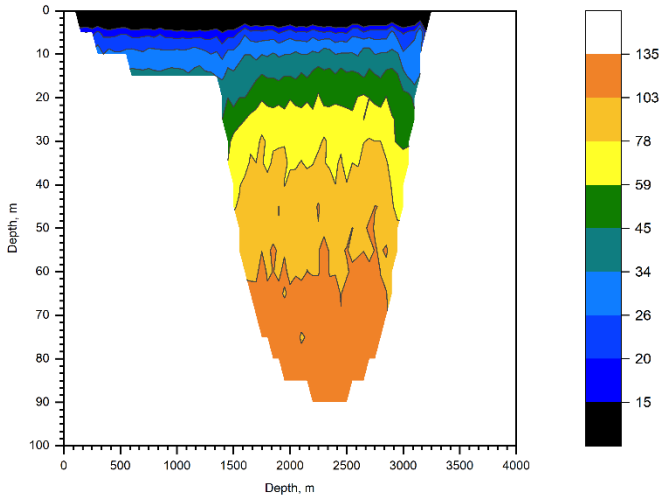

Figure 4-46: Variation of Average Shear Stress Increment (abs value) of six artificial earthquake records on the Orleans profile of Section A-B

The maximum shear stress increment is calculated in each zone using the concepts illustrated earlier using Mohr circle, and are illustrated in Figure 4-45 and Figure 4-46 for the soil deposit. Maximum shear stress increment observed at the base of the section C-D model is up to 84 kPa and it reduces in the shallow layers and reach to zero stress at the ground surface. The zero-stress obtained at the ground surface is consistent with the compatibility requirements of stress relationship at the free surface.

Similar observations are recorded in section A-B but the shear stress increment at the bottom of the soil deposit shows the maximum of 135kPa and it reduces in the shallow layers and become zero at the free surface. Even though both sections show similar pattern in the variation of shear stress increment, the magnitude is 75% more in section A-B

compared to the magnitude recorded in section C-D. Again, this variation is attributed to the narrow valley profile of A-B comparing section C-D.

4.8.7 Average CSR of 6 artificial earthquakes

Cyclic stress ratio (CSR) is a parameter that is used to understand the severity of the shear stress increment on soil deposit due to an earthquake motion, and to assess the potential for soil liquefaction. It is defined in different ways depending on the engineering application, and the characterization method used. In triaxial condition, the CSR is defined as half the cyclic the deviatoric stress divided typically by the minor principal stress, or by the average effective stress (Vaid et al., 2001) if an attempt is made to be consistent with the simple shear definition to the extent possible (i.e., $CSR = (\sigma_1 - \sigma_3)/(\sigma'_{1c} + \sigma'_{3c})$ or $CSR = (\sigma_1 - \sigma_3)/2\sigma'_{3c}$ under triaxial loading). But in simple shear condition, the CSR is defined as the cyclic shear stress on the horizontal plane divided by the vertical consolidation stress. Prasanna (2020) proposed the use of Horizontal stress ration (HSR) to refer to the ratio of shear stress on the horizontal plane to the effective stress, and cyclic stress ratio (CSR) to refer to the ratio of maximum shear stress (i.e., half the deviatoric stress) by the mean effective stress. Technically the cyclic stress ratio computed under simple shear loading represents the HSR and that under triaxial loading represents the CSR. The CSR is calculated from the maximum shear stress increment divided by the initial vertical effective stress. Because during dynamic shaking the maximum value of shear stress happens only

at one instant, and thus it is factorized to obtained an average value that represents the entire duration of the loading.

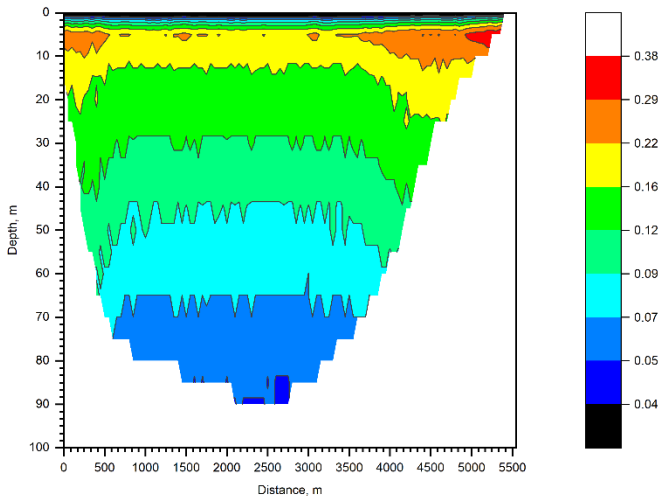

Figure 4-47: Variation of Average CSR of six artificial earthquake records on the Orleans profile of Section C-D

Similar to the Seed's simplified method of finding equivalent shear stress from peak ground acceleration, a factor of 0.65 is used to get the representative shear stress increment from the actual maximum shear stress recorded during the duration of applied earthquake motion.

The value of CSR is computed as per the recommendation of Prasanna (2020), and shown in Figure 4-47 and Figure 4-48 for section C-D and A-B respectively. It is fairly small at depth, and the highest just below the ground surface. It is generally less than 0.5. CSR is 0.5 means that the increment in shear stress is equal to half of the initial vertical effective stress.

According to the shear stress results observed from the FLAC 2-D analysis of section A-B and C-D of Orleans profile, section A-B shows CSR values for all the applied earthquakes. Figure 4-47showing the distribution of CSR for the section C-D. Each artificial earthquake applied individually to the model and analyzed to get the variations and got the average plot as shown. Here the CSR values varies from 0.05 to 0.38 and it is high near ground surface. The peak value range of 0.29 to 0.38 is only observed at the interface of soil and bedrock near the ground level. Next higher values of 0.16 to 0.29 observed are from 5 to 15m elevation from the ground surface. Below 15m up to 30m depth, the values vary between 0.12 to 0.16.

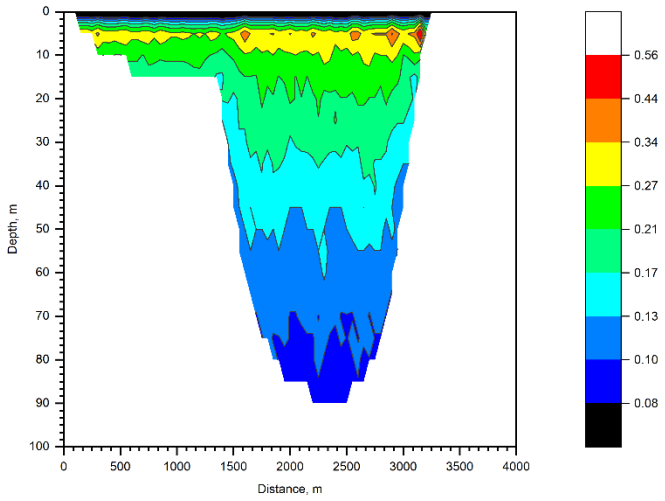

Figure 4-48: Variation of Average CSR of six artificial earthquake records on the Orleans profile of Section A-B

In general, the CSR values reduce with depth but near the rock soil interface the values are slightly higher compare to the values observed in the middle of the soil layer. Reduction of CSR with depth is due to the increase in overburden confining stress coming from the top soil layers where the overburden pressure getting larger with depth. However, the soil bedrock interface shows an increased value compare to the middle soil layers at the same elevation is may cause due to the influence of rock motion.

Although section A-B shows the similar variation as section C-D in terms of reduction in CSR with depth, the values are higher in each layer in section A-B due to the narrow valley deposit. As shown in Figure 4-48, the largest CSR in section A-B is about 0.44 and it occurs at a depth of about 5m (CSR larger than 0.44 is also noted but it is not taken into consideration because it is limited to very few zones). Overall, most portions of the 5m to 15m layer are subject to CSR of at least 0.27. The high value of CSR in section C-D is about 0.29, and the comparable range of CSR in the 5-15m layers in C-D is in the range of 0.27 to 0.16. In the horizontal bedrock model, the CSR in the 5-15m layer varies from 0.15 to 0.23. Table 4-4 summarizes the variation of CSR values from the analysis using artificial earthquakes in same layers of section A-B and C-D against horizontal bedrock model and confirm the importance of the geological change on seismic analysis.

Table 4-4: Comparison of average CSR values observed for all size artificial earthquakes in among section A-B and section C-D s of Orleans profile

Depth of Layer from GL	CSR in Horizontal bedrock Model	CSR in Section C-D	CSR in Section A-B
5~15	0.23~0.15	0.29~0.16	0.44~0.27
15~30	0.15~0.1	0.16~0.12	0.27~0.21
30~45	0.1~0.08	0.12~0.09	0.21~0.17
45~60	0.08~0.07	0.09~0.07	0.17~0.13
>60	<0.07	<0.07	<0.13

4.8.8 Comparison of artificial and real earthquake effects

The results presented previously considered the response due to spectra matching input time histories, or 'artificial' earthquakes. As discussed earlier these were generated according to the design spectrum for the local site. While their use is widespread in seismic analysis for geotechnical purposes, it is preferable to analyses the response of the sites to real earthquake motions since such motion capture the anticipated frequency content better. Two components of the Val-des-Bois earthquake motion were used as two separate time histories to assess the response of the soil profiles along sections A-B and C-D. The E-W motion is called motion R1 and the N-S record motion R2. The CSR computed from the response of section C-D is shown in Figure 4-49 and Figure 4-50 for input motions R1 and

R2 respectively. The CSR values reach about 0.3 for motion R1, and about 0.24 for R2. It should be noted that the scaling used to obtain the motions was not the simpler PGA scaling and thus R1 and R2 have different peak accelerations. The PGA of R1 is 0.032g and R2 is 0.033g, and that plays a key role on the resulting CSR. The scaling considering the spectral periods, as computed in this research, is considered to yield better and more representative deformation characteristics of the soil deposit. The nature of the CSR variation is similar in both earthquake time histories, and the trends are very comparable to those obtained using the artificial records in the previous sections. This similarity in the variation of observed CSR for the Val-des-Bois Earthquake recorded at station OT012 for both North-South (R2) motion and East-West (R1) motion is shown in Table 4-5 and compared to the average values obtained from the artificial motions.

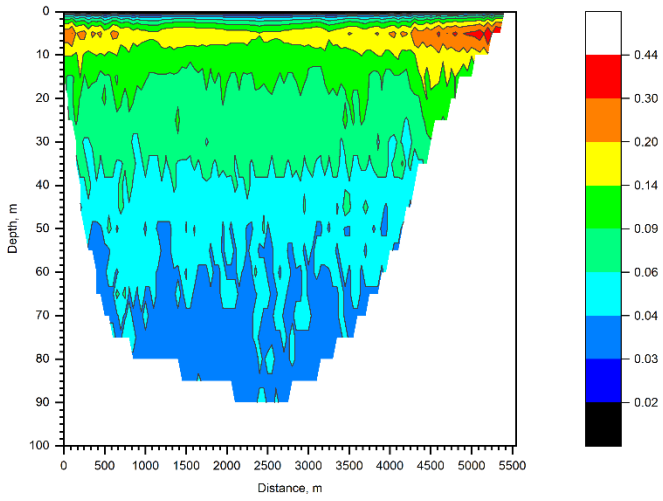

Figure 4-49: Variation of CSR for the Val-des-Bois E-W motion records on the Orleans profile of Section C-D

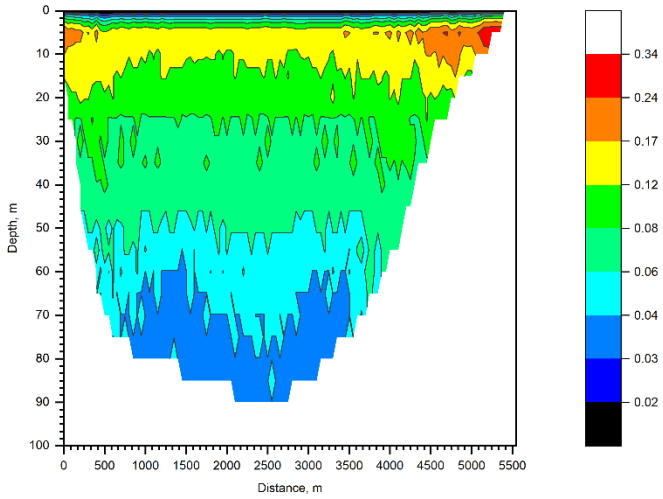

Figure 4-50: Variation of CSR for the Val-des-Bois N-S motion records on the Orleans profile of Section C-D

Table 4-5: Comparison of average CSR values observed from artificial earthquake and E-W motion and N-S motion of Val-des-Bois in section C-D of Orleans Profile

Depth of Layer from GL	CSR due to Artificial Earthquake	CSR due to Val-des-Bois E-W	CSR due to Val-des-Bois N-S
5~15	0.29~0.16	0.30~0.14	0.24~0.12
15~30	0.16~0.12	0.14~0.09	0.12~0.08
30~45	0.12~0.09	0.09~0.08	0.08~0.06
>45	<0.09	<0.08	<0.06

However, the East-West motion had comparatively severe effects than North-South directional motion and the distribution of artificial earthquake records being in the middle of both motions if we compare the maximum values. However, it's a small portion of top layers showing higher CSR values in red band may be due to higher shear stress development at some localized regions or it may be numerical latent. As the region is small compare to other regions, it can be ignored. Except to that, the variation of CSR from the artificial earthquake slightly higher than the values observed from the real earthquake.

The response of section A-B is shown in Figure 4-51 and Figure 4-52. There were difficulties running the analysis with section A-B subjected to the N-S motion (motion R2). FLAC grids had to be re-generated due to large deformations which were not present in the prior analysis. Very large CSR values, as high as 5, which are quite unrealistic were obtained from the analysis for large portions of the soil deposit. Similar to Table 4-5, the variation observed from the seismic analysis using Val-des-Bois N-S component at station OTT 12 as earthquake input motion as shown in the Table 4-6. The reasons for the drastic departure of the response for this combination of soil profile (A-B) and the time history (N-S) are unknown at this time. It is speculated that it may be due to issues with the incompatibility of the numerical routines in FLAC that implement the hysteretic damping and the re-meshing algorithms.

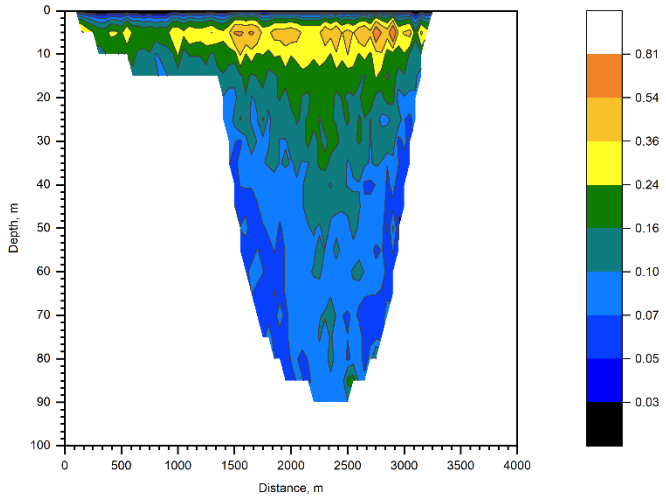

Figure 4-51: Variation of CSR for the Val-des-Bois E-W motion records on the Orleans profile of Section A-B

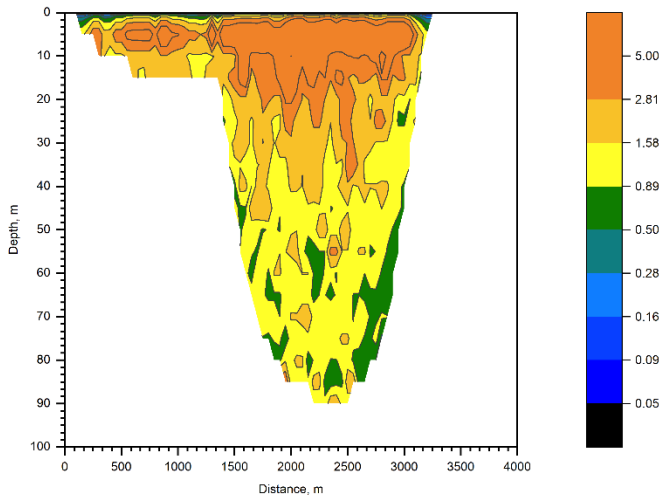

Figure 4-52: Variation of CSR for the Val-des-Bois N-S motion records on the Orleans profile of Section A-B

Table 4-6: Comparison of average CSR values observed from artificial earthquake and E-W motion and N-S motion of Val-des-Bois in section A-B of Orleans Profile

Depth of Layer from GL	CSR due to Artificial Earthquake	CSR due to Val-des-Bois E-W motion	CSR due to Val-des-Bois N-S motion
5~15	0.44~0.27	0.54~0.24	>5
15~30	0.27~0.21	0.24~0.16	5~2.81
30~45	0.21~0.17	0.16~0.10	2.81~1.58
>45	<0.17	<0.1	<1.58

Table 4-7: Comparison of maximum horizontal acceleration due to E-W and N-S motion of Val-des-Bois in sections C-D and A-B of Orleans Profile

Location	Section C-D		Section A-B	
	Val-des-Bois EW motion	Val-des-Bois NS motion	Val-des-Bois EW motion	Val-des-Bois NS motion
GL (at 0m)	0.18g~0.13g	0.13g~0.11g	25.8g~4.36g	>17.78g
Shallow layers up to 30m	0.18g~0.07g	0.13g~0.08g	8.88g~3.05g	>17.78g
Rock-soil interface	0.82g~0.24g	0.19g~0.11g	25.8g~8.88g	>17.78g

Table 4-8: Comparison of maximum shear stress due to E-W and N-S motion of Val-des-Bois in sections C-D and A-B of Orleans Profile (in MPa)

Location	Section C-D		Section A-B	
	Val-des-Bois EW motion	Val-des-Bois NS motion	Val-des-Bois EW motion	Val-des-Bois NS motion
5~15	8~24	4~22	10~72	>564
15~30	24~32	15~30	33~72	>564
30~45	24~42	22~42	33~107	>564
>45	32~72	30~59	33~235	>564

In summary, the results presented above show reasonable response in all cases (except the case of Val-de-Bois N-S motion applied to cross section A-B). The cyclic shear stress variation among both sections of A-B and C-D clearly shows the effect of geology on seismic analysis. Also, the results obtained from both real and artificial earthquake gives the confidence on the analysis using the artificial earthquakes that are generated from the design spectra for the local site.

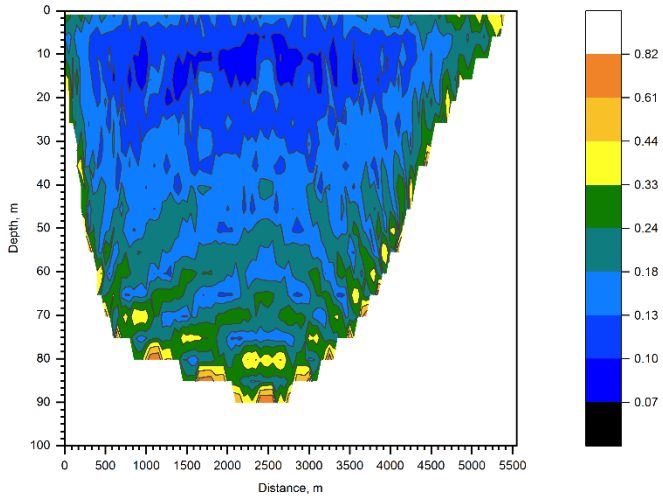

Figure 4-53: Variation of Maximum Horizontal Acceleration for the Val-des-Bois E-W motion records on the Orleans profile of Section C-D

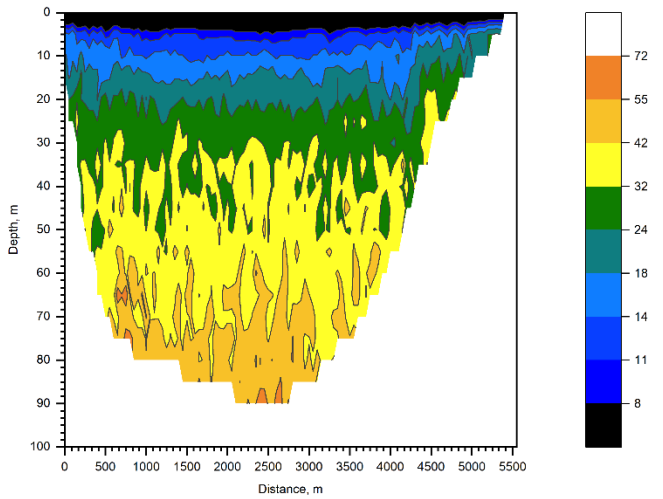

Figure 4-54: Variation of Maximum shear stress increment for the Val-des-Bois E-W motion records on the Orleans profile of Section C-D

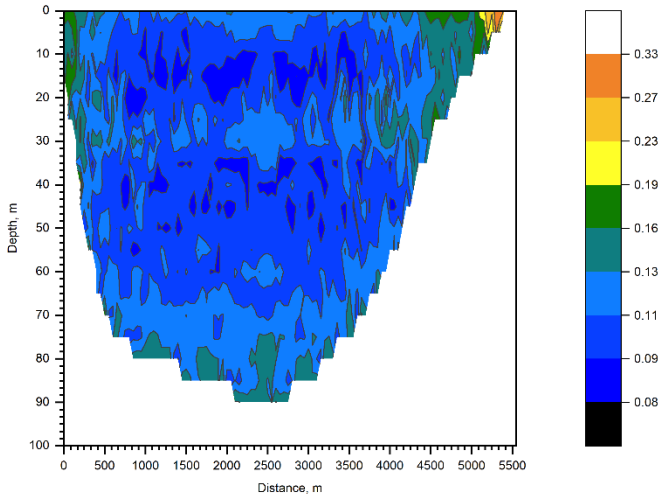

Figure 4-55: Variation of Maximum Horizontal acceleration for the Val-des-Bois N-S motion records on the Orleans profile of Section C-D

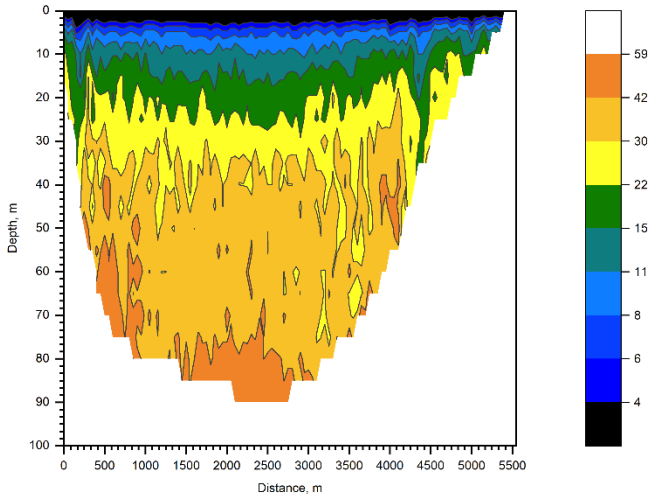

Figure 4-56: Variation of Maximum shear stress increment for the Val-des-Bois N-S motion records on the Orleans profile of Section C-D

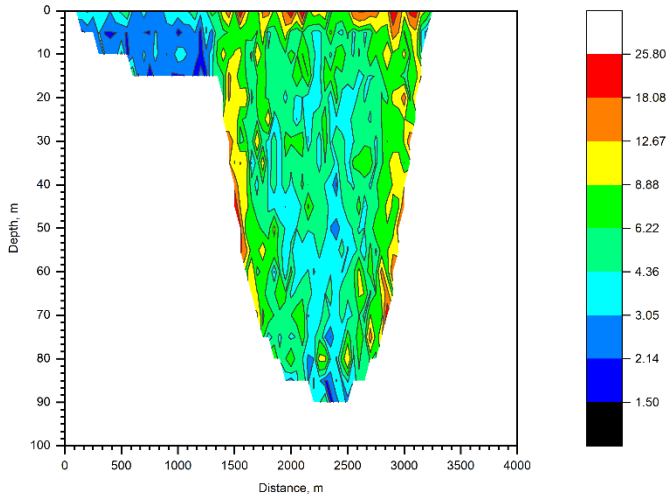

Figure 4-57: Variation of Maximum Horizontal acceleration for the Val-des-Bois E-W motion records on the Orleans profile of Section A-B

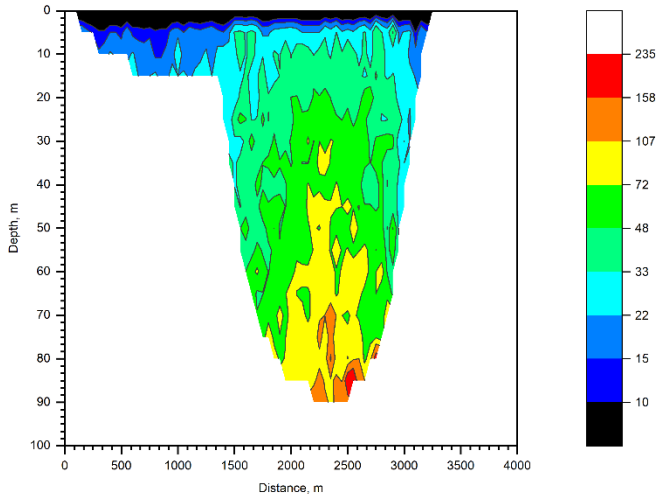

Figure 4-58: Variation of Maximum shear stress increment for the Val-des-Bois E-W motion records on the Orleans profile of Section A-B

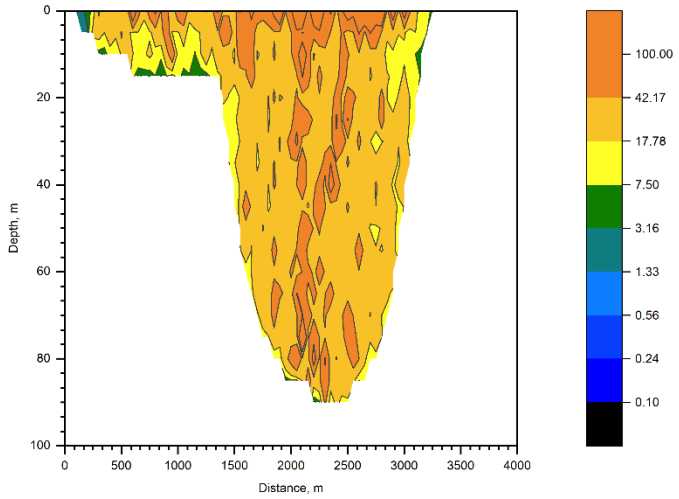

Figure 4-59: Variation of Maximum Horizontal Acceleration for the Val-des-Bois N-S motion records on the Orleans profile of Section A-B

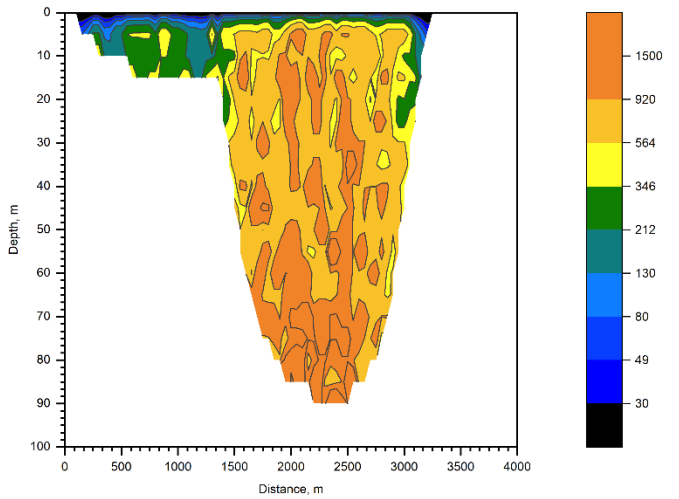

Figure 4-60: Variation of Maximum shear stress increment for the Val-des-Bois N-S motion records on the Orleans profile of Section A-B

CHAPTER 5

SUMMARY AND CONCLUSION

5.1 SUMMARY

The influence of basin geometry on seismic amplifications in Leda clay is studied in this research to assess the implications of the simplifying assumptions made in current design practice. The seismic response of a site is complicated and depends on both material properties and input motion characteristics. A local site with about 94m thick soft Leda clay deposit at the centre was modelled. Two perpendicular cross sections at the site, one with moderate inclinations of soil-bedrock interface (Section C-D), and another with somewhat steeper soil-bedrock interface inclinations (Section A-B), were considered in the 2-D analysis.

The bedrock at the Orleans valley site is concave shaped with a basin that is roughly 5.5km × 4.0km at ground surface, and 94m deep. A 100m deep rectangular model was considered in the analysis to facilitate the application of vertically propagating shear waves at the bottom bed-rock boundary. These configurations represent bed rock inclinations in the range of 3° to 12° which are often considered rather minor, and approximated as horizontal. Wave reflection and refraction effects due to non-normal incidence at the sloping soil-bedrock interface leads to behaviour different than the one typically considered in practice (which assumes a horizontal bedrock and normal incidence). The non-normal incidence leads to simultaneous shear and compression wave loading in soils whereas current practice

only considers the shear loading. The properties of the clay were considered to be a function of depth at the site and obtained from the literature. The relatively low impedance of the soft Leda clay and the high impedance of the bedrock lead to a large impedance contrast at the site, which leads to the wave trapping phenomenon.

The response of the Orleans valley is modelled with its 2-dimensional soil bedrock interface due to a number of input motions, both artificially generated and recorded during the 2010 Val-des-Bois earthquake, was assessed and analyzed. Also, a horizontal bedrock model was created to validate the FLAC output against the 1-dimensional analysis from ProShake, and also to compare the response of geological basin effects. The response of the two sections compared to the horizontal bedrock model highlight the effects of basin geometry on seismic amplifications.

Analysis and comparison of seismic response focussed on peak values of shear stress increment, horizontal accelerations and cyclic stress ratio at various locations within the soil deposit. Also, response spectra are used to compare the acceleration response, and spectral ratio method is used to compare the amplification or attenuation of earthquakes.

5.2 Conclusions

Bedrock geometry effects lead to cyclic changes in both the shear stress on the horizontal plane, and the vertical and horizontal normal stresses. The changes in normal stresses are caused by p-waves, and in shear stresses by s-waves. The Rayleigh wave effect of the incoming motion in the surface layers due to reflection and refraction on nonlinear soil

bedrock interface showed more prominent variation in seismic response compared to 1-dimensional analysis. The differences were a function of the bedrock-soil interface inclination and basin geometry. Following conclusions are derived from the observed outputs of the numerical analysis.

1. The numerical 2-D model developed in FLAC yields results that are somewhat different at specific periods but overall comparable to those obtained in 1-D equivalent linear analysis in ProShake. Observations showed a close match of peak acceleration and spectral amplitudes at short period values. However, the FLAC analysis showed 30%~35% increased values compare to ProShake spectral accelerations at moderate to long period. These differences are due to the fundamental difference of analysis between these two packages where FLAC is time domain analysis and ProShake is frequency domain analysis. The observations of higher spectral amplitudes in FLAC compared to SHAKE are in alignment with the findings of other researchers in the literature assessing different soils.

2. Effects of geology on the seismic analysis appears to be an important factor. Amplification of peak ground motion, shear stress increment and cyclic stress ratio (CSR) vary considerably between 1-D and 2-D analysis, and with the basin geometry in 2-D analysis. The maximum values of these quantities recorded within the soil deposit are shown in Table 5-1 considering the response to the artificial time histories, and the recorded East-West motion during the Val-des-Bois earthquake. The table

shows that the 2D bedrock profile results in larger peak horizontal accelerations and larger cyclic stress ratio values.

Table 5-1: Summary of seismic response between 1-dimensional horizontal bedrock model and 2-dimensional concave bedrock model

Parameters	Section A-B	Section C-D	Flat
CSR	0.44	0.29	0.23
PHA	0.917g	0.275g	0.227g
$\Delta\tau_{xy}$	135kPa	84kPa	70kPa

The higher amplitudes of acceleration and CSR in 2D model compared to the flat model is a reflection of the basin geometry which focusses the earthquake energy towards the centre of the valley. Such effects cannot be captured by the simple 1-D, horizontal bedrock models.

3. Strong spectral amplitudes observed in the long period range is consistent with the deep thickness of the soft Leda clay deposit at the centre of the site. The natural site periods, $T_n = 1/(2n+1).(4H/V_S)$, will be higher in such cases on account of both the depth of the soil deposit, and the stiffness of the soft soils.
4. Peak horizontal acceleration, shear stress increment and cyclic stress ratio shows up to 1.3 times, 1.2 times and 1.2 times respectively in section C-D compared to the flat soil bedrock interface model. These observations of higher amplitudes in these parameters confirm the influence of the geological basin on seismic response. Comparison between the broad valley of section C-D and narrow valley of AB illustrates how critical is the

steepness of the slope in seismic analysis, and points to the need for establishing the basic shape as accurately as possible.

5. Steepness of the concave profiles varies between section A-B and section C-D, and clearly the soil-rock interface inclination has an effect on the response. The soil-bedrock interface in Section A-B has up to 12° inclination (1V:5H) whereas it the maximum inclination in section C-D is about 3°. The peak ground acceleration, shear stress increment and cyclic stress ratios in section A-B shows 4 times, 1.9 times and 1.9 times of the horizontally stratified model output where the values are higher compare to section C-D response. This comparison again confirms the significant impact of geology on seismic response. Particularly the steepness of the concave profile increases the vulnerability of the site against an earthquake.
6. The average response obtained from the analysis using the six artificial earthquakes, that are mathematically formulated by matching target response spectra, are relatively comparable to the of the scaled real earthquakes, except in the case of the N-S time history applied to the steep A-B section. This specific combination resulted in very large loads and deformations, and required dynamic re-meshing in the program. The results in this case were very different from all the other analysis (about 20 of them) and the reasons are unknown. It is suggested this possibly due to issues with the implementation of hysteretic damping at large strains in the program. The results of that specific case are not considered when drawing conclusions.

The response shows fairly same or slightly higher output compare to the seismic records observed from artificial earthquakes. Cyclic stress ratio observed maximum of up to 0.54 in section A-B and 0.30 at section C-D for the input motion R1. Both of these CSR values are 1~1.2 times the values obtained from the artificial earthquake records. This gives a confidence and reliability of output result analysed with the artificial earthquakes.

The differences in CSR values are a special concern since it suggests that current practice might calculate a factor of safety against liquefaction to be larger than one (based on "Flat" bedrock model), whereas in fact the true factor of safety might be less than one due to basin effects. A slight deviation from presumed horizontal bedrock profile may change the nature of wave reflection and refraction in both p- and s- waves, and could lead to different seismic response. This behavior become more evident from the response of nonlinear concave soil-bedrock interface of Orleans results in CSR as high as 0.44 at some locations but 1-D FLAC analysis would only have produced a CSR of 0.23. Again, the steepness of the basin and its depth significantly influence on the amplification of the seismic response. plays and important role in the seismic effects.

7. Typically, Leda clay does not undergo large deformations until CSR exceeds about 0.3 to 0.35 for the earthquake magnitudes expected in this region. If the CRR data in the literature for Leda clay is representative of the clays at the Orleans site then there would

be “liquefaction” is certain parts of the soil deposit which would not be detected by the conventional analysis.

8. Table 5-2 shows experimental data (Theenathayarl, 2015) on Leda clay as a function of CSR vs number of cycles to liquefaction, and lists the CSR obtained from different analysis techniques. Theenathayarl (2015) determined the behaviours at initial confining stresses of 100kPa, 200kPa and 400kPa, which would roughly translate to about 10m, 20m and 40m depth given that water table was presumed to be near the ground surface.

Table 5-2: Comparison of CSR in both 1D and 2D analysis at different stress levels against the Experimental Study done by Theenathayarl, 2015

Depth	Experimental Data		CSR from Numerical analysis		
	CSR	No of Cycles for liquefaction	FLAC 1D	FLAC 2D Section C-D	FLAC 2D Section A-B
10m	0.35	3~4	0.20	0.25	0.30
	0.3	10			
	0.25	40			
	0.2	>100			
20m	0.3	<1	0.15	0.15	0.20
	0.25	2~3			
	0.2	10			
	0.15	40			
	0.1	>100			
40m	0.25	<1	0.10	0.10	0.15
	0.2	1~2			
	0.15	40			
	0.1	>100			

A comparison of the CSR values obtained from both 1D and 2D FLAC analysis with the experimental data provides insights into the issues that could be encountered in liquefaction susceptibility assessment. There is considerable variation in the cycle stress ratio values obtained in the shallow layers depending on the numerical model (Table 5-2).

At 10m from the ground level (GL), the 1D analysis gives a CSR of 0.20, whereas the 2D analysis in section C-D results in a CSR of 0.25. Based on the experimental study done by Theenathayarl (2015), a CSR of 0.20 will not fail the Leda clay even after 100 cycles. But, a CSR of 0.25 causes liquefaction in 40 cycles. The difference is even more prominent in the 2D analysis of section A-B where the CSR is 0.30 at 10m from GL. The experimental data shows that Leda clay at 10m depth will liquefy in 10 cycles at a CSR of 0.3.

At 20m, the CSR obtained from the numerical analysis varies from 0.15 to 0.20. At this depth, a CSR of 0.2 will liquefy the soil in 10 cycles, but the soil would not liquefy until 40 cycles at a CSR of 0.15. At 40m, a CSR of 0.15 fails the soil in 40 cycles, but the soil would not liquefy at a CSR of 0.10 even after 100 cycles. As the steepness of the concave soil bedrock interface is narrower in section A-B, it shows more prominent variation in CSR values compared to the 1D analysis which assumes horizontal bedrock soil interface.

These data again emphasize that the basin geometry should be incorporated in to the numerical seismic analysis to understand the behavior of local site under an earthquake loading.

5.3 RECOMMENDATION FOR FUTURE WORK

This research study focussed on the effects of basin geometry on seismic amplification in Leda clay, and compared the results of the 2-D site response analysis with the current practice, which generally is a 1-D analysis (with presumed horizontal layering and bedrock). The 2-D analysis was conducted using a relatively simple, non-linear elastic model to facilitate comparisons with the design practice. The comparisons were assessed using horizontal acceleration, shear stress and cyclic stress ratio. However, additional factors that could be considered to enhance the understanding further could be studied in future research. The recommendations below could improve the quality of the numerical model, as well as the understanding of the basin effects.

- FLAC 2-D package is used for this numerical study as the focus was on comparing the effects of 2D bedrock profile to the typical assumption of horizontal bedrock. But, 2-dimensional modelling not sufficient to fully represent the variations of the actual field profile. A 3-dimensional analysis might be more appropriate to capture the seismic response as close as to the field response.
- FLAC analysis provides a wide range of information, and only the magnitude of the horizontal shear stress was considered in calculating the CSR this study. A more comprehensive evaluation of the stress state changes due to cyclic changes in shear

and normal stresses would provide more insights into the effects of 3-D loading conditions, and the implications of the current definition of CSR and CRR.

- Real earthquake motions are recorded in two horizontal directions (E-W and N-S) and in vertical direction. In this study, both the E-W and N-S motions of Val-des-Bois earthquake were used independently for the analysis as two different earthquakes. But the real earthquake is the combination of all three motions. A FLAC 3D model will be more suitable tool to analyse the actual earthquake effect which is the combined effect of horizontal (E-W and N-S) and vertical motions. So that the particle motion corresponding to the vertically propagating shear waves will be captured more accurately with respect to the appropriate orientation of the site.
- The soil behaviour was modelled using a non linear, total stress model in the analysis to facilitate comparisons with SHAKE. A proper elasto-plastic model under undrained condition will yield more realistic results. Such an analysis can also assess the effects of pore pressure boundary conditions in-situ (Sivathayalan & Logeswaran, 2007, 2008), and the potential for void redistribution during, or following, the earthquake and its effects on the overall stability.

REFERENCES

Abrahamson , N., & Youngs, R. (1992). A stable algorithm for regression analysises using the random effects model. *Bulletin of the Seismological Society of America, 82*(1), 505-510.

Andersen, K., Kleven, A., & Heien, D. (1988). Cyclic soil data for design of gravity structures. *Journal of Geotechnical Engineering, 114*(5), 517-539.

Ansal, A., & Erken, A. (1989). Undrained behavior of clay under cyclic shear stresses. *Journal of Geotechnical Engineering, 115*(7), 968-983.

Armen , K. D. (1980). *A response spectrum method for random viberations.*

Arthur, J., & Menzies, B. (1972). Inherent Anisotropy in a sand. *Géotechnique, 22*(1), 115–128.

Arthur, J., Chua, K., & Dunstan, T. (1977). Induced anisotropy in a sand. *Géotechnique, 27*(1), 13–30.

Atik, L., & Abrahamson, N. (2010). An Improved Method for Nonstationary Spectral Matching. *Earthq. Spectra, 26*, 601–617.

Atik, L., Abrahamson, N., & Eeri, M. (2010). An Improved Method for Nonstationary Spectral Matching. *Earthquake Spectra, 26*(3), 601–617. doi:10.1193/1.3459159

Atkinson , G., & Beresnev, I. (1998). *Compatible ground-motion time histories for new national seismic hazard maps.*

Atkinson, G., & Assatourians, K. (2010). Attenuation and Source Characteristics of the June 23, 2010 M5.0 Val-des-Bois, Quebec earthquake. *Seismological Research Letters, 81*, 849–860.

Bard, P.-Y., & Bouchon, M. (1980). The seismic response of sediment-filled valleys. Part 1. The case of incident SH waves. *Bull. Seism. Soc. Am, 70*(4), 1263-1286.

Bardet, J., Ichii , K., & Lin, C. (2000). *EERA, A computer program for Equivalent linear Earthquake site Response Analysis of layered soils deposits.* University of Southern California, Los Angeles.

Bardet, J., Ichii, K., & Lin , C. (2000). *EERA, A computer program for Equivalent linear Earthquake site Response Analysis of layered soils deposits.* University of Southern California, Los Angeles.

Bolt, B. (1999). *Earthquakes.* W.H. Freeman and Company, New York, NY, USA.

Borcherdt, R. (1970). Effects of local geology on ground motion near San Francisco Bay. *Bull. Seism Soe. Am, 60*, 29-61.

Borouchaki, H., Villard, J., Laug, P., & George, P. (2005). Surface mesh enhancement with geometric singularities identification. *Computer Methods in Applied Mechanics and Engineering, 194*(48). doi: 10.1016/j.cma.2004.11.017

Boulanger, R., & Idriss , I. (2004). *Evaluating the potential for liquifaction or cyclic failure of silts and clays.*

Boulanger, R., & Idriss, I. (2004). *Evaluating the potential for liquefaction or cyclic failure of silts and clays (p. 131).* Center for Geotechnical Modeling, Dept. of Civil and Environmental Engineering, Univ. of California, Davis.

C.M Snelson, T. M. Brocher, Miller K.C, & Pratt T. L. (2007). Seismic Amplification within the Seattle Basin, Washington State: Insights from SHIPS Seismic Tomography Experiments. *97*, 1432–1448. doi:10.1785/0120050204

Canadian Foundation Engineering Manual (4 ed.). (2006).

Carballo, J., & Cornell, C. (2000). *Probabilistic Seismic Demand Analysis: Spectrum Matching and Design.* Report No. RMS-41, 313, Stanford University, USA.

Casagrande, A., & Carillo, N. (1944). Shear failure of anisotropic materials. *J. Boston Soc. Civil Eng, 31*(4), 122–135.

Castro, G. (1969). *Liquefaction of sands.* Ph.D. thesis, Harvard University, Cambridge, Mass.

Castro, G., & Poulos, S. (1977). Factors Affecting Liquefaction and Cyclic Mobility. *Journal of Geotechnical Engineering, ASCE, 103*, 501-516.

Craig, R. (2004). *Soil mechanics.* CRC Press.

D, M., J.A, H., A, P., & H, C. (2011). Development of a Vs30 (NEHRP) map for the city of Ottawa, Ontario, Canada. *Canadian Geotechnical Journal, 48*, 458–472.

Dobry, R., & Vucetic, M. (1987). Dynamic properties and seismic response of soft clay deposits.

Drysdale, J, & Cajka, M. (1989). *Intensity Report of the November 25, 1988 Saguenay, Quebec Earthquake.* GSC Open File Report #3279.

Duncan, J., & Chang, C. (1970). Nonlinear analysis of stress and strain in soils. Journal of Soil Mechanics and Foundations Division. *ASCE, 96*(SM5), 1629-1653.

Edward , F., & Klaus, J. (1993). The Theoritical Response of Sedimentary Layers to Ambient Seismic Noice. *Geophysical Research Letters, 20*(24), 2925-2928.

Elnashai, A., & Sarno, L. (2008). *Fundamentals of earthquake engineering.* John Wiley & Sons Ltd, UK.

Erhart, T., Wolfgang, A., & Ramm, E. (2005). Robust adaptive remeshing strategy for large deformation, transient impact simulations. *International Journal for Numerical Methods in Engineering, 65*(13), 2139-2166. doi:https://doi.org/10.1002/nme.1531

Farzad , N., Arzhang , A., & Shahram Pezeshk. (2004). Selection and Scaling of Ground Motion Time Histories for Structural Design Using Genetic Algorithms. *Earthquake Spectra, 20*(2), 413-426.

Field, E. (2000). A modified ground-motion attenuation relationship for southern California that accounts for detailed site classification and a basin-depth effect. *Bulletin of the Seismological Society of America, 90*(6).

Frankel, A, W. Stephenson, & D. Carver. (2009). Sedimentary basin effects in Seattle, Washington: Ground-motion observations and 3D simulations. *99*, 1579–1611.

Frankel, A. D., D. L. Carver, & R. A. Williams. (2002). Nonlinear and linear site response and basin effects in Seattle for the M 6.8 Nisqually, Washington, earthquake. *92*, 2090–2109.

Gangsig, S., & Ohseop , S. (2016). A Time-Domain Method to Generate Artificial Time History from a Given Reference Response Spectrum. *48*(3), 831-839.

Gasparini , D., & VanMarcke, E. (1976). *Simulated Earthquake Motion Compatible with Prescribed Response Spectra.* M.I.T. Department of Civil Engineering Research Report R76-4.

Georges, K., Olivier, V., & Calogero , C. (2011). Finite-Dynamic Model for Infinite Media: Corrected Solution of Viscous Boundary Efficiency. *American Society of Civil Engineers*. doi:DOI: 10.1061/(ASCE)EM.1943-7889.0000250

Gutenberg, B. (1957). Effects of ground on earthquake motion. *Bulletin of the Seismological Society of America, 47*(3), 221–250. doi:https://doi.org/10.1785/BSSA0470030221

Han, T., & Williams, K. (2008). Multilevel Investigation of Adaptive Performance Individual- and Team-Level Relationships. *Group & Organization Management, 33*(6), 657-684. doi:10.1177/1059601108326799

Hancock, J., Lamprey, J., & Norman, A. (2006). An improved method of matching response spectra of recorded earthquake ground motion using wavelets. *Journal of earthquake engineering*, 67-89. doi:10.1080/13632460609350629

Housner, G. (1965). Intensity cf the Ground Shaking Near the Causative Fault. *Proceedings of the Third World Conference on Earthquake Engineering*, *1.* New Zealand.

Hunter J. A., Crow, H. L., Brooks, G. R., Pyne, M., Motazedian, D., Khaheshi-Banab, K., Lamontagne, M., et al. ,2010, Seismic site classification and site period mapping in the Ottawa area using geophysical methods. Ottawa, ON: Geological Survey of Canada, Open File 6237

Idriss, I. (1999). An update to the Seed-Idriss simplified procedure for evaluating liquefaction potential. *TRB Workshop on New Approaches to Liquefaction.* Publication No. FHWARD-99-165, Federal Highway Administration.

Idriss, I., & Seed, H. (1968). Seismic Response of Horizontal Soil Layers. *Journal of the Soil Mechanics and Foundations Division, 94*, 1003-1031.

Idriss, I., & Sun, J. (1992). *User's Manual for SHAKE91.* Center for Geotechnical Modeling, Department of Civil Engineering, University of California, Davis.

Idriss, I., & Sun, J. (1992). *User's Manual for SHAKE91: A Computer Program for Conducting Equivalent Linear Seismic Response Analyses of Horizontally Layered Soil Deposits.* University of California, Davis, California.

Ishihara, K. (1996). *Soil behaviour in earthquake geotechnics.* Oxford University Press, New York.

Itasca Consulting Group, I. (2019). *FLAC-Fast Lagrangian Analysis of Continua, Ver. 8.1.* Minneapolis: Itasca.

Kanai , K., & Tanaka, T. (1951). Observations of the Earthquake Motion at the Different Depths of the Earth. *Part I, BUZZ. Earthq. Res. Inst, 29*, 107.

Khaheshi Banab, K. (2010). *Site Response Analysis and Seismic Surveying of High Contrast Soil Profiles for the City of Ottawa.* Ph.D thesis, Carleton University.

Kodaka, T., Itabashi, K., Fukuzawa, H., & Kato, S. (2010). Cyclic Shear Strength of Clay under Simple Shear Condition. *In Soil Dynamics and Earthquake Engineering, ASCE*, 234-239.

Kramer, S. (1996). *Geotechnical Earthquake Engineering.* Prentice-Hall, Inc.

Lade, P., & Kirkgard, M. (2000). Effects of stress rotation and changes of b-values on cross-anisotripic behavior of natural, K0-consolidated soft clay. *Soils and Foundations, 40*(6), 93–105.

Lilhanand , K., & Tseng, W. (1988). Development and application of realistic earthquake time histories compartible with multible-damping design spectra. *Proceedings of Ninth World Conference on Earthquake Engineering.* Tokyo-Kyoto, Japan (Vol.II).

Locat, J., Lefebvre, G., & Ballivy, G. (1984). Mineralogy, chemistry, and physical properties interrelationships of some sensitive clays from Eastern Canada. *Canadian Geotechnical Journal, 21*(3), 530-540.

Lysmer, J., & Kuhlemeyer , R. (1969). Finite dynamic model for infinite media. *Journal of the Engineering Mechanics Division, ASCE, 95*(4), 859-877.

Mackerle, J. (2001). Finite elements in the analysis of pressure vessels and piping. *International Journal of Pressure Vessels and Piping, 79*(1), 1-26.

Mahmood, A., & Mitchell, J. (1974). Fabric-property relationships in fine granular materials. *Clays and Clay Minerals, 22*(5–6), 397–408.

Malek, A., Azzouz, A., Baligh, M., & Germaine, J. (1989). Behavior of foundation clays supporting compliant offshore structures. *Journal of Geotechnical Engineering, 115*(5), 615-636.

Mazzotti S, Leonard L. J, Hyndman R. D, & Cassidy J. F. (2008). Tectonics, Dynamics and Seismic Hazard in the Canada–Alaska Cordillera. *179*.

Mejia, L., & Dawson, E. (2016). Earthquake deconvolution for FLAC. *4th International FLAC Symposium on Numerical Modelling in Geomechanics*.

Naeim, F., & Bhatia, H. (2000). *Time Domain Scaling via Nonlinear Programming.*

NRC (2022), Natural Resources Canada, Important Canadian Earthquakes, https://earthquakescanada.nrcan.gc.ca/historic-historique/map-carte-en.php (accessed on Jan 21, 2022)

Peterson, R., & Treagust, D. (1998). Learning to teach primary science through problem-based learning. *Science Education, 82*(2), 215-237.

Phillips, A., & May, P. (1967). *A Form of Anisotropy in Granular Media.* Special Task Report, Dept. of Civil and Municipal Engineering, University College, London.

Prasanna, R. (2020). *Assessment of Liquefaction Characteristics of sand under coupled action of p- and s- waves,* PhD Thesis. *Carleton University*, 349p.

Prasanna, R., & Sivathayalan, S. (2021). *A Hollow Cylinder Torsional Shear Device to Explore Behavior of Soils Subjected to Complex Rotation of Principal Stresses* Geotechnical Testing Journal, 44(6):1595-1616. https://doi.org/10.1520/

Pratt T.L, T. M. Brocher, C. S. Weaver, & K. C. C. (2003). Amplification of seismic waves by the Seattle basin, Washington State. *93*, 533–545. doi:10.1785/0120010292

Pratt, T. L, & T. M. Brocher. (2006). Site response and attenuation in the Puget Lowland, Washington State. *96*, 536–552. doi:10.1785/0120040200

Riepl, J., Bard, P., Hatzfeld, D., Papaioannou, C., & Nechtschein, S. (n.d.). Detailed evaluation of site-response wtimation methods across and along the sedimentary valley of Volvi (EURO-SEISTEST). *Bull. Seism. SW Am, 88*, 488-502.

Sangrey, D., Henkel, D., & Esrig, M. (1969). The effective stress response of a saturated clay soil to repeated loading. *Canadian Geotechnical Journal, 6*(3), 241- 252.

Schnabel, P., Lysmer, J., & Seed, H. (1972). *SHAKE – A computer program for earthquake response analysis of horizontally layered soils.* Report No. EERC-72/12, University of California, Berkeley.

Seed, H., & Idriss, I. (1970). *Soil moduli and damping factors for dynamic response analyses.* Earthquake Engineering Research Center, University of California, Berkeley.

Seed, H., & Idriss, I. (1971). Simplified procedure for evaluating soil liquefaction potential. *Journal of the Soil Mechanics and Foundations Engineering Division, ASCE, 97*(9), 1249–1274.

Seed, H., & Idriss, I. (1982). *Ground motions and soil liquefaction during earthquakes (Vol. 5).* Oakland, CA: Earthquake Engineering Research Institute.

Seed, H., & Sun, J. (1989). *Implication of site effects in the Mexico City earthquake of September 19, 1985 for earthquake-resistance-design criteria in the San Francisco Bay Area of California.* Report No. UCB/EERC-89/03, University of California, Berkeley, California.

Seed, H., Idriss, I., & Arango, I. (1983). Evaluation of liquefaction potential using field performance data. *Journal of Geotechnical Engineering, 109*(3), 458-482.

Seed, R., & Harder, L. (1990). SPT-based analysis of cyclic pore pressure generation and undrained residual strength. In J. Duncan (Ed.), *In Proceedings of H.B. Seed Memorial Symposium, University of California Berkeley, Berkeley, Calif. 2*, pp. 351–376. BiTech Publishers, Vancouver, B.C.

Seed, R., Cetin, K., Moss, R., Kammerer, A., Wu, J., Pestana, J., & Kayen, R. (2003). Recent advances in soil liquefaction engineering: a unified and consistent framework. *In Proceedings of the 26th Annual ASCE Los Angeles Geotechnical Spring Seminar.* Long Beach, CA.

Silva, W., & Lee, K. (1987). *WES RASCAL Code for Synthesizing Earthquake Ground Motions.*

Silva, W., & Lee, K. (1987). *WES RASCAL Code for Synthesizing Earthquake Ground Motions, Stateof-the-Art for Assessing Earthquake Hazards in the United States.* Report 24. U.S. Corps of Engineers Waterways Experiment Station, Miscellaneous Paper S-73-1, 120 p.

Sivathayalan, S. & Logeswaran, P., 2007, Behaviour of sands under generalised boundary conditions. Canadian Geotechnical Journal, 44(2): 138-150.

Sivathayalan, S. & Logeswaran, P., 2008, Experimental assessment of the response of sands under shear–volume coupled deformation, Canadian Geotechnical Journal, 45(9): 1310-1323.

Sivathayalan, S., & Ha, D. (2011). Effect of static shear stress on the cyclic resistance of sands in simple shear loading. *Canadian Geotechnical Journal, 48*(10), 1471–1484.

Skempton, A., & Northey, R. (1952). The Sensitivity of Clays. *Geotechnique, 3*(1), 30-53.

Strenk , P., & Wartman, J. (2011). Uncertainty in seismic slope deformation model predictions. *Engineering Geology*, 61–72.

Strenk, P., & Wartman , J. (2011). Uncertainty in seismic slope deformation model predictions. *Engineering Geology, 122*, 61–72.

Thiers, G., & Seed, H. (1969). Strength and stress-strain characteristics of clays subjected to seismic loading conditions. In Vibration effects of earthquakes on soils and foundations. *ASTM International*.

Thompson, M, E. A. Wirth, A. D. Frankel, J. Renate Hartog, & J. E. Vidale. (2020). Basin Amplification Effects in the Puget Lowland, Washington, from Strong-Motion Recordings and 3D Simulations. *110*, 534–555. doi:10.1785/0120190211

Tremblay, R., Atkinson, G., & Bouaanani, N. (2015). Selection and scaling of ground motion time histories for seismic analysis using NBCC 2015 . *Canadian Association for Earthquake Engineering*.

Tsai, N., & Housner, G. (1970). Calculation of surface motions of a layered half-space. *Bull. Seismol. Soc. Amer, 60*(5), 1625-1651.

Vaid, Y., & Chern, J. (1985). Cyclic and monotonic undrained response of sands. *Proceedings Advances in the Art of Testing Soils under Cyclic Loading Conditions, Detroit*, 120-147.

Vaid, Y., & Sivathayalan, S. (1996). Static and cyclic liquefaction potential of Fraser Delta sand in simple shear and triaxial tests. *Canadian Geotechnical Journal, 33*(2).

Vaid, Y., & Sivathayalan, S. (2000). Fundamental factors affecting liquefaction susceptibility of sands. *Canadian Geotechnical Journal 37(3)*, 592-606.

Vaid, Y., & Thomas, J. (1995). Liquefaction and postliquefaction behavior of sand. *Journal of Geotechnical Engineering, 121*(2), 163–173.

Vaid, Y.P., Stedman, J.D., and Sivathayalan, S. 2001. Confining stress and static shear effects in cyclic liquefaction, Canadian Geotechnical Journal, 38(3): 580-591.

Wang, W. (1979). *Some findings in soil liquefaction.* Earthquake Engineering Department, Water Conservancy and Hydroelectric Power Scientific Research Institute.

Wichtmann, T., Andersen, K., & Sjursen, M. (2013). Cyclic tests on high-quality undisturbed block samples of soft marine Norwegian clay. *Canadian Geotechnical Journal, 50*(4), 400-412.

Wong, R., & Arthur, J. (1985). Induced and inherent anisotropy in sand. *Geotechnique, 35*(4), 471–481.

Youd, T.L., Idriss, I.M., Andrus, R.D., Arango, I., Castro, G., Christian, J.T., Dobry, R., Finn, W.D.L., Harder Jr, L.F., Hynes, M.E., Ishihara, K., Koester, J.P., Liao, S.C., Marcuson III, W.F., Martin, G.R., Mitchell, J.K., Moriwaki, Y., Power,M.S., Robertson, P.K., Seed, R.B., and Stokoe II, K.H. (2001). *Liquefaction Resistance of Soils: Summary Report from the 1996 NCEER and 1998 NCEER/NSF Workshops on Evaluation of Liquefaction Resistance of Soils*, Journal of Geotechnical and Geoenvironmental Engineering, 127(10): 817-833.

Zergoun, M., & Vaid, Y. (1994). Effective stress response of clay to undrained cyclic loading. *Canadian Geotechnical Journal, 31*(5), 714-727.

APPENDIX A

COMPARISON OF THE EFFECTS OF AMPLITUDE SCALING *VS* AMPLITUDE AND FREQUENCY SCALING

Scaling of a real earthquake to match the target design spectrum of the specific site is a critical step. As the amplitude varies with the epicentral distance, the amplitude scaling is often considered appropriate for a selected site to match with its target design spectrum if the motion was recorded at a different epicentral distance. However, the frequency content of seismic shaking depends on the magnitude of the earthquakes. Larger earthquakes are known to have relatively stronger long period motions. Thus, scaling of a recorded earthquake motion by adjusting the recorded time interval can be an effective way to simulate a shaking record due to a different magnitude earthquake. Again, the purpose of analyzing an earthquake is to incorporate natural variations of earthquake motion in to the model. So, both frequency and amplitude scaling enable the selected motion history to match with the target design spectrum while representing the natural variations of earthquake motions in the analysis.

The scaling of Val-des-Bois earthquake is done in two stages. First, the amplitude is scaled to get a closest possible match with the target design spectrum. In this case, the scaling was done such that the spectral ordinate at 0.1s approximately matches the design spectral ordinate at 0.1s. After this scaling, the overall frequency content of the East-West motion was reasonably similar to the design spectrum. However, the North-South motion was

shifted towards the higher frequency side from the target design spectrum. In order to get a better match, the frequency content of the scaled N-S motion was shifted toward long period by adjusting the data interval in the time history file.

Initially, the history was recorded with the frequency of 100Hz where the time interval between data points is 10ms. The time interval was changed to 12ms in order to get a good match with the design spectrum. The effect of this change on the resulting soil response has been relatively minor.

Contours of acceleration, maximum shear stress and CSR within the soil deposits are shown in Figures A1-A5 and Table A-1 compares the recorded maximum soil response values when the analyses were run with amplitude scaled motion and amplitude and frequency scaled motion. There is a slight increase observed in terms of maximum acceleration, maximum shear stress increments and CSR values. However, the differences are not considerably high. This is a reflection of the fact that the frequency scaling was rather small in this case since the recorded motions had frequency content fairly close to the design spectrum

Table A 1: Comparison between the soil response of amplitude scaled motion vs amplitude and frequency scaled of N-S motion of Val-des-Bois Earthquake on Section C-D Model

Parameters	Amplitude and Frequency scaled N-S Motion of Val-des-Bois	Amplitude scaled N-S Motion of Val-des-Bois
Maximum Horizontal Acceleration	0.34g	0.31g
Maximum Shear Stress Increment	59kPa	50kPa
CSR	0.34	0.31

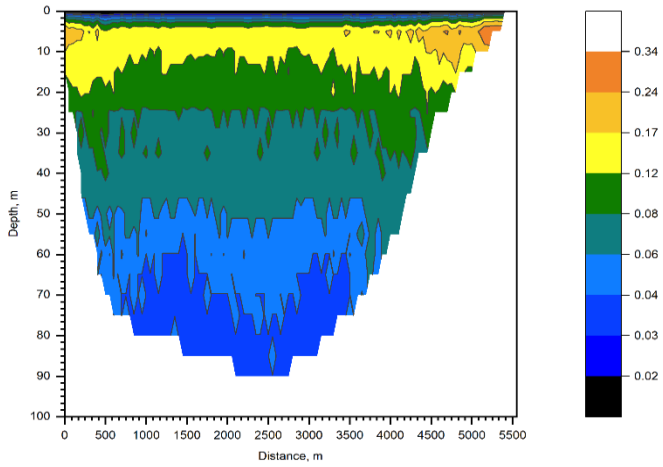

Figure A 1: Variation of CSR in section C-D for the N-S motion of Val-des-Bois (frequency scaled)

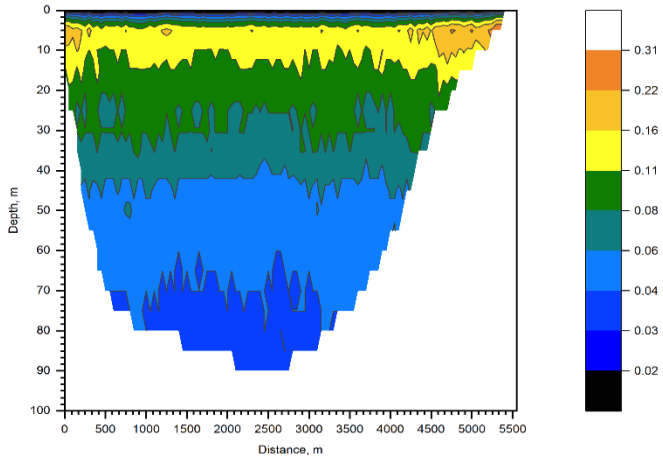

Figure A 2:Variation of CSR in section C-D for the N-S motion of Val-des-Bois (frequency not scaled)

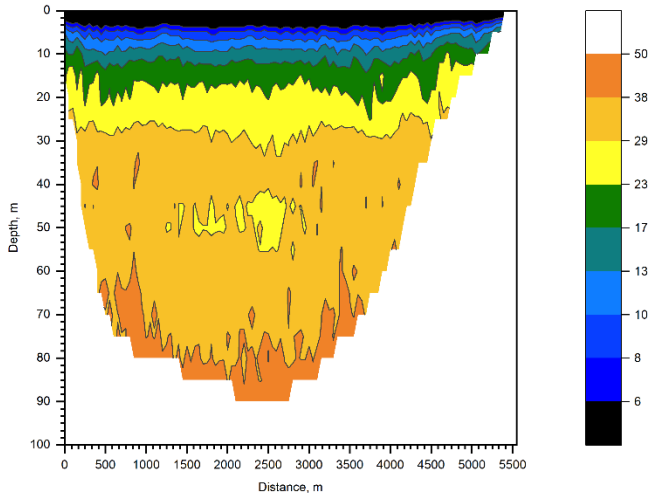

Figure A 3: Variation of maximum shear stress increment in section C-D for the N-S motion of Val-des-Bois (frequency not scaled)

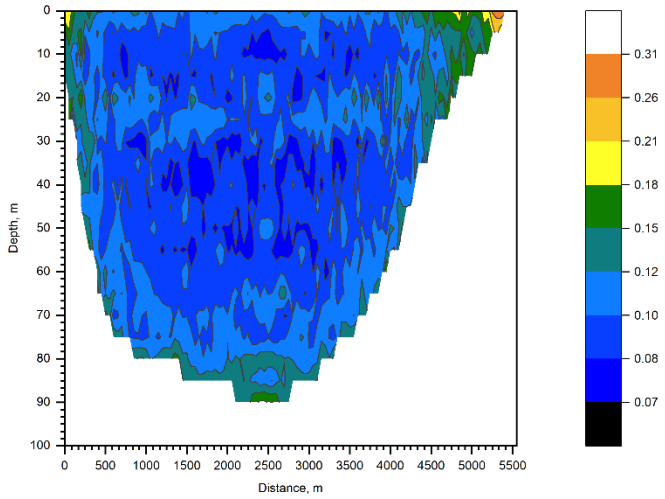

Figure A 4: Variation of maximum horizontal acceleration in section C-D for the N-S motion of Val-des-Bois (frequency not scaled)

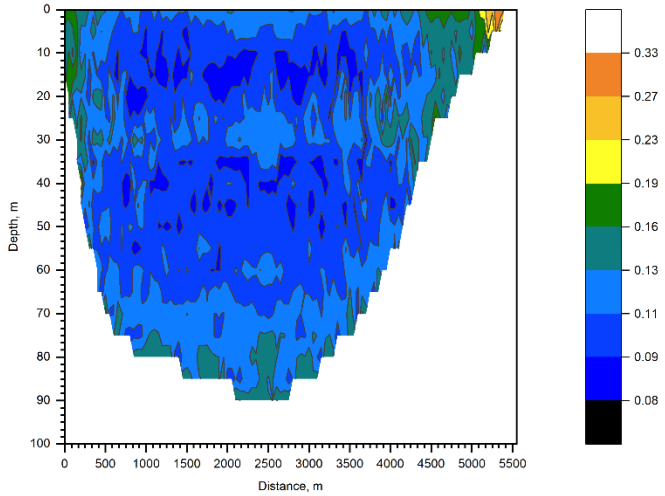

Figure A 5: Variation of maximum horizontal acceleration in section C-D for the N-S motion of Val-des-Bois (frequency scaled)

APPENDIX B

DIFFERENT DEFINITIONS OF CYCLIC STRESS RATIO (CSR)

Cyclic stress ratio is defined differently depending on the context as explained in Chapter 2. In typical design practice, and in the analysis presented in Chapter 4, the cyclic stress ratio is defined based on the cyclic shear stress increment on the horizontal plane. Under 3D loading conditions this definition may not represent the effect of the maximum shear stress, since the shear stress on the horizontal plane need not be the largest shear stress acting on the soil element. This is especially the case if the soil is subjected to the effects of both p- and s- waves simultaneously.

One of the approaches under such circumstances can be by defining the CSR as the ratio between the maximum shear stress increment and the initial vertical effective stress, or the effective normal stress on the plane of maximum shear stress. An assessment is considered in this appendix by defining the cyclic stress ratio as $CSR = K\frac{\Delta\tau_{max}}{\sigma'_{vo}}$. Here the $\Delta\tau_{max}$ is defined as the difference between the maximum shear stress during the dynamic condition and the static shear stress on the same plane of the maximum dynamic shear stress, and K is a constant to account for the transient nature of earthquake loading. This is computed from the magnitude of the maximum shear stress τ_{max} during dynamic loading, which is calculated from horizontal stress $\sigma_{x,dyn}$,vertical stress $\sigma_{z,dyn}$ and the shear stress $\tau_{xz,dyn}$.

$$|\tau_{max}| = \sqrt{\left(\frac{\sigma_{x,dyn} - \sigma_{z,dyn}}{2}\right)^2 + \tau_{xz,dyn}^2}$$

Then the angle ϕ_s to the maximum shear stress is calculated from the horizontal, vertical and shear stress components that corresponds to the maximum shear stress as,

$$\tan(2\phi_s) = -\frac{\left(\frac{\sigma_{x,dyn}-\sigma_{z,dyn}}{2}\right)}{\tau_{xz,dyn}}$$

Then the maximum dynamic shear stress is calculated as,

$$\tau_{max,dyn} = -\left(\frac{\sigma_{x,dyn}-\sigma_{z,dyn}}{2}\right)\sin(2\phi_s) + \tau_{xz,dyn}\cos(2\phi_s)$$

And the static shear stress at the same plane of dynamic maximum shear stress is calculated as,

$$\tau_{st} = -\left(\frac{\sigma_{x,st}-\sigma_{z,st}}{2}\right)\sin(2\phi_s) + \tau_{xz,st}\cos(2\phi_s)$$

Finally, CSR is calculated as,

$$CSR = 0.65 \times \frac{\tau_{max,dyn}-\tau_{st}}{\sigma'_{v,st}}$$

As the CSR is defined by considering the maximum shear stress on the principal plane, the previously calculated values are termed here as horizontal stress ratio (HSR) since they were calculated from the shear stress increment on the horizontal plane. Based on the dynamic analysis of six artificial earthquakes, the cyclic stress ratio (CSR) values were computed by considering the maximum shear stress increment, and these CSR values were compared to the HSR. in Figure B-1 and Figure B-2. The general characteristics are similar, but, the CSR maximum is found to be higher (about 0.44) whereas the maximum HSR is only about 0.29 (in section C-D) in those zones located in the shallow depth. For section A-B, the maximum CSR was recorded as 0.71 where the HSR is only up to 0.44. However,

the CSR is smaller compared to HSR in the deeper layers. The magnitude of the CSR and HSR both decrease as the depth increases (Table B-1).

Table B 1: Comparison of average CSR values observed for all size artificial earthquakes in among section A-B and section C-D s of Orleans profile

Depth from GL	CSR in Horizontal bedrock Model	Section C-D		Section A-B	
		HSR	CSR	HSR	CSR
5~15	0.23~0.15	0.29~0.16	0.44~0.06	0.44~0.27	0. 71~0.2
15~30	0.15~0.1	0.16~0.12	0.06~0.04	0.27~0.21	0.2~0.1
30~45	0.1~0.08	0.12~0.09	0.04~0.02	0.21~0.17	0.1~0.08
45~60	0.08~0.07	0.09~0.07	0.02~0.01	0.17~0.13	0.08~0.05
>60	<0.07	<0.07	<0.02	<0.13	<0.05

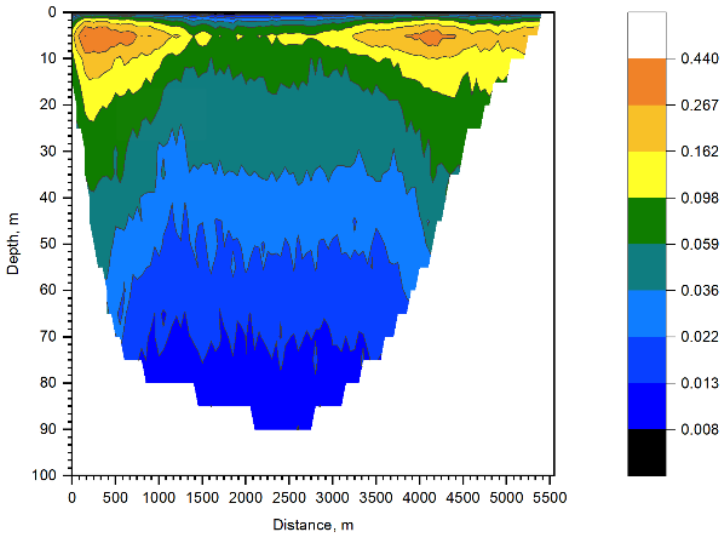

Figure B 1: Variation of Average CSR of six artificial earthquake records on the Orleans profile of Section C-D

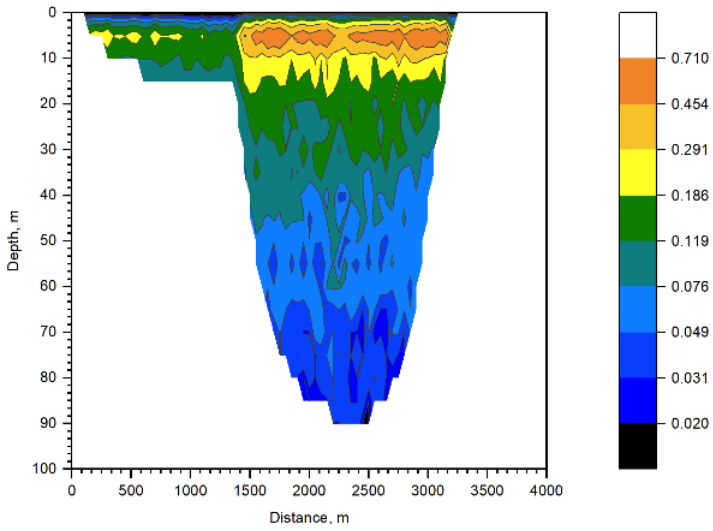

Figure B 2: Variation of Average CSR of six artificial earthquake records on the Orleans profile of Section A-B